Thèse de Mei Qi, Lille 1, 2016

THÈSE DE DOCTORAT
DE L'UNIVERSITÉ LILLE I - SCIENCES ET TECHNOLOGIES

LABORATOIRE DE MÉCANIQUE DE LILLE (UMR CNRS 8107)

Présentée par

Mei Qi

pour obtenir le grade de

DOCTEUR DE L'UNIVERSITÉ LILLE I - SCIENCES ET TECHNOLOGIES

Domaine

GÉNIE CIVIL

Sujet de la thèse

Modélisation micromécanique de l'endommagement et du frottement dans des géomatériaux initialement anisotropes

Soutenue le 24 février 2016 devant le jury composé de :

Pr. J. SULEM	NAVIER, Ecole des Ponts ParisTech	*Président du jury*
Pr. D. HOXHA	PRISME, Université Orléans	*Rapporteur*
Pr. D. KONDO	IJLRDA, UPMC	*Rapporteur*
Pr. A. GIRAUD	INPL, Ecole de Géologie	*Examinateur*
Pr. Q.Z. ZHU	University of Hohai	*Examinateur*
Pr. J.B. COLLIAT	LML, USTL	*Co-directeur de thèse*
Pr. J.F. SHAO	LML, USTL	*Directeur de thèse*

LML-L'UNIVERSITÉ LILLE I

© 2016 Tous droits réservés.

doc.univ-lille1.fr

© 2016 Tous droits réservés.

doc.univ-lille1.fr

Abstract

The objective of this thesis aims to propose a micromechanical method for modelling induced damage and friction sliding for a class of initially anisotropic quasi-brittle materials. To this end, two three-dimensional micromechanical damage models have been developed respectively for open and closed microcracks. The key step of these two models is an efficient numerical method to estimate Hill's tensor for three dimensional spheroidal microcracks in a transversely isotropic solid matrix. Then, the effective elastic properties of cracked material are determined through a rigorous up-scaling procedure based three homogenization methods (*Dilute* scheme, MT scheme, PCW scheme) and analysed by a series of sensitivity studies. Further, a damage model based on the irreversible thermodynamics framework is proposed to account for interactions between initial anisotropy and induced growth of cracks. Furthermore, the second micromechanical model for frictional closed cracks is developed for the description of induced damage and frictional sliding in initially anisotropic materials. The effective elastic properties of cracked materials are estimated using a MT scheme. The evolutions of inelastic strains due to frictional sliding and induced damage by the propagation of microcracks are coupled and described by specific local friction and damage criteria as functions of conjugate thermodynamic forces. The main features of mechanical behaviours of initially anisotropic quasi-brittle materials are taken into account, such as induced growth of micro-cracks, irreversible deformation and hysteretic loops due to friction effects of crack surfaces, coupling between inherent anisotropy and induced anisotropy, effects of confining pressure and volumetric dilatancy.

© 2016 Tous droits réservés.

doc.univ-lille1.fr

© 2016 Tous droits réservés.

doc.univ-lille1.fr

Résumé

L'objectif de cette thèse est de proposer une approche micromécanique pour modéliser l'endommagement et le frottement dans des géomatériaux initialement anisotropes. Dans ce but, deux modèles d'endommagement micromécaniques en 3D ont été développés. L'estimation du tenseur de Hill pour les microfissures sphéroïdales dans une matrice isotrope transverse est le cœur de ces deux modèles. Les propriétés élastiques effectives du milieu fissuré sont déterminées par trois méthodes d'homogénéisation (schéma *Dilué*, schéma MT, schéma PCW) et analysées par une série d'études de sensibilité. Le premier modèle d'endommagement basé dans le cadre de la thermodynamique irréversible est proposé pour prendre en compte des interactions entre l'anisotropie initiale et la fissuration induite. De plus, le deuxième modèle micromécanique pour des fissures fermées frottantes est développé pour modéliser l'endommagement et le glissement dissipatif par frottement. Les évolutions des déformations inélastiques sont provoquées par deux phénomènes couplés: le glissement avec frottement et l'endommagement induit par la propagation des microfissures. Elles sont décrites par des critères spécifiques locaux de l'endommagement et du frottement en fonction des forces thermodynamiques conjuguées. Les principales caractéristiques du comportement mécanique des géomatériaux initialement anisotropes (la croissance des microfissures induites, les déformations irréversibles, boucles d'hystérésis causées par les effets du frottement qui apparaissent sur les lèvres des microfissures fermées, le couplage entre l'anisotropie inhérente et celle induite, les effets de la pression de confinement et de la dilatance volumétrique) sont prises en compte.

© 2016 Tous droits réservés.

doc.univ-lille1.fr

© 2016 Tous droits réservés.

doc.univ-lille1.fr

Acknowledgement

I would like firstly to express my most sincere gratitude to my main supervisor Professor Jianfu Shao for his precious guidances, patiences, confidences and courages during three years of my research and it is a great honour for me to be one of his students.

I would like also to acknowledge my secondary supervisor, Professor Jean-Baptiste Colliat, for his support, motivation and enthusiasm throughout the duration of my research.

I am deeply grateful to Professor Albert Giraud, for his helps, fruitful discussions and to share work with me. I would like specially to thank Professor Qizhi Zhu for his very useful advice. I am deeply grateful for the comments from Professor Dashnor Hoxha, Professor Djimédo Kondo as the reviewers of the manuscript of my dissertation. My sincerely gratitude goes to Professor Jean Sulem as the president jury.

Great thanks also give to my colleagues in paysagé 3 of Laboratoire mécanique de Lille for agreeable ambiance, their assistance, specially for French. They are Dr. Paul Hauseux, Dr. Mahban Hosseini, Alexis Vallade, Hanaa Taif, Andrey Suchkov. I would like also to thank the ones who gave support and helpful advice during the studies: Dr. Wanqing Shen, Dr. Hamid Ghorbanbeigi, Christian Bikong, Dr. Wei Yang, Dr. Mingyao Li, Dr. Yuanyuan Zheng, Dr. Yu Zhang ...

Thanks to my friends Yu xiaohan, Wang Yang, Yang Xue for their support far from China. Great thanks also give to Zhou Hang, I would never be in France without him.

Finally, I have to give a great appreciation to my parents for their unconditional support and encouragement during my academic career.

Mei

© 2016 Tous droits réservés.

doc.univ-lille1.fr

© 2016 Tous droits réservés.

doc.univ-lille1.fr

Table Of Contents

Notations v

General Introduction ix

I Mechanical behaviours of anisotropic materials 1

1 Introduction . . . 1
2 Anisotropic linear elastic behaviour . . . 2
2.1 Monoclinic symmetry materials . . . 5
2.2 Orthotropic materials . . . 5
2.3 Transversely isotropic materials . . . 6
2.4 Isotropic materials . . . 10
3 Behaviour of initial anisotropic rocks . . . 11
3.1 Some experimental data . . . 11
3.2 Determination of elastic parameters . . . 16
3.3 Failure criteria . . . 23
4 Induced anisotropy in rocks . . . 27
4.1 Effect of micro-cracks on macroscopic behaviour of rocks . . . 27
4.2 Some examples on the characterization of induced damage . . . 29
5 Conclusion . . . 30

II Some fundamentals for damage modelling of anisotropic materials 33

1 Introduction . . . 33
2 Basic homogenization schemes of cracked materials . . . 34
2.1 Description of a crack-matrix system . . . 34
2.2 Effective elastic property of cracked materials . . . 35
2.3 Dilute scheme . . . 38
2.4 Mori-Tanaka scheme estimations . . . 40
2.5 PCW scheme estimations . . . 42
3 Eshelby problem . . . 43
3.1 Eshelby's equivalent eigenstrain method . . . 43
3.2 Green's function for Eshelby's problem . . . 45

© 2016 Tous droits réservés.

doc.univ-lille1.fr

Thèse de Mei Qi, Lille 1, 2016

3.3 Hill tensor for arbitrarily oriented spheroidal inclusion in a transversely isotropic matrix . . . 46
4 Conclusion . . . 60

III Numerical study of effective elastic properties of initially transversely isotropic materials 61
1 Introduction . . . 61
2 An approximation of limit case of tensor $\mathbb{T}$ for penny-shaped crack in a transversely isotropic material . . . 62
3 Sensitivity study of effective elastic properties . . . 64
3.1 Effect of crack orientation on effective elastic properties . . . 65
3.2 Effects of micro-cracks on elastic properties in arbitrary direction . . . 70
4 Conclusion . . . 73

IV Micromecanical damage model of transversely isotropic materials with unilateral effects 75
1 Introduction . . . 75
2 Formulation of anisotropic damage model . . . 77
2.1 Free energy and state equations . . . 78
2.2 Damage criterion and evolution law . . . 78
2.3 Computational aspect . . . 79
3 Numerical application . . . 81
3.1 Modelling pre-existing cracks . . . 81
3.2 Uniaxial tension test . . . 84
3.3 Uniaxial compression test . . . 85
3.4 Simple shear test . . . 87
4 Conclusion . . . 88

V Coupling between damage evolution and frictional sliding in an initially anisotropic material 91
1 Introduction . . . 92
2 Description of cracked material . . . 94
2.1 Deformation of cracked material . . . 94
2.2 Effective properties of cracked materials . . . 95
2.3 Free enthalpy with damage-friction . . . 97

© 2016 Tous droits réservés.

doc.univ-lille1.fr

Thèse de Mei Qi, Lille 1, 2016

3 Hill tensor for arbitrarily oriented spheroidal cracks in a transversely isotropic material . . . 98
4 Description of friction-damage evolutions . . . 102
4.1 Friction criterion . . . 103
4.2 Damage criterion . . . 104
4.3 Damage-friction coupling . . . 105
4.4 Numerical implementation . . . 106
5 Numerical assessment and experimental verification . . . 107
5.1 Parameters identification . . . 108
5.2 Simulation of triaxial compression test . . . 110
5.3 Direct shear tests . . . 115
6 Conclusion . . . 115

VI Conclusions and perspectives **119**

A Walpole decomposition of elasticity tensor for transversely isotropic materials **121**

B Derivative of Green's function for transversely isotropic materials **123**

C Chapter 3 supplements **127**
1 Some illustrations of effect of the microcracks on the macrocopic property for initially isotropic matrix . . . 127
1.1 Anisotropic distribution of microcracks . . . 127
1.2 Effects of the microcracks on the elastic modulus in arbitrary direction: comparison with the initially transversely isotropic matrix . . . 130
1.3 Isotropic distribution of microcracks . . . 133

Bibliography **137**

© 2016 Tous droits réservés.

doc.univ-lille1.fr

Thèse de Mei Qi, Lille 1, 2016

© 2016 Tous droits réservés.

doc.univ-lille1.fr

Notations

Tensor notations

a	scalar	$.$	simple contraction
$\underline{a}$	vector	$:$	double contraction
$\mathbf{a}$	second-order tensor	$\otimes$	tensor product
$\mathbb{A}$	fourth-order tensor	$\mathbb{I}$	fourth-order identity tensor
$\boldsymbol{\delta}$	second-order identity tensor	$\mathbb{K}$	$= \mathbb{I} - \mathbb{J}$
$\mathbb{J}$	$= \frac{1}{3}\boldsymbol{\delta} \otimes \boldsymbol{\delta}$		
$\mathbb{E}_i$	fourth order transverse isotropic tensors		
$(\boldsymbol{a} \otimes \boldsymbol{b})_{ijkl}$	$= a_{ij}b_{kl}$		
$(\boldsymbol{a} \overline{\underline{\otimes}} \boldsymbol{b})_{ijkl}$	$= \frac{1}{2}(a_{ik}b_{jl} + a_{il}b_{jk})$		

© 2016 Tous droits réservés.

doc.univ-lille1.fr

Thèse de Mei Qi, Lille 1, 2016

Material parameters

$\mathbb{C}^s$	elastic stiffness tensor of the solid matrix
$\mathbb{S}^s$	elastic compliance tensor of the solid matrix
$\mathbb{C}^f$	fictitious elastic stiffness tensor of cracks
$\mathbb{C}^{hom}$	homogenized drained elastic stiffness tensor
$\mathbb{S}^{hom}$	homogenized drained elastic compliance tensor
E_i^s	elastic Young's modulus of the solid phase in 3 different directions
G_i^s	elastic shear modulus of the solid phase in 3 different directions
ν_i^s	Poisson's ratio of the solid phase in 3 different directions
k^f	elastic bulk modulus of cracks
μ^f	elastic shear modulus of cracks
ϵ	aspect ratio of cracks

Model parameters

$R(d)$	the function of the crack resistance to damage propagation
c_0, c_1, c_m	damage criterion parameters
η	friction coefficient
r_c	critical (maximal) damage resistance
d_0	initial damage value
d_c	critical damage value
λ_d	damage multiplier
λ_s	friction multiplier

© 2016 Tous droits réservés.

doc.univ-lille1.fr

Thèse de Mei Qi, Lille 1, 2016

Common notations in all chapters

$\mathbf{E}$ macroscopic strain tensor

$\mathbf{\Sigma}$ macroscopic stress tensor

$\boldsymbol{\varepsilon}$ microscopic strain tensor

$\boldsymbol{\sigma}$ microscopic stress tensor

$\underline{n}$ unit normal vector of one microcrack family

$\mathbb{P}$ Hill tensor

$\mathbb{S}$ Eshelby's tensor

$\mathbb{A}$ strain concentration tensor

$\boldsymbol{\sigma}^*$ macroscopic stress tensor for Eshelby's problem

$\boldsymbol{\varepsilon}^*$ macroscopic strain tensor for Eshelby's problem

$\boldsymbol{G}$ Green's function

$\boldsymbol{\varepsilon}^t$ eigenstrain tensor

$\boldsymbol{\sigma}^I$ polarization tensor (the eigenstrain tensor)

$\boldsymbol{\varepsilon}^I$ strain tensor in the inclusion for Eshelby's problem

© 2016 Tous droits réservés.

doc.univ-lille1.fr

Thèse de Mei Qi, Lille 1, 2016

© 2016 Tous droits réservés.

doc.univ-lille1.fr

Thèse de Mei Qi, Lille 1, 2016

General Introduction

Damage due to growth of micro-cracks is an essential dissipation mechanisms in a large range of quasi brittle materials such as rocks and concretes. The induced damage affects not only mechanical properties but also physical properties such as permeability and heat conductivity. Further, frictional sliding along crack surfaces is also at the physical origin of macroscopic irreversible deformation in such materials. These two dissipation mechanisms, crack growth and frictional sliding, are generally coupled. Significant efforts have been made during the last decades on modelling of induced damage in different engineering materials. A number of macroscopic damage models have been developed in the framework of irreversible thermodynamics. In these models, spatial distribution of micro-cracks is mathematically represented by scalar or tensorial variables. Effective properties of cracked materials are determined by postulating a specific form of thermodynamic potential. Damage evolution is determined through definition of a specific damage criterion in terms of conjugate thermodynamic forces. Directly calibrated from experimental data, most of such models are able to capture main features of macroscopic behaviors of brittle materials. However, macroscopic approaches are not able to consider physical mechanisms involved at relevant material scales and usually meet difficulties in dealing with some specific features such as unilateral effects, damage-friction coupling etc. On the other hand, for a class of quasi-brittle materials, important irreversible strains are observed and coupled with damage evolution. By considering such irreversible strains as plastic strains, different macroscopic models have also been developed for description of coupled elastic-plastic strains and damage evolution. Most models have been formulated in the framework works of irreversible thermodynamics by choosing suitable internal variables for damage state and plastic strains. The key step is to define an appropriate thermodynamics framework incorporating coupling between two dissipation mechanisms. A number of specific models have been proposed for concrete materials and rock materials. In these models, plastic strains have been described by using macroscopic yield criteria and plastic potentials, depending on macroscopic stresses and damage state. However,

© 2016 Tous droits réservés.

doc.univ-lille1.fr

Thèse de Mei Qi, Lille 1, 2016

the physical origin of macroscopic plastic strains was not explicitly explained. In concrete and rock like materials, it is known that macroscopic plastic strains are generally related to frictional sliding along closed micro-cracks.

On the other hand, significant advances have also been achieved on micro-mechanical modelling of induced damage and coupling with friction. The main objective is to consider the growth and frictional sliding of micro-cracks at appropriate material scales and then to determine effective properties of cracked materials by a up-scaling method. Different features can be properly considered such as induced anisotropy, interaction between cracks and unilateral effects. Two categories of micro-mechanical damage models can be found. In the first category, the micro-mechanical models are directly formulated in the framework of Linear Fracture Mechanics, without using a rigorous up-scaling procedure to determine effective properties of cracked materials. On the other hand, a second category of micro-mechanical models are developed by using rigorous linear homogenization procedures for heterogeneous materials. In this context, cracks are considered as a inclusion phase embedded in an elastic matrix. Effective elastic properties of cracked materials are estimated using an Eshelby solution based homogenization method. In a number of models, coupling between crack growth and frictional sliding has been taken into account. Further, micro-mechanical models have even been extended to saturated brittle materials by taking into account effects of fluid pressure.

Most micro-mechanical models so far developed generally deal with crack growth and frictional sliding in initially isotropic materials. However, for many engineering materials such as rocks, there exist different kinds of inherent anisotropy due to the presence of bedding planes, preferential orientations of mineral grains or pores etc. It is therefore an important issue to consider effects of the initial structural anisotropy on induced crack growth. In the context of Eshelby solution based micro-mechanical approaches, an essential step of homogenization procedure is to establish a suitable relation between prescribed macroscopic strain (or stress) and local strain (stress) field inside crack phases using a specific strain concentration (or stress localization) tensor. Such a concentration tensor is directly related to the so-called Eshelby tensor or equivalently Hill's tensor and depends on homogenization schemes considering or not crack interactions and spatial distribution. In the case of spheroidal micro-cracks embedded in an isotropic elastic solid matrix, it is possible to obtain a closed-form of such a tensor. However, when cracked materials with inherent anisotropy are concerned, it is no more possible to get such closed-form solutions. Suitable numerical methods have to be developed to computer Hill's tensor.

The main objective of this thesis is to develop a micro-mechanics based model for the

© 2016 Tous droits réservés.

doc.univ-lille1.fr

Thèse de Mei Qi, Lille 1, 2016

description of induced damage and frictional sliding in initially anisotropic materials. To this end, an Eshelby's solution based linear homogenization method will be extended in order to take into account effects of initial anisotropy. The present thesis is composed of the following Chapters.

In Chapter I , a bibliographic review will be given on basic mechanical behaviours of anisotropic rock materials. Firstly, the inherent structural anisotropy of mechanical and physical properties is shortly discussed such in terms of different types of symmetry such as transversely isotropic symmetry, orthotropic symmetry, monoclinic symmetry etc. Then a series of experimental investigations are presented in order to show anisotropic elastic and failure properties of typical rocks. Some anisotropic failure criteria are also presented. Finally, loading induced anisotropy by material damage is presented. It will be shown that nucleation and growth of micro-cracks strongly effect deformation behaviour and failure process in many rock-like material.

In Chapter II , we present a short review of some theoretical fundamentals of different Eshelby solution based homogenization techniques for micro-mechanical modelling of cracked random materials. The emphasis is put on the determination of strain concentration tensor for both isotropic and anisotropic materials. In particular, an efficient numerical method is proposed to computer Eshelby or Hill tensor for three-dimensional ellipsoidal micro-cracks embedded in a transversely isotropic material.

Chapter III is devoted to a numerical study of effective elastic properties of initially anisotropic cracked materials. The emphasis is put on the study of interaction between the initial anisotropy and induced oriented micro-cracks. Three different homogenization schemes (*Dilute* scheme, Mori-Tanaka scheme (MT) and Ponte Castaneda and Willis scheme (PCW)) are considered. A series of numerical results are presented in show effects of induced micro-cracks on effective elastic properties in initially transversely isotropic materials with different anisotropic degrees and different micro-crack orientations.

In Chapter IV , a micro-mechanical damage model is proposed for initially transversely isotropic materials with the definition of a specific damage criterion in the framework of irreversible thermodynamics to describe the progressive growth of open micro-cracks. The idea of this model is to combine linear homogenization methods (*Dilute* scheme, MT scheme, PCW scheme) with the thermodynamic reasoning based on the energy released rate, and the assumption of normality rule will be employed to build the evolution law of

© 2016 Tous droits réservés.

doc.univ-lille1.fr

Thèse de Mei Qi, Lille 1, 2016

damage. And then, the proposed model is implemented in a computer code and applied to study elastic-damage behaviours of brittle materials respectively under uniaxial tension and compression as well as simple shear tests.

In Chapter V , the micro-mechanical damage model is extended to modelling coupling between damage evolution and frictional sliding for closed micro-cracks in an initially transversely isotropic materials. A specific local criterion is proposed to describe inelastic frictional sliding with is inherently coupled with the damage evolution law. A series of numerical assessments are presented for different loading paths such as triaxial compression and simple shear. The micro-mechanical model is also verified through experimental validation for a typical clayey rock that was extensively investigated in the context of geological disposal of radioactive waste and shale gas exploration. In particular, interactions between the initial anisotropy and induced damage are analysed. Coupling between damage by crack growth and frictional sliding is also studied through numerical examples.

© 2016 Tous droits réservés.

doc.univ-lille1.fr

Chapter I

Mechanical behaviours of anisotropic materials

Contents

1 Introduction 1
2 Anisotropic linear elastic behaviour 2
2.1 Monoclinic symmetry materials 5
2.2 Orthotropic materials 5
2.3 Transversely isotropic materials 6
2.4 Isotropic materials 10
3 Behaviour of initial anisotropic rocks 11
3.1 Some experimental data 11
3.2 Determination of elastic parameters 16
3.3 Failure criteria 23
4 Induced anisotropy in rocks 27
4.1 Effect of micro-cracks on macroscopic behaviour of rocks 27
4.2 Some examples on the characterization of induced damage 29
5 Conclusion 30

1 Introduction

Generally, anisotropy is the property of being directionally dependent, as opposed to isotropy, which implies identical properties in all directions. It can be defined as a difference, when measured along different axes, in a material's physical or mechanical property

© 2016 Tous droits réservés.

doc.univ-lille1.fr

Thèse de Mei Qi, Lille 1, 2016

(elastic modulus, mechanical strength, permeability, conductivity, etc). It means that the behaviour of an anisotropic material has a preferred direction and its mechanical response depends on loading orientation.

The objective of this chapter is to present a short review of various features of mechanical behaviours of anisotropic rock-like materials. Indeed, most rocks exhibit anisotropic behaviours related to their microstructure morphology and geological origin. For example, the structure of sedimentary rocks takes place during the accumulation of sediments and the process of consolidation or lithification (compaction, cementation and recrystallization). The geological origin is further influenced by external environments such as loading history, surrounding temperature, etc. These elements are the causes of various transformations of rocks. Moreover, during subsequent loading, an induced anisotropy can produce due to oriented growth and propagation of micro-cracks. There will be interactions between the inherent initial anisotropy and induced one.

In this short review, the linear elasticity theory of anisotropic materials will be first recalled. Then some representative studies will be presented on the experimental characterization and modelling of both elastic and failure properties of a class of transversely isotropic rocks. Finally, some results will be presented on the characterization and description of induced anisotropy in rock-like materials.

2 Anisotropic linear elastic behaviour

The linear elastic behaviour means that the stress tensor ($\boldsymbol{\Sigma}$) remains proportional to the deformation tensor ($\boldsymbol{E}$) during loading procedure. In general, the elastic behaviour of the material is characterized by the elasticity tensor (the stiffness tensor $\mathbb{C}$ and the compliance tensor $\mathbb{S}$).

We assume a linear, elastic, homogeneous medium which satisfies the generalized Hooke's law. So, we have:

$$\boldsymbol{\Sigma}_{ij} = \mathbb{C}_{ijkl}\boldsymbol{E}_{kl} \tag{I .1}$$

with $\mathbb{C}_{ijkl}$ the components of the elastic stiffness tensor of material.

Its inverse form can be written as:

$$\boldsymbol{E}_{ij} = \mathbb{S}_{ijkl}\boldsymbol{\Sigma}_{kl} \tag{I .2}$$

$\mathbb{S}_{ijkl}$ refers to the components of the compliance tensor.

The both elastic stiffness tensor $\mathbb{C}$, and elastic compliance tensor $\mathbb{S}$ have major symmetries. The symmetry of the initial structure of materials is reflected in its elastic properties.

© 2016 Tous droits réservés.

doc.univ-lille1.fr

Thèse de Mei Qi, Lille 1, 2016

The number of elastic coefficients is reduced accordingly. They are characterized by 21 independent components in the general (triclinic) anisotropic case. The corresponding matrix is symmetric, $6-6$ dimension. According to the Voigt notation, the components of these tensors can be written as [Walpole, 1984] (see also [Ponte-Castaneda and Willis, 1995]):

$$\mathbb{A}_{ijkl} = \begin{bmatrix} A_{1111} & A_{1122} & A_{1133} & \sqrt{2}A_{1123} & \sqrt{2}A_{1131} & \sqrt{2}A_{1112} \\ A_{1122} & A_{2222} & A_{2233} & \sqrt{2}A_{2223} & \sqrt{2}A_{2231} & \sqrt{2}A_{2212} \\ A_{1133} & A_{2233} & A_{3333} & \sqrt{2}A_{3323} & \sqrt{2}A_{3331} & \sqrt{2}A_{3312} \\ \sqrt{2}A_{1123} & \sqrt{2}A_{2223} & \sqrt{2}A_{3323} & 2A_{2323} & 2A_{2331} & 2A_{2312} \\ \sqrt{2}A_{1131} & \sqrt{2}A_{2231} & \sqrt{2}A_{3331} & 2A_{2331} & 2A_{3131} & 2A_{3112} \\ \sqrt{2}A_{1112} & \sqrt{2}A_{2212} & \sqrt{2}A_{3312} & 2A_{2312} & 2A_{3112} & 2A_{1212} \end{bmatrix} \tag{I .3}$$

However, the 21 components of compliance tensor is conventionally written in terms of the elastic modulus which have physical significations of the elastic behaviour of the material.

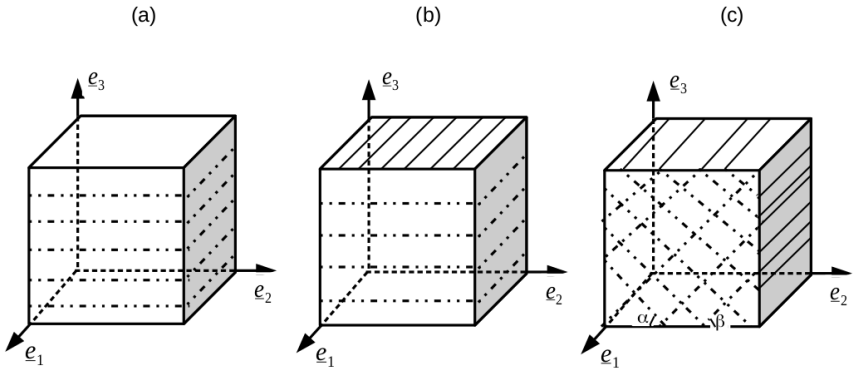

Figure I .1: Structural models: (a) axial, (b) orthotropic, (c)monoclinic.

At the macroscopic scale, the material can be classed in four types according to the symmetry system of the initial structural anisotropy, see Figure (I .1):

- axial symmetry (transversely isotropic material): this is a spacial case of orthotropic symmetry, with the rotational variance around one of the symmetry axes, (I .1 (a)).

© 2016 Tous droits réservés.

doc.univ-lille1.fr

Thèse de Mei Qi, Lille 1, 2016

- orthotropic symmetry (orthotropic material): an orthotropic material is one for which there are two orthogonal planes of symmetry. It means that the material properties are variant under reflections relative to two orthogonal planes, (I .1 (b)).
- monoclinic symmetry (monoclinic material): it presents an axis of symmetry and a perpendicular plane. It means that it has two preferential planes by any angle between them. If there is a third preferential plane, it must be perpendicular to the others, (I .1 (c)).
- triclinic symmetry: in this case, there is not symmetry, only a center of symmetry is presented.

Among these four symmetry systems, the axial symmetry and orthotropic symmetry are two symmetries which frequently appear in the sedimentary rocks. Different mechanical domains, the elastic domain, the elastic limit, the plastic flow, the rupture of the material, can be influenced by initial anisotropy of the material.

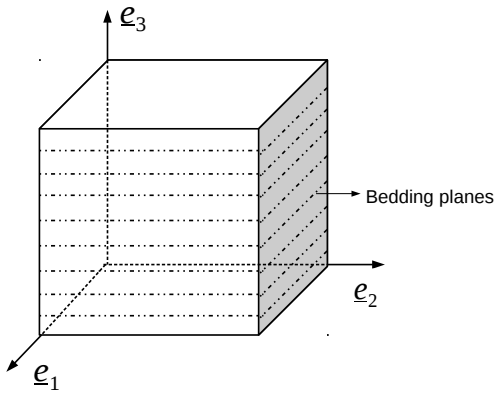

Figure I .2: Definition of structural axes

In most cases, anisotropic rocks are considered as orthotropic or transversely isotropic materials in a coordinate system in their structure or their apparent symmetry directions. In the following subsections, we take into account the three principal directions $(\underline{e}_1, \underline{e}_2, \underline{e}_3)$, as shown in Figure I .2. Three special symmetry classes to present the elastic properties of the material, including orthotropic, transversely isotropic, isotropic symmetries. In these special cases of symmetry, three general independent coefficients are used usually: the Young moduli E_i, the shear moduli G_i and the Poisson's ratio ν_i in three different directions to characterize the elastic property of material.

© 2016 Tous droits réservés.

doc.univ-lille1.fr

Thèse de Mei Qi, Lille 1, 2016

2.1 Monoclinic symmetry materials

A monoclinic symmetry material is symmetry about a plane. In other words, if the material properties are invariant under reflections relative to one plane, say the plane $\underline{e}_1 - \underline{e}_2$, all components of the stiffness tensor having and odd number of indices taking the value 3 can be shown to be zero:

$$\mathbb{C}_{ijkl} = \begin{bmatrix} C_{1111} & C_{1122} & C_{1133} & 0 & 0 & \sqrt{2}C_{1112} \\ C_{2211} & C_{2222} & C_{2233} & 0 & 0 & \sqrt{2}C_{2212} \\ C_{3311} & C_{3322} & C_{3333} & 0 & 0 & \sqrt{2}C_{3312} \\ 0 & 0 & 0 & 2C_{2323} & 2C_{2331} & 0 \\ 0 & 0 & 0 & 2C_{2331} & 2C_{3131} & 0 \\ \sqrt{2}C_{1112} & \sqrt{2}C_{2212} & \sqrt{2}C_{3312} & 0 & 0 & 2C_{1212} \end{bmatrix} \tag{I .4}$$

The number of independent elastic coefficients is reduced to 13.

2.2 Orthotropic materials

An orthotropic material is one for which there are two orthogonal planes of symmetry. In other words, orthotropic materials have three planes/axes of symmetry. Their material properties are different along each axis. If the orthogonal planes are chosen to be normal to the $\underline{e}_1$ and $\underline{e}_2$ directions, the stiffness matrix can be written as:

$$\mathbb{C}_{ijkl} = \begin{bmatrix} C_{1111} & C_{1122} & C_{1133} & 0 & 0 & 0 \\ C_{2211} & C_{2222} & C_{2233} & 0 & 0 & 0 \\ C_{3311} & C_{3322} & C_{3333} & 0 & 0 & 0 \\ 0 & 0 & 0 & 2C_{2323} & 0 & 0 \\ 0 & 0 & 0 & 0 & 2C_{3131} & 0 \\ 0 & 0 & 0 & 0 & 0 & 2C_{1212} \end{bmatrix} \tag{I .5}$$

Note that the material is symmetry about a 180-degree rotation about this axis and also there are 9 independent coefficients where we supposed that the 3 symmetry directions

© 2016 Tous droits réservés.

doc.univ-lille1.fr

Thèse de Mei Qi, Lille 1, 2016

are known.

It is obvious that the compliance tensor $\mathbb{S}$ will have the same symmetry as the stiffness tensor $\mathbb{C}$:

$$\mathbb{S}_{ijkl} = \begin{bmatrix} \frac{1}{E_1} & \frac{-\nu_{21}}{E_2} & \frac{-\nu_{31}}{E_3} & 0 & 0 & 0 \\ \frac{-\nu_{12}}{E_1} & \frac{1}{E_2} & \frac{-\nu_{32}}{E_3} & 0 & 0 & 0 \\ \frac{-\nu_{13}}{E_1} & \frac{-\nu_{23}}{E_2} & \frac{1}{E_3} & 0 & 0 & 0 \\ 0 & 0 & 0 & \frac{1}{G_{23}} & 0 & 0 \\ 0 & 0 & 0 & 0 & \frac{1}{G_{31}} & 0 \\ 0 & 0 & 0 & 0 & 0 & \frac{1}{G_{12}} \end{bmatrix} \tag{I .6}$$

where E_1, E_2, E_3 are the 3 Young's moduli in $\underline{e}_1$, $\underline{e}_2$, $\underline{e}_3$ directions; G_{23}, G_{31}, G_{12} are the shear moduli in the planes $(\underline{e}_2, \underline{e}_3)$, $(\underline{e}_3, \underline{e}_1)$, $(\underline{e}_1, \underline{e}_2)$ respectively. Poisson's ratio ν_{ij} correspond to a contraction in direction j when an extension is applied in direction i. The Poisson's ratio of an orthotropic material is different in each direction ($\underline{e}_1$, $\underline{e}_2$ and $\underline{e}_3$). However, the symmetry of the stress and strain tensors implies that not all the six Poisson's ratios in the equation are independent. There are only nine independent material parameters: three elastic moduli, three shear moduli, and three Poisson's ratios. The remaining three Poisson's ratios can be obtained from the relations: $\frac{\nu_{12}}{E_1} = \frac{\nu_{21}}{E_2}$, $\frac{\nu_{13}}{E_1} = \frac{\nu_{31}}{E_3}$, $\frac{\nu_{23}}{E_2} = \frac{\nu_{32}}{E_3}$.

2.3 Transversely isotropic materials

This is the special case of the orthotropic materials which are symmetric about an axis that is normal to a plane of isotropy. If we choose $\underline{e}_3$ as the symmetry axis, then the stiffness tensor takes the following form:

© 2016 Tous droits réservés.

doc.univ-lille1.fr

Thèse de Mei Qi, Lille 1, 2016

$$\mathbb{C}_{ijkl} = \begin{bmatrix} C_{1111} & C_{1122} & C_{1133} & 0 & 0 & 0 \\ C_{1122} & C_{1111} & C_{1133} & 0 & 0 & 0 \\ C_{1133} & C_{1133} & C_{3333} & 0 & 0 & 0 \\ 0 & 0 & 0 & 2C_{3131} & 0 & 0 \\ 0 & 0 & 0 & 0 & 2C_{3131} & 0 \\ 0 & 0 & 0 & 0 & 0 & C_{1111} - C_{1122} \end{bmatrix} \tag{I .7}$$

which has only 5 independent elastic coefficients to characterize the mechanical behaviour.

The corresponding compliance tensor is conventionally written in terms of the longitudinal and transverse Young's moduli ($E_L = E_3$ and $E_T = E_1 = E_2$), the transverse and longitudinal Poisson's ratios ($\nu_T = \nu_{12} = \nu_{21}$ and $\nu_{TL} = \nu_{13} = \nu_{23}$, $\nu_{LT} = \nu_{31} = \nu_{32}$) and the longitudinal shear modulus $G_L = G_{31}$, as:

$$\mathbb{S}_{ijkl} = \begin{bmatrix} \frac{1}{E_T} & \frac{-\nu_T}{E_T} & \frac{-\nu_{TL}}{E_L} & 0 & 0 & 0 \\ \frac{-\nu_T}{E_T} & \frac{1}{E_T} & \frac{-\nu_{TL}}{E_L} & 0 & 0 & 0 \\ \frac{-\nu_{LT}}{E_T} & \frac{-\nu_{LT}}{E_T} & \frac{1}{E_L} & 0 & 0 & 0 \\ 0 & 0 & 0 & \frac{1}{G_L} & 0 & 0 \\ 0 & 0 & 0 & 0 & \frac{1}{G_L} & 0 \\ 0 & 0 & 0 & 0 & 0 & \frac{2(1+\nu_T)}{E_T} \end{bmatrix} \tag{I .8}$$

It may be interesting to introduce standard notation and the corresponding simplified algebra for fourth-order transversely isotropic tensor (see [Kunin, 1983],[Walpole, 1984] and for recent application to micro-mechanics in [Sevostianov et al., 2005], [Levin and Alvarez-Tostado, 2006],[Dormieux et al., 2006], [Sevostianov and Kachanov, 2007]).

By denoting $\underline{n}$ the unit vector of symmetry axis of the material, let us introduce the second-order tensors $\underline{\underline{i}}_N$ and $\underline{\underline{i}}_T$:

$$\underline{\underline{i}}_N = \underline{n} \otimes \underline{n} = n_i\, n_j\, \underline{e}_i \otimes \underline{e}_j \quad , \quad \underline{\underline{i}}_T = \underline{\underline{i}} - \underline{\underline{i}}_N \tag{I .9}$$

© 2016 Tous droits réservés.

doc.univ-lille1.fr

Thèse de Mei Qi, Lille 1, 2016

In the particular case of $\underline{n} = \underline{e}_3$, (I .9) writes:

$$\underline{\underline{i}}_N = \underline{e}_3 \otimes \underline{e}_3 \quad , \quad \underline{\underline{i}}_T = \underline{e}_1 \otimes \underline{e}_1 + \underline{e}_2 \otimes \underline{e}_2 \tag{I .10}$$

One introduces fourth-order tensors:

$$\begin{aligned} &\mathbb{E}_1 = \frac{1}{2}\underline{\underline{i}}_T \otimes \underline{\underline{i}}_T \quad , \quad \mathbb{E}_2 = \underline{\underline{i}}_N \otimes \underline{\underline{i}}_N \\ &\mathbb{E}_3 = \underline{\underline{i}}_T \overline{\otimes} \underline{\underline{i}}_T - \mathbb{E}_1 \quad , \quad \mathbb{E}_4 = \underline{\underline{i}}_T \overline{\otimes} \underline{\underline{i}}_N + \underline{\underline{i}}_N \overline{\otimes} \underline{\underline{i}}_T \end{aligned} \tag{I .11}$$

It is readily seen that:

$$\begin{aligned} &\mathbb{E}_1 + \mathbb{E}_2 + \mathbb{E}_3 + \mathbb{E}_4 = \mathbb{I} \\ &\mathbb{E}_p : \mathbb{E}_q = \mathbb{E}_p \quad \text{if } p = q \quad , \quad \mathbb{E}_p : \mathbb{E}_q = 0 \quad \text{if } p \neq q \end{aligned} \tag{I .12}$$

Two others elementary tensors are also introduced:

$$\mathbb{E}_5 = \underline{\underline{i}}_N \otimes \underline{\underline{i}}_T \quad , \quad \mathbb{E}_6 = \underline{\underline{i}}_T \otimes \underline{\underline{i}}_N \tag{I .13}$$

and with the Voigt notation, the matrix expressions of these six decomposition tensors are shown in Appendix A.

It may be shown that any transversely isotropic fourth-order tensor can be decomposed as:

$$\mathbb{L} = l_1\,\mathbb{E}_1 + l_2\,\mathbb{E}_2 + l_3\,\mathbb{E}_3 + l_4\,\mathbb{E}_4 + l_5\,\mathbb{E}_5 + l_6\,\mathbb{E}_6 \tag{I .14}$$

and transversely isotropic second-order tensors write:

$$\underline{\underline{a}} = a_N\,\underline{\underline{i}}_N + a_T\,\underline{\underline{i}}_T \quad , \quad Tr(\underline{\underline{a}}) = \underline{\underline{a}} : \underline{\underline{i}} = a_N + 2a_T \tag{I .15}$$

The (non commutative) tensor products $\mathbb{L} : \mathbb{H}$ and $\mathbb{H} : \mathbb{L}$ write:

$$\begin{aligned} &\mathbb{L} : \mathbb{H} = (h_1\,l_1 + 2h_5\,l_6)\;\mathbb{E}_1 + (h_2\,l_2 + 2h_6\,l_5)\;\mathbb{E}_2 + h_3\,l_3\,\mathbb{E}_3 + \\ &+ h_4\,l_4\,\mathbb{E}_4 + (h_5\,l_2 + h_1\,l_5)\;\mathbb{E}_5 + (h_6\,l_1 + h_2\,l_6)\;\mathbb{E}_6 \\ &\mathbb{H} : \mathbb{L} = (h_1\,l_1 + 2h_6\,l_5)\;\mathbb{E}_1 + (h_2\,l_2 + 2h_5\,l_6)\;\mathbb{E}_2 + h_3\,l_3\,\mathbb{E}_3 + \\ &+ h_4\,l_4\,\mathbb{E}_4 + (h_2\,l_5 + h_5\,l_1)\;\mathbb{E}_5 + (h_1\,l_6 + h_6\,l_2)\;\mathbb{E}_6 \end{aligned} \tag{I .16}$$

The inverse of $\mathbb{L}$ is:

$$\begin{aligned} &(\mathbb{L})^{-1} = \frac{l_2}{\Delta}\,\mathbb{E}_1 + \frac{l_1}{\Delta}\,\mathbb{E}_2 + \frac{1}{l_3}\mathbb{E}_3 + \frac{1}{l_4}\mathbb{E}_4 - \frac{l_5}{\Delta}\,\mathbb{E}_5 - \frac{l_6}{\Delta}\,\mathbb{E}_6 \\ &\Delta = l_1\,l_2 - 2l_5\,l_6 \end{aligned} \tag{I .17}$$

© 2016 Tous droits réservés.

doc.univ-lille1.fr

Thèse de Mei Qi, Lille 1, 2016

Any fourth-order transversely isotropic tensor $\mathbb{T}$ with a direction of anisotropy $\underline{n}$ can be written as ([Bornert et al., 2001]):

$$\begin{aligned}\mathbb{T} &= (\mathbb{E}_1 :: \mathbb{T})\,\mathbb{E}_1 + (\mathbb{E}_2 :: \mathbb{T})\,\mathbb{E}_2 + \frac{1}{2}(\mathbb{E}_3 :: \mathbb{T})\,\mathbb{E}_3 + \frac{1}{2}(\mathbb{E}_4 :: \mathbb{T})\,\mathbb{E}_4 \\ &+\frac{1}{2}(\mathbb{E}_6 :: \mathbb{T})\,\mathbb{E}_5 + \frac{1}{2}(\mathbb{E}_5 :: \mathbb{T})\,\mathbb{E}_6\end{aligned} \tag{I .18}$$

One considers an arbitrary anisotropic fourth-order tensor $\mathbb{T}^{ani}$ which has the minor symmetries. In this case, application of the double contractions $\mathbb{T}^{ani}$ gives the projection of $\mathbb{T}^{ani}$ onto the subspace generated by $\mathbb{E}_i$ $(i = 1, 6)$, to obtain a transversely isotropic tensor with a direction of anisotropy $\underline{n}$:

$$\mathbb{T}^{TrIso} = \left(\mathbb{E}_1 :: \mathbb{T}^{ani}\right)\mathbb{E}_1 + \left(\mathbb{E}_2 :: \mathbb{T}^{ani}\right)\mathbb{E}_2 + \frac{1}{2}\left(\mathbb{E}_3 :: \mathbb{T}^{ani}\right)\mathbb{E}_3 \tag{I .19}$$

$$+\frac{1}{2}\left(\mathbb{E}_4 :: \mathbb{T}^{ani}\right)\mathbb{E}_4 + \frac{1}{2}\left(\mathbb{E}_6 :: \mathbb{T}^{ani}\right)\mathbb{E}_5 + \frac{1}{2}\left(\mathbb{E}_5 :: \mathbb{T}^{ani}\right)\mathbb{E}_6 \tag{I .20}$$

This method has been applied to the tangent operator. The compliance tensor $\mathbb{S}$ of a transversely isotropic medium with symmetry axis $\underline{n} = \underline{e}_3$ writes:

$$\begin{aligned}&\mathbb{S} = s_1\,\mathbb{E}_1 + s_2\,\mathbb{E}_2 + s_3\,\mathbb{E}_3 + s_4\,\mathbb{E}_4 + s_5\,\mathbb{E}_5 + s_6\,\mathbb{E}_6 \\ &s_1 = \frac{1-\nu_T}{E_T}, \quad s_2 = \frac{1}{E_L}, \quad s_3 = \frac{1+\nu_T}{E_T} \\ &s_4 = \frac{1}{2\mu_{LT}}, \quad s_5 = s_6 = -\frac{\nu_{LT}}{E_L}\end{aligned} \tag{I .21}$$

By using its inverse relation (I .17), the corresponding stiffness tensor writes:

$$\begin{aligned}&\mathbb{C} = \mathbb{S}^{-1} = c_1\,\mathbb{E}_1 + c_2\,\mathbb{E}_2 + c_3\,\mathbb{E}_3 + c_4\,\mathbb{E}_4 + c_5\,\mathbb{E}_5 + c_6\,\mathbb{E}_6 \\ &c_1 = 1/\left(\frac{1-\nu_T}{E_T} - \frac{2\nu_{LT}^2}{E_L}\right) \quad , \quad c_2 = E_L/\left(1 - \frac{2\nu_{LT}^2}{E_L}\frac{E_T}{1-\nu_T}\right) \\ &c_3 = \frac{E_T}{1+\nu_T}, \quad c_4 = 2G_{LT}, \quad c_5 = c_6 = \nu_{LT}/\left(\frac{1-\nu_T}{E_T} - \frac{2\nu_{LT}^2}{E_L}\right)\end{aligned} \tag{I .22}$$

In the particular case of transversely isotropic material with the symmetry axis $\underline{n} = \underline{e}_3$, the 5 elastic constants characterizing the transversely isotropic stiffness tensor $\mathbb{C}$ are given by:

$$\begin{aligned}&C_{1111} = C_{2222} = C_{11} \ , \quad C_{3333} = C_{33} \ , \quad C_{1212} = C_{66} \ , \\ &C_{1122} = C_{2211} = C_{12} \ , \quad C_{1133} = C_{3311} = C_{2233} = C_{3322} = C_{13} \ , \\ &C_{1313} = C_{2323} = C_{1331} = C_{2332} = C_{3113} = C_{3223} = C_{3131} = C_{3232} = C_{44}\end{aligned} \tag{I .23}$$

© 2016 Tous droits réservés.

doc.univ-lille1.fr

Thèse de Mei Qi, Lille 1, 2016

The compliance tensor $\mathbb{S}$ may be written:

$$
\begin{aligned}
&S_{1111} = S_{2222} = \frac{1}{E_1} \ , \quad S_{3333} = \frac{1}{E_3} \ , \quad S_{1122} = -\frac{\nu_{12}}{E_1} \ , \\
&S_{1133} = -\frac{\nu_{31}}{E_3} \ , \quad S_{1212} = \frac{1+\nu_{12}}{2\,E_1} \ , \quad S_{2323} = S_{3131} = \frac{1}{4\,G_{31}} \ , \\
&C_{11} = -\frac{1-\nu_{31}^2\frac{E_1}{E_3}}{(1+\nu_{12})\left(\frac{2\,\nu_{31}^2}{E_3}-\frac{1-\nu_{12}}{E_1}\right)} \ , \quad C_{33} = \frac{E_3\left(\frac{1-\nu_{12}}{E_1}\right)}{\frac{2\,\nu_{31}^2}{E_3}-\frac{1-\nu_{12}}{E_1}} \ , \\
&C_{12} = -\frac{\nu_{12}+\nu_{31}^2\frac{E_1}{E_3}}{(1+\nu_{12})\left(\frac{2\,\nu_{31}^2}{E_3}-\frac{1-\nu_{12}}{E_1}\right)} \ , \quad C_{13} = -\frac{\nu_{31}}{\frac{2\,\nu_{31}^2}{E_3}-\frac{1-\nu_{12}}{E_1}} \ , \\
&C_{44} = G_{31} \ , \quad C_{66} = \frac{C_{11}-C_{12}}{2} = \frac{E_1}{2\,(1+\nu_{12})}
\end{aligned}
\tag{I .24}
$$

with the correspondence notation (see relation I .22).

2.4 Isotropic materials

The property of isotropic materials is uniformly in all directions. It is the simplest case. An isotropic elastic stiffness tensor can be expressed in terms of the two fourth-order projection tensors $\mathbb{J}$ and $\mathbb{K}$.

$$
\mathbb{C} = 3\,k\,\mathbb{J} + 2\,\mu\,\mathbb{K} \tag{I .25}
$$

may be written as:

$$
\left[C^{IJ}\right] = \begin{pmatrix}
k+\frac{4\mu}{3} & k-\frac{2\mu}{3} & k-\frac{2\mu}{3} & 0 & 0 & 0 \\
k-\frac{2\mu}{3} & k+\frac{4\mu}{3} & k-\frac{2\mu}{3} & 0 & 0 & 0 \\
k-\frac{2\mu}{3} & k-\frac{2\mu}{3} & k+\frac{4\mu}{3} & 0 & 0 & 0 \\
0 & 0 & 0 & 2\mu & 0 & 0 \\
0 & 0 & 0 & 0 & 2\mu & 0 \\
0 & 0 & 0 & 0 & 0 & 2\mu
\end{pmatrix}
\tag{I .26}
$$

where $\mathbb{J}$ and $\mathbb{K}$ play the role of the eigentensors, and the shear and bulk moduli of the material, k_i and μ_i, are corresponding eigenvalues.

© 2016 Tous droits réservés.

doc.univ-lille1.fr

Thèse de Mei Qi, Lille 1, 2016

The compliance stiffness tensor can be obtained as follows:

$$\mathbb{S} = \frac{1}{3\,k}\,\mathbb{J} + \frac{1}{2\,\mu}\,\mathbb{K} \tag{I .27}$$

$$\left[S^{IJ}\right] = \begin{pmatrix} \frac{1}{9}\left(\frac{3}{\mu}+\frac{1}{k}\right) & \frac{1}{9k}-\frac{1}{6\mu} & \frac{1}{9k}-\frac{1}{6\mu} & 0 & 0 & 0 \\ \frac{1}{9k}-\frac{1}{6\mu} & \frac{1}{9}\left(\frac{3}{\mu}+\frac{1}{k}\right) & \frac{1}{9k}-\frac{1}{6\mu} & 0 & 0 & 0 \\ \frac{1}{9k}-\frac{1}{6\mu} & \frac{1}{9k}-\frac{1}{6\mu} & \frac{1}{9}\left(\frac{3}{\mu}+\frac{1}{k}\right) & 0 & 0 & 0 \\ 0 & 0 & 0 & \frac{1}{2\mu} & 0 & 0 \\ 0 & 0 & 0 & 0 & \frac{1}{2\mu} & 0 \\ 0 & 0 & 0 & 0 & 0 & \frac{1}{2\mu} \end{pmatrix} \tag{I .28}$$

3 Behaviour of initial anisotropic rocks

3.1 Some experimental data

During the last decades, a large number of experimental investigations have been performed to study influences of inherent anisotropic structure of materials on their mechanical behaviours. The first significant experimental studies of anisotropic materials were performed by Müller (1930), Lepper (1949), Priee (1958) and Hobbs (1960). These studies have essentially shown the existence of anisotropy of the moduli as well as the existence of anisotropy of resistance in the condition of compression with the sample tested parallel or perpendicular to the bedding planes.

In particular, many studies were focused on transversely isotropic rocks, for instance [Hoek, 1964, Chenevert and Gatlin, 1965, Attewell, 1974, Hobbs, 1964, Singh, 1973, Singh et al., 1973, NIANDOU, 1994, Nasseri et al., 2003, JALBOUT, 2005]. In order to characterize mechanical behaviours of such anisotropic materials, due to their material symmetry, it is generally proposed to compression tests on cylindrical samples which are cut with angle varying from 0° to 90° between the sample axis and bedding planes. The mechanical behaviours of transversely isotropic rocks can be characterized by the following features:

- The maximum mechanical strength is generally reached in the perpendicular direction of the bedding planes, hardly in the parallel direction of the bedding planes.

© 2016 Tous droits réservés.

doc.univ-lille1.fr

Thèse de Mei Qi, Lille 1, 2016

The minimum strength always appears between the angle 30° and 60° with the bedding planes. As an example, the results in figure I .3 for a schist rock ([Akai and Arioka, 1970]) show the evolution of compression failure strength as a function of the orientation of loading. The strength reaches an maximum value at the angles 0° and 90° and its minimum value is at 30°. The coefficient of anisotropy of schist is about 10. In Table (3.1), we show the loading angle for maximal strength as well as the anisotropy coefficient for different types of anisotropic rocks. A classification of rock anisotropy on the basis of these coefficients is proposed by [Singh et al., 1973] in Table 3.1.

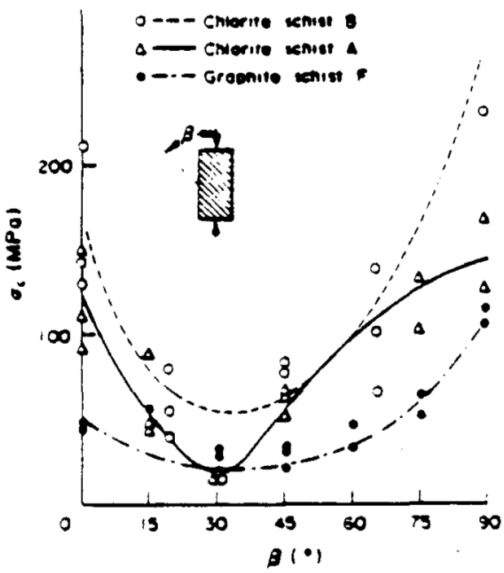

Figure I .3: Anisotropy of Schist strength under unixial compression ([Akai and Arioka, 1970])

- Under triaxial compression, the failure mechanisms and the behaviour of material depend on the orientation and the confining pressure, see figure I .4. Generally, the anisotropy of the failure strength as well as the anisotropy of the elastic modulus decrease by increasing the confining pressure. It means that the confining pressure permits to reduce effects of structure in the failure mechanisms. For example, in the case of the Green River shale I, the ratio between the minimum strength (corresponding $\theta = 30°$) and the maximum strength is equal to 0.63 for confining pressure 100psi; to 0.89 for 25000psi [McLAMORE and GRAY, 1967]. A similar variation

© 2016 Tous droits réservés.

doc.univ-lille1.fr

Thèse de Mei Qi, Lille 1, 2016

Nature of the rock	Angle θ for maximal strength	Coefficient of the anisotropy	Source
Martinsburg slate	90°	13.46	[Donath, 1964]
Fractured sandstone	90°	6.37	[Horino and Ellickson, 1970]
Barnsley Hard coal	90°	5.18	[POMEROY et al., 1971]
Penrhyn slate	90°	4.85	[Attewell, 1974]
South African slate	0°	3.68	[Hoek, 1964]
Texas slate	90°	3.00	[McLAMORE and GRAY, 1967]
Permian shale	90°	2.33	[Chenevert and Gatlin, 1965]
Green River shale I	0°	1.62	[McLAMORE and GRAY, 1967]
Green River shale II	0°	1.41	[McLAMORE and GRAY, 1967]
Green River shale	0°,90°	1.37	[Chenevert and Gatlin, 1965]
Kota sandstone	0°	1.12	[RAO et al., 1984]
Arkansas sandstone	0°	1.10	[Chenevert and Gatlin, 1965]
Quartizitic	90°	2.19	[Singh et al., 1973]
Carbonaceous	90°	2.19	
Micaceous	90°	6.00	

Table I .1: Strength anisotropy of different rocks

is observed by [Donath, 1964] for Martinsburg slate. Meanwhile, it is necessary to note that [ALLIROTE and BOEHLER, 1970] on diatomite of Andance mountain (in France), to conclude that anisotropy of strength, also anisotropy of elastic modulus, increase with the confining pressure, see figure I .5.

© 2016 Tous droits réservés.

doc.univ-lille1.fr

Thèse de Mei Qi, Lille 1, 2016

Anisotropic ratio	Class	Type of rock
$1.0 - 1.1$	isotropic	Sandstone
$> 1.1 - 2.0$	slightly anisotropic	Sandstone, Argillite
$> 2.0 - 4.0$	Anisotropic	Argillite, Slate, Phyllite
$> 4.0 - 6.0$	Strongly anisotropic	Slate, Phyllite
> 6.0	Very strongly anisotropic	Slate, Phyllite

Table I .2: Classification of inherent anisotropy of rocks

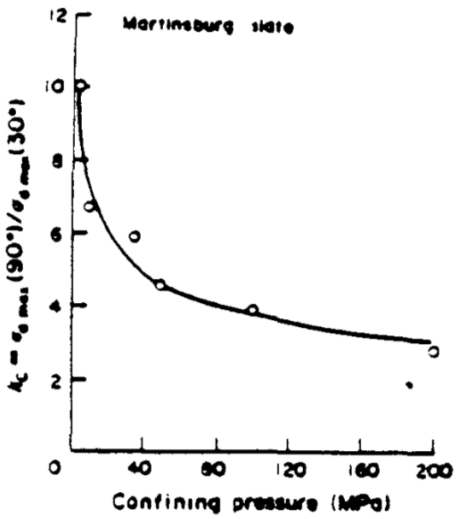

Figure I .4: Coefficient of anisotropy of strength under compression of Martinsburg slate in function of the confining pressure [KWASNIEWSKI, 1993, Donath, 1964]

- The increasing rate of failure strength of a sedimentary rock by increasing of the confining pressure is often smaller for the angle θ between 30° and 45° and reaches its maximal value at 0°, see figure I .6.
- Several failure mode are observed. The failure occurs in two principle modes: extension and shearing. Generally, the fracture angle strongly depends on the loading orientation as well as confining pressure. For loading orientations $0° \leqslant \theta \leqslant 15°$, the failure takes place by extension of the bedding plane for low confining pressure and

© 2016 Tous droits réservés.

doc.univ-lille1.fr

Thèse de Mei Qi, Lille 1, 2016

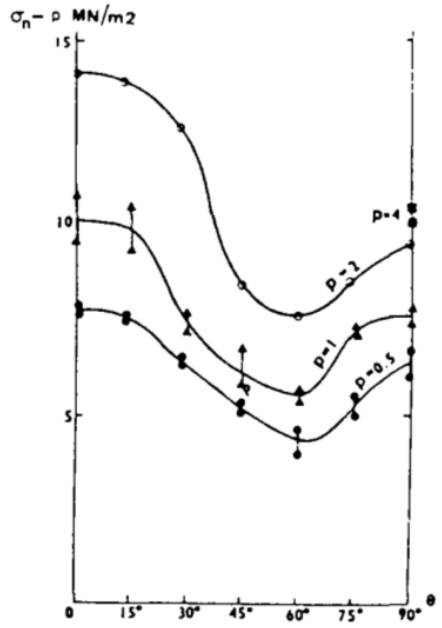

Figure I .5: Evolution of anisotropy of yield strength with the confining pressure ([ALLIROTE and BOEHLER, 1970])

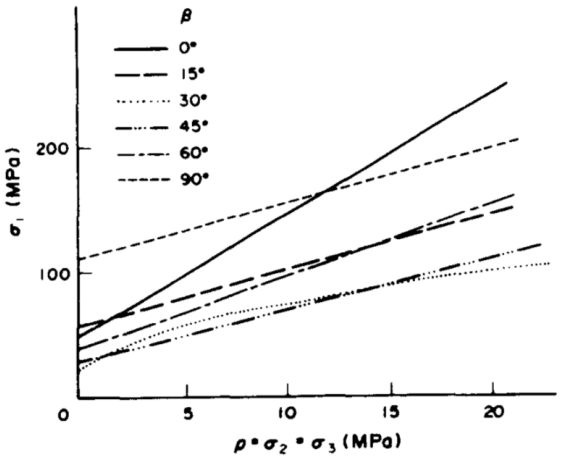

Figure I .6: The increasing rate of strength of a Schist: the maximum principal stress as a function of the confining pressure with different angles θ [Akai and Arioka, 1970]

© 2016 Tous droits réservés.

doc.univ-lille1.fr

Thèse de Mei Qi, Lille 1, 2016

shear band for high confining pressure. For loading orientations $15° \leqslant \theta \leqslant 60°$, the failure generally takes place because of the sliding of bedding planes and the fracture orientation is nearly equal to θ. When the confining pressure is high, shear band by strain localisation can occur and the fracture may cross bedding planes, see figure I .8 and I .7.

- The anisotropy of the modulus are generally more important than anisotropy of failure strength.

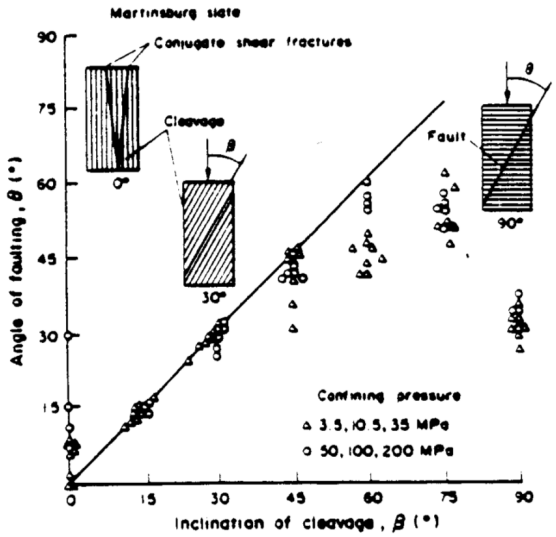

Figure I .7: Angle and failure mode of Martinsburg slate following the main principal stress ([Donath, 1964])

3.2 Determination of elastic parameters

Most experimental studies on elastic behaviour of anisotropic rocks show the variation of the elastic modulus as a function of the state of stress [Muller, 1930, McLAMORE and GRAY, 1967, ALLIROTE and BOEHLER, 1970, NIANDOU, 1994].

Given that we are often interested in elastic constants of orthotropic or transversely isotropic rocks, a question that often proposes in practice is, "what are the possible variation of the elastic constants of these areas?" [Amadei et al., 1987] based on the experimental data conclude as following:

- For most of the rock that we studied, the ratio $\frac{E_2 E_3{}^{\frac{1}{2}}}{E_1}$ and $\frac{E_2}{E_1}$ are above 1, indicating

© 2016 Tous droits réservés.

doc.univ-lille1.fr

Thèse de Mei Qi, Lille 1, 2016

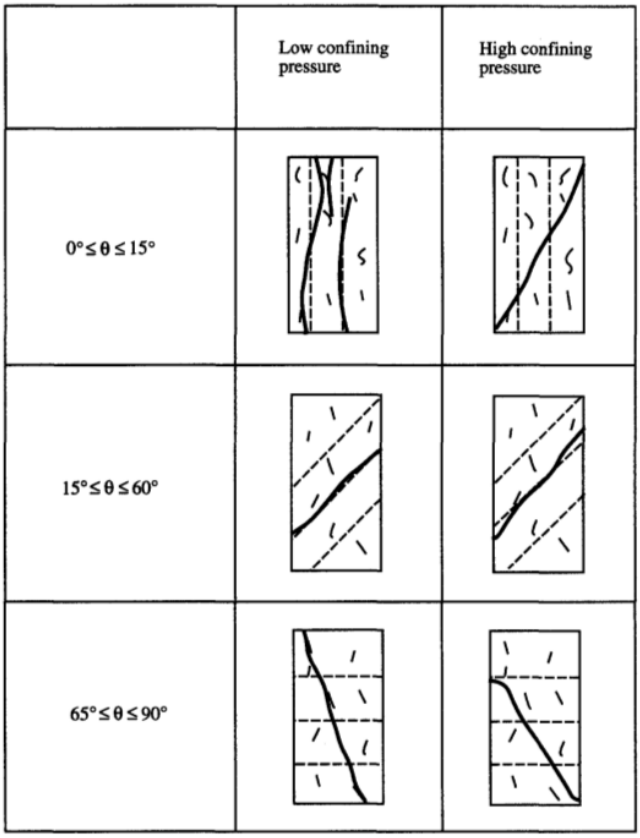

Figure I .8: Main failure modes of Tournemire shale [NIANDOU, 1994]

lower rigidities in the direction normal to the plane major anisotropy $\underline{e}_2 - \underline{e}_3$. However, these ratios seem to be lower than 3. Several cases in which the two previous ratios are below 1 by several articles, and above 0.70.

- All of Poisson's ratio are positive and the value are below 0.5. Most of the value of ν_{23} are in the domain $(0.1 - 0.35)$ and $(\nu_{21}\nu_{31})^{\frac{1}{2}}$ varies in the domain $(0.1 - 0.7)$.

- Several points of experimental data do not diverge a lot from the isotropic case, for which $\frac{E_2}{E_1}$, $\frac{G_{23}}{G_{12}}$, $\frac{\nu_{21}}{\nu_{23}}$ are equal to unity.

Now, we choice a typical shale (Tournemire shale) as an example to present the evolution of the elastic parameters. The Tournemire shale can be initially considered as a transversely isotropic material according to the experimental data which is proposed by [Homand et al., 1993]. We proposed that $\underline{e}_3$ the axis normal to bedding planes which are defined in the isotropic plane $\underline{e}_1\underline{e}_2$, see Fig. I .10. We are 5 elastic parameters (E_1, E_3,

© 2016 Tous droits réservés.

doc.univ-lille1.fr

Thèse de Mei Qi, Lille 1, 2016

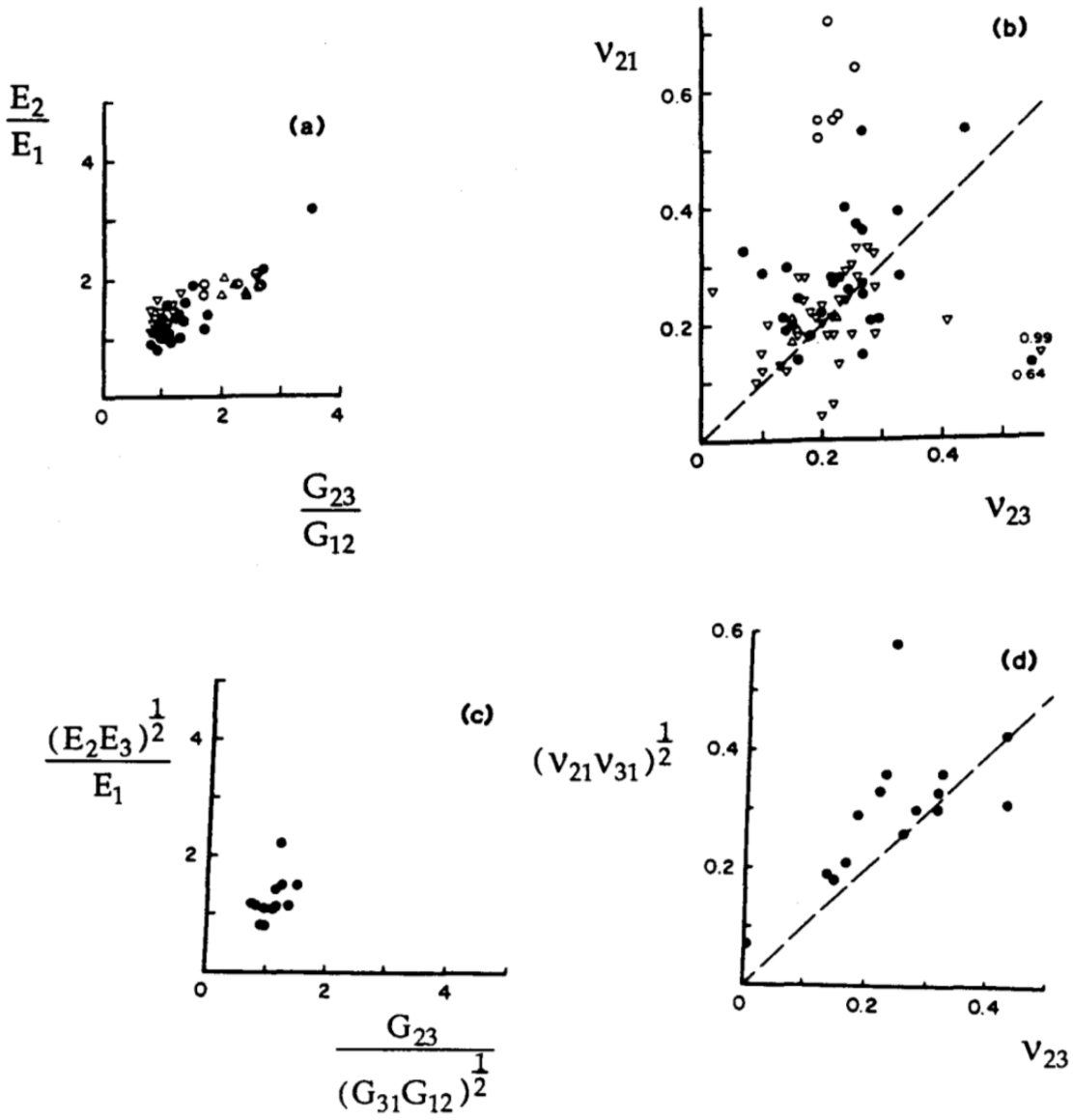

Figure I .9: Elastic parameters for different anisotropic rocks: (a) and (b) transversely isotropic, (c) and (d) orthotropic [Amadei et al., 1987]

ν_{12}, ν_{31}, G_{31}) to take into account in order to characterizer this material.

Initially anisotropic cracked media

© 2016 Tous droits réservés.

doc.univ-lille1.fr

Thèse de Mei Qi, Lille 1, 2016

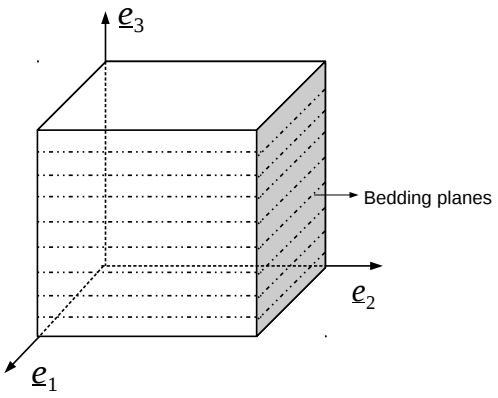

Figure I .10: Definition of structural axes

3.2.1 Evolution of Young's moduli (E_T and E_L)

There are two experimental methods to determine the evolution of principle Young's moduli:

- Generally, the elastic constant can be determined from material responses during unloading paths. Two Young's moduli E_T and E_L corresponding two structural directions $\underline{e}_1$ (or $\underline{e}_2$) and $\underline{e}_3$ can be obtained from tests performed in parallel and perpendicular with the bedding plane respectively.

  [NIANDOU, 1994] presented triaxial compression test including unloading-reloading cycles to determine Young's modulus as shown in Fig. I .11 and I .12. The important hysteresis buckles were obtained in the Fig. I .11, so it is difficult to determine the slope of the unloading or reloading curves. It means that it will have big error to determine the elastic constant with the slope in Fig.I .11. In order to avoid hysteresis buckles, a short relaxation phase was included before each unloading cycle. In the Fig.I .12, unloading and reloading curves were nearly the same with a short relaxation phase. The Young's modulus can be determined by measuring the slope of unloading and reloading curves.

- According to the various experimental data on the Tournemire shale, it conclude that the initial elastic parameters generally depend on the confining pressure, see Fig.I .13 by [NIANDOU, 1994].

  We can note that the Young's modulus E_L is strongly influence by confining pressure. That is because the confining pressure tightens the bedding planes and the material

© 2016 Tous droits réservés.

doc.univ-lille1.fr

Thèse de Mei Qi, Lille 1, 2016

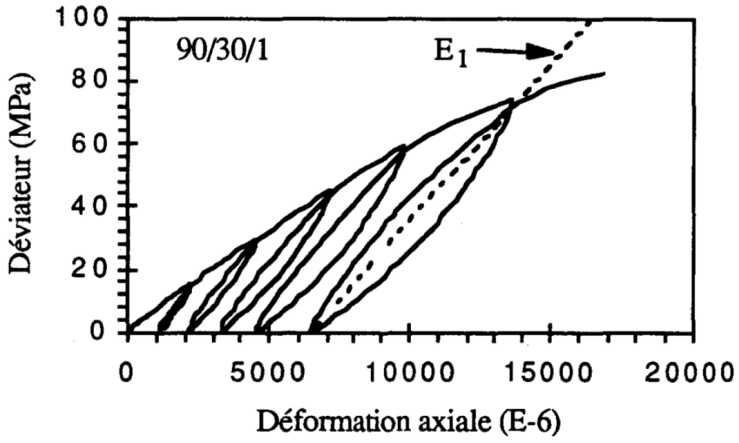

Figure I .11: Stress-strain curves including unloading cycles during triaxial test without relaxation phase.

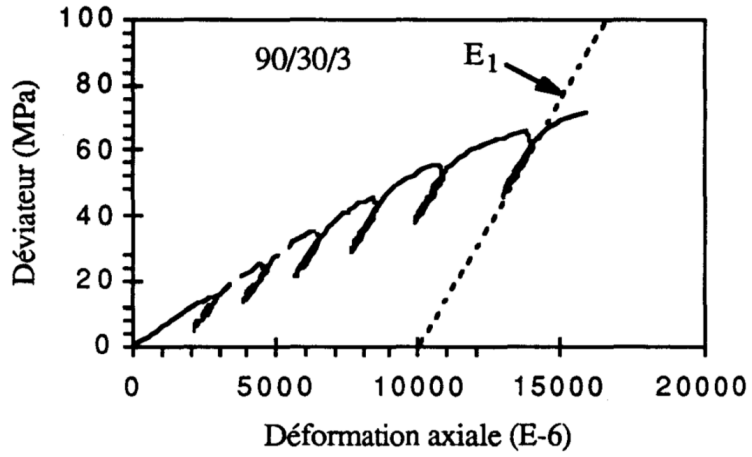

Figure I .12: Stress-strain curves including unloading cycles during triaxial test with relaxation phase.

becomes more stiff.

As a function of confining pressure, most commonly used the empirical laws of evolution of Young's modulus [Santarelli, 1987]:

$$E_L = E_0(1 + \frac{\sigma_3}{P_a})^m \qquad \text{(I .29)}$$

which σ is the confining pressure and P_a is a reference pressure equal to the atmo-

© 2016 Tous droits réservés.

doc.univ-lille1.fr

Thèse de Mei Qi, Lille 1, 2016

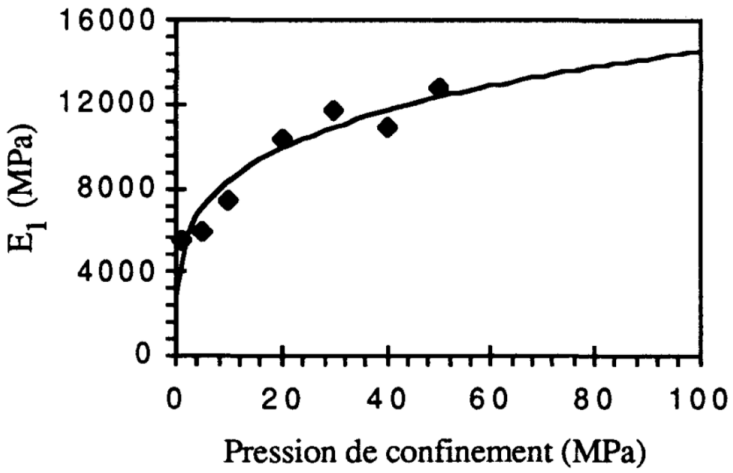

Figure I .13: Variation of the elastic modulus E_L as a function of confining pressure: comparison between experimental and theoretical values [NIANDOU, 1994].

spheric pressure. And E_0 is the value of Young's modulus for zero confining pressure. And

$$E_L = E_0(1 + a(\frac{\sigma_3}{P_a})^m) \tag{I .30}$$

for which E_0, m and a are three parameter to determine.

For the values of Young's modulus E_T, [NIANDOU, 1994] shows it can be determined by average values of the experimental data with different confining pressures.

3.2.2 Evolution of Poisson's ratios (ν_T and ν_{TL}, ν_{LT})

All of Poisson's ratios correspond to the ratio of two elastic strains. The strain will take place from the loading-unloading cycles.

- Evolution of Poisson's ratio ν_{LT}

The Poisson's ratio ν_{LT} is equal to ratio of the variation of longitudinal strain ε_L and transversal strain ε_T for a variation stress, Fig. I .14.

[NIANDOU, 1994] show that ν_{LT} depend on the confining pressure σ and the deviatoric stress $q = \sigma_3 - \sigma_1$. An empirical laws of evolution of Poisson's ratio ν_{LT} is proposed:

$$\nu_{LT} = \nu_i(\sigma_3)\exp(\alpha(\sigma_3)\frac{q}{P_a}) \tag{I .31}$$

© 2016 Tous droits réservés.

doc.univ-lille1.fr

Thèse de Mei Qi, Lille 1, 2016

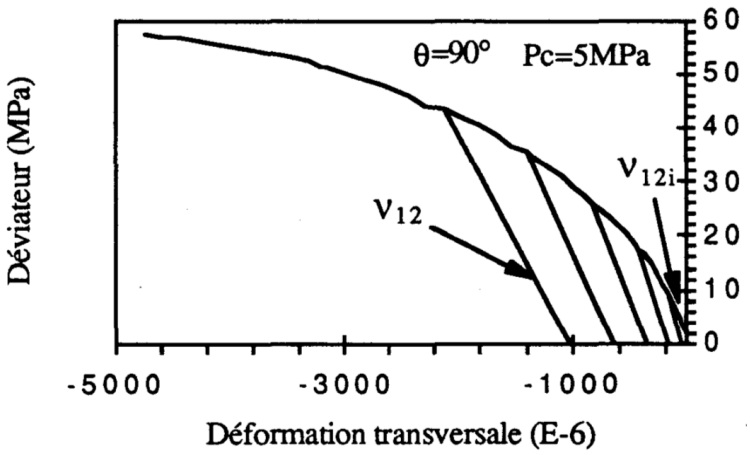

Figure I .14: Scheme of identification of the Poisson's ratio ν_{LT} [NIANDOU, 1994]

where $\nu_i(\sigma_3)$ present the elastic ratio at the initial slope of the curves of the conventional triaxial test. P_a is the atmospheric pressure and $\alpha(\sigma_3)$ is model parameter which can be determined by experimental data.

- Evolution of Poisson's ratio ν_L and ν_{TL}

The experimental data [NIANDOU, 1994] shows that the confining pressure do not have enough influence on Poisson's ratio ν_L and ν_{TL}. Consequently, the value of Poisson's ratio ν_L and ν_{TL} takes the average value of the several experimental data.

3.2.3 Evolution of longitudinal shear modulus (G_L)

Longitudinal shear modulus G_L can not be directly measure by the shear test because of fragility of samples. The dynamic test have been performed by Cuxac (1991) for characterize dynamic elastic moduli. The static shear modulus can be determine from a triaxial test on a inclined 45° specimen.

$$G_L = \frac{\sigma_3}{2(\varepsilon_3 - \varepsilon_{1p})} \tag{I .32}$$

where ε_3 is the longitudinal strain and ε_{1p} is the transversal strain. But [NIANDOU, 1994] note an important experimental dispersion which is related to the difficulties of measuring ε_{1p}.

© 2016 Tous droits réservés. doc.univ-lille1.fr

Thèse de Mei Qi, Lille 1, 2016

So many studies try to express the shear modulus as a function of the other elastic parameters (Wolf, 1944; Carrier, 1946; Tan-Tjong-Kie, 1941; Barden, 1963; Wiendieck, 1964; Zienkiewicz, 1972; Garnier, 1973), see [NIANDOU, 1994].

By making a transformation of the coordinate system, one of the relation is obtained theoretically:

$$\frac{1}{E_0} = \frac{sin^4\theta}{E_L} + (\frac{1}{G_L} - 2\frac{\nu_{LT}}{E_L})sin^2\theta cos^2\theta + \frac{cos^4\theta}{E_T} \qquad \text{(I .33)}$$

where E_0 is the axial Young modulus which is determined form a test performed in the θ orientation. Thus, the shear modulus can be easily obtained from this equation.

3.3 Failure criteria

Different kinds of criteria have been proposed to take into account for the directional character of failure strength of anisotropic rocks. Generally, they are divided into two groups: Discontinuous models and continuous models. The continuous models follow the continuous variation of the mechanical strength of material with loading orientation. The discontinuous models consider that the material is interrupted by oriented discontinuity surfaces such as cracks or inclusions. Among the discontinuous models, the first attempt seems to be Jaeger's single weakness plane theory [Jaeger, 1960] and more recently [Hoek and Brown, 1980]. The continuous models can be further divided into two sub-groups: the one ignoring the intermediate principal stress and the one taking into account it. For the first sub-group, several anisotropic criteria have been proposed by [Jaeger, 1960, McClintock and Walsh, 1962, Welsh and Brace, 1964, McLAMORE and GRAY, 1967, Hoek, 1964, Bieniawski, 1967, Hoek and Brown, 1980]. These empirical criteria are simple in their formulation and very practical for use but require a lot of experimental data for their calibration. Some criteria have been formulated in three dimensional stress space, for instance [Pariseau, 1972, Boehler and Sawczuk, 1977, Boehler and Sawczuk, 1980, Dafalias, 1979, Dafalias, 1982, Boehler and Sawczuk, 1986].

3.3.1 Jaeger's single weakness plane theory

[Jaeger, 1960] has proposed an extension of Mohr-Coulomb criterion to anisotropic rocks. Consider a rock sample which presents a direction of plane anisotropy, with an inclination angle Ψ, related to the direction of major principal stress σ_1 at a state of compressive stresses (σ_1, σ_3), Fig. I .15(a). On any weakness plane of failure angle (or fracture angle) α relative to the direction of σ_1 (Fig. I .15(b)), the shear strength is given by following expression:

© 2016 Tous droits réservés.

doc.univ-lille1.fr

Thèse de Mei Qi, Lille 1, 2016

$$\tau = c_\alpha + \sigma_n tan\phi \tag{I .34}$$

where c_α and ϕ are respectively the cohesion of rock and the frictional angle to the failure plane.

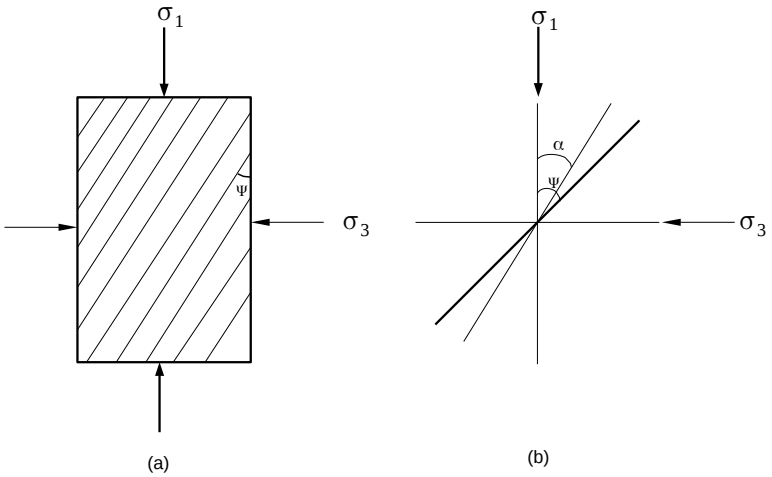

Figure I .15: Jaeger's theory

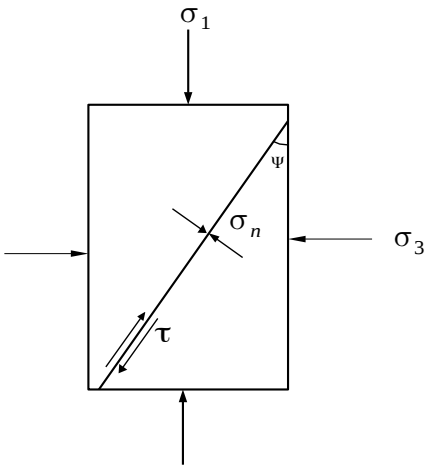

Figure I .16: Schematic diagram defining stress orientations along and across a plane.

© 2016 Tous droits réservés.

doc.univ-lille1.fr

Thèse de Mei Qi, Lille 1, 2016

The shear stress and normal stress applied to the failure plane in Fig. I .16 can be expressed in terms of principal stresses using Mohr's circle method:

$$2\tau = (\sigma_1 - \sigma_3)sin(2\alpha) = (\sigma_1 - \sigma_3)cos(\phi) \tag{I .35}$$

$$2\sigma_n = (\sigma_1 + \sigma_3) - (\sigma_1 - \sigma_3)cos(2\alpha) = (\sigma_1 + \sigma_3) - (\sigma_1 - \sigma_3)sin(\phi) \tag{I .36}$$

Substituting I .35 and I .36 for I .34, one gets:

$$(\sigma_1 - \sigma_3)_r = \frac{2(c_\alpha + \sigma_3 tan\phi)}{\sqrt{tan^2\phi + 1} - tan\phi} \tag{I .37}$$

It is worthy to note that the friction angle and fracture angle have a relation $\alpha = \frac{\pi}{4} \pm \frac{\phi}{2}$ for isotropic materials. But for anisotropic materials, such a relation does not exist any more. The cohesion c_α is not constant, it varies depending on the angle of anisotropic plane inclination:

$$c_\alpha = A - Bcos2(\alpha - \Psi) \tag{I .38}$$

A and B are two parameters which can be determined by experimental data.

3.3.2 Jaeger's criterion modified by McLamore and Gray

The McLamore and Gray's criterion [McLAMORE and GRAY, 1967] is obtained from a modification of Jaeger's criterion [Jaeger, 1960]. This criterion describes the shear strength of anisotropic rocks with a continuous variation of cohesion c_Ψ and friction angle $tan\phi_\Psi$ with the orientation Ψ of the bedding plane. The following empirical relations have been introduced:

$$c_\Psi = A - B[cos2(\Psi_{min,c} - \Psi)]^n \tag{I .39}$$

$$tan\phi_\Psi = C - D[cos2(\Psi_{min,\phi} - \Psi)]^m \tag{I .40}$$

where A, B, C, D, m, n are model parameters which should be determined from experimental tests. Ψ is defined in Fig. I .15. $\Psi_{min,c}$ and $\Psi_{min,\phi}$ are the values of Ψ corresponding to the minimum value of c_Ψ and $\tan\phi_\Psi$ respectively. For example, in Fig. I .18, $\Psi_{min,c} = \Psi_{min,\Psi} = 30°$. The power index n is an anisotropic factor. The authors proposed to take $n = 1$ or $n = 3$ for the rocks to bedding plane and $n = 5$ or $n = 6$ for the rocks to linear anisotropy. Figure I .17 presents several n for the variation of cohesion.

© 2016 Tous droits réservés.

doc.univ-lille1.fr

Thèse de Mei Qi, Lille 1, 2016

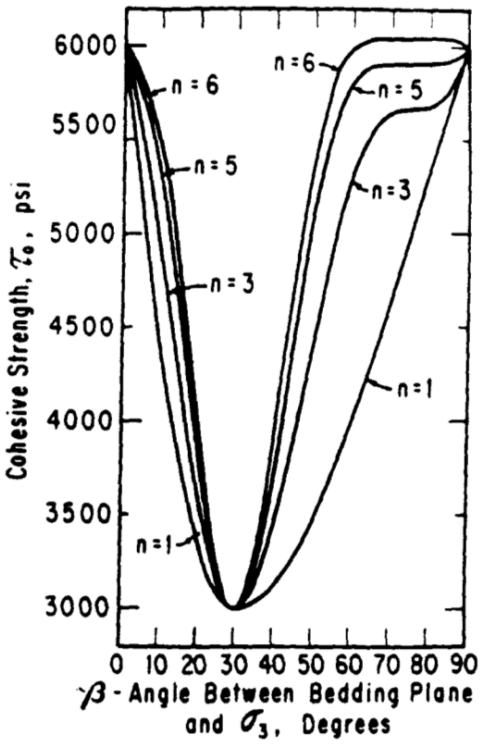

Figure I .17: Evolution of the cohesion as a function of the orientation for different value of n [McLAMORE and GRAY, 1967]

© 2016 Tous droits réservés.

doc.univ-lille1.fr

Thèse de Mei Qi, Lille 1, 2016

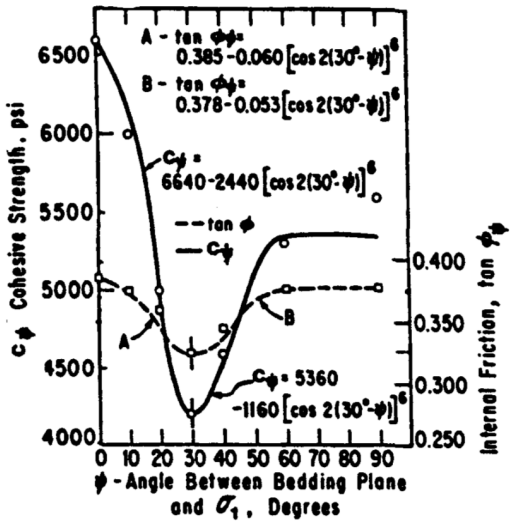

Figure I .18: Failure deviatoric stress as a function of confining pressure [McLAMORE and GRAY, 1967]

4 Induced anisotropy in rocks

This section is dedicated to describe macroscopic mechanical behaviours of anisotropic rocks, which exhibit an induced anisotropy due to oriented growth of micro-cracks. The mechanical behaviour of many rocks is mainly characterized by anisotropic degradation of elastic properties and inelastic strains. This degradation of elastic properties is mainly due to the nucleation and growth of micro-cracks while the inelastic deformation is related to the frictional sliding along micro-cracks. The macroscopic failure is generally induced by the coalescence of micro-cracks. Further, other physical properties of materials such as permeability are also affected by induced micro-cracks.

4.1 Effect of micro-cracks on macroscopic behaviour of rocks

Macroscopic behaviours of rock-like materials are closely related to their microstructure evolutions. Many works have been dedicated to the characterization of micro-cracks in quasi-brittle materials (rocks, concrete, etc) and effects of micro-cracks on macroscopic mechanical properties. The first reference experimental study was proposed by [Bieniawski, 1967], which allowed to establish relationships between different stages of macroscopic behaviour of rocks and evolution states of micro-cracks in uniaxial compression. Optical microscope investigations of micro-cracks have been presented by [Peng and Johnson,

© 2016 Tous droits réservés.

doc.univ-lille1.fr

Thèse de Mei Qi, Lille 1, 2016

1972], and finer solutions have been obtained by [Tapponier and Brace, 1976, paterson, 1982], thanks to the Scanning Electron Microscope investigations. A quite comprehensive review on micro-crack evolutions in quasi-brittle rocks was given by [Paterson, 1978].

Physical mechanisms of nucleation and propagation of micro-cracks have been investigated by a number of previous experimental investigations, for instance [Hori and Nemat-Nasser, 1983, Hori and Nemat-Nasser, 1985, Brace and Bombolakis, 1963, Steif, 1984, paterson, 1982]. Three essential crack propagation modes have generally been identified: (1) purely tensile propagation, corresponding to the mode I in Fracture Mechanics and leading to the separation of materials particles in crack plane; (2) tensile–shear mode, in which both the tensile loading and shear loading contribute to the growth of crack size, (3) compression-shear mixed mode associated with the breaking of internal bands by facial sliding, which generally occurs under compression-dominated loading paths. In the present work, the emphasis is put on mechanical behaviours of rock-like materials under some conventional laboratory tests (uniaxial tension test, uniaxial and triaxial compression test).

- The mechanical behaviour of rock-like materials in tension presents a very fragile character. One can observe softening and failure behaviours in the level of relatively moderate strain.

- The mechanical behaviour of rock-like materials in uniaxial or triaxial compression test presents different stages during loading and reloading state that they connects with the micro-cracks state [Bieniawski, 1967, Paterson, 1978, Pensee et al., 2002b]:

  In Fig. I .19, at the beginning of loading process, the closure of pre-existing cracks is observed in a very low stress level. Then, the material shows a linear stress-strain relationship, but this straight line is soon interrupted as a consequence of pre-existing cracks or new micro-cracking. The final stage of the mechanical behaviour, which occurs around the peak stress, corresponds to the coalescence of micro-cracks and to the macroscopic fracture.

  A progressive degradation of elastic stiffness can be seen from the slopes of successive unloading-reloading cycles. In practice, the loading-unloading cycles make it possible to evaluate current elastic stiffness in axial and lateral directions. This degradation of elastic properties is the consequence of nucleation and growth of oriented micro-cracks. Furthermore, irreversible strains can also be observed during unloading paths and such strains are generally due to frictional sliding along micro-cracks surfaces in

© 2016 Tous droits réservés.

doc.univ-lille1.fr

Thèse de Mei Qi, Lille 1, 2016

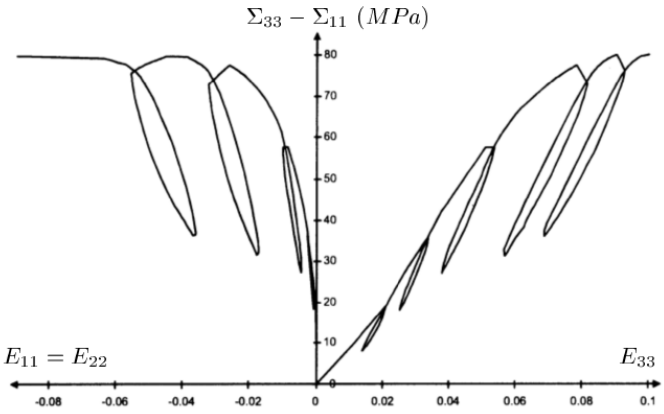

Figure I .19: Example of the stress-strain curves in a triaxial compression test with unloading-reloading cycles on claystone (with confining pressure $10MPa$) [Khazraei, 1995], LML.

rocks.

4.2 Some examples on the characterization of induced damage

In this subsection, we show some experimental results on the quantitative characterization of induced damage in rock materials, such as anisotropic spatial orientation of micro-cracks. Among many experimental studies devoted to this feature, we just mention here some representative ones for instance [Zhao, 1998, Homand et al., 2000, paterson, 1982].

Most of studies related to the evolution of induced micro-cracks have been made under compression condition. It has been found that the propagation of micro-cracks is preferentially observed in a direction close to the loading direction. In connection with this anisotropy of micro-crack, a question is proposed that it exist two types of micro-cracks (open crack and closed crack) during loading path. For example, [Homand et al., 2000] showed that the propagation of micro-cracks is oriented and generally preferred in some directions, which means that the induced damage of material is inherently anisotropic in nature. Fig. I .20 shows that with the augmentation of the deviatoric stress, the propagation of the crack density shows an anisotropic behaviour.

The other important point is to characterize the nucleation of new micro-cracks. [Zhao, 1998] combines SEM observations and quantitative stereological techniques, and observed variations of accumulated crack length with the direction according to the axis of loading

© 2016 Tous droits réservés.

doc.univ-lille1.fr

Thèse de Mei Qi, Lille 1, 2016

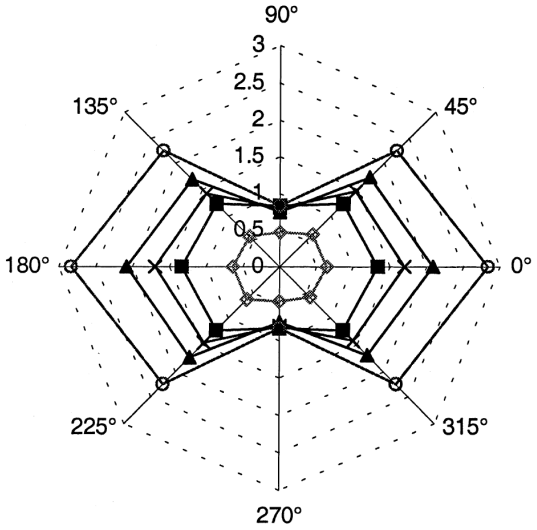

Figure I .20: Variation of cracks density as a function of the orientation under different diviatoric stress.

stress. In Fig. I .21, the values of normalized stress relative to the strength under compression ($\frac{\Sigma_{33}}{\Sigma_c}$) are shown for each case. These results indicate a relatively distribution in orientation, clearly show the existence of micro-cracks whose direction does not coincide with the loading direction.

5 Conclusion

In this chapter, we have presented a short review on mechanical behaviour of anisotropic rocks. It is found that many rocks exhibit an initial structural anisotropy due to the formation process and material heterogeneities. Both elastic and failure properties depend on loading orientation with respect to the material symmetries. Further, during subsequent loading, an induced anisotropy can be produced due to the nucleation and propagation of micro-cracks. There are interactions between the induced micro-cracks and initial material anisotropy. In the next Chapters, the objective will be the development of a micro-mechanical approach for modeling induced damage and friction in initially anisotropic rock-like materials. The micro-mechanical approach will be based on a Eshelby solution based linear homogenization procedure. Both open and closed micro-cracks will be considered. However, in the present work, the study will be limited to a class of transversely isotropic materials, such as shale, slate, schist etc.

© 2016 Tous droits réservés.

doc.univ-lille1.fr

Thèse de Mei Qi, Lille 1, 2016

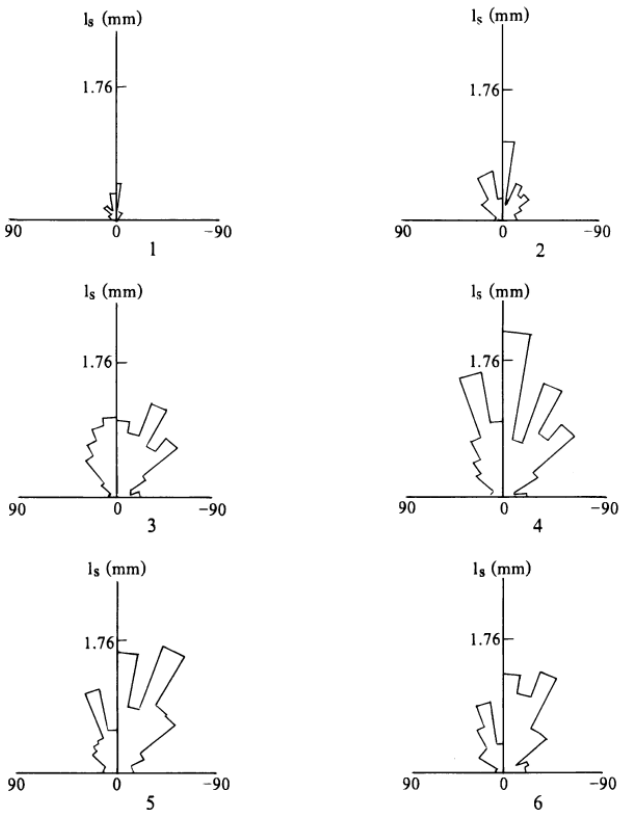

Figure I .21: Rose diagrams showing the variation of summarized crack length at different levels of the stress which is normalized with strength under unixial compression [Zhao, 1998]: a) $\Sigma_{33} = 0.59\Sigma_c$, b) $\Sigma_{33} = 0.73\Sigma_c$, c) $\Sigma_{33} = 0.88\Sigma_c$, d) $\Sigma_{33} = 0.96\Sigma_c$, e) $\Sigma_{33} = \Sigma_c$, f) unloaded.

© 2016 Tous droits réservés.

doc.univ-lille1.fr

Thèse de Mei Qi, Lille 1, 2016

© 2016 Tous droits réservés.

doc.univ-lille1.fr

Chapter II

Some fundamentals for damage modelling of anisotropic materials

Contents

1 Introduction 33

2 Basic homogenization schemes of cracked materials 34

2.1 Description of a crack-matrix system 34

2.2 Effective elastic property of cracked materials 35

2.3 Dilute scheme 38

2.4 Mori-Tanaka scheme estimations 40

2.5 PCW scheme estimations 42

3 Eshelby problem 43

3.1 Eshelby's equivalent eigenstrain method 43

3.2 Green's function for Eshelby's problem 45

3.3 Hill tensor for arbitrarily oriented spheroidal inclusion in a transversely isotropic matrix 46

4 Conclusion 60

1 Introduction

As mentioned in chapter I , most rock-like materials are subjected to oriented nucleation and propagation of micro-cracks leading to anisotropic damage of materials. The induced damage effects not only mechanical but also transport properties of rock-like materials. In the present work, we propose to develop a micro-mechanical approach for the

© 2016 Tous droits réservés.

doc.univ-lille1.fr

Thèse de Mei Qi, Lille 1, 2016

description of induced damage in both initially isotropic and anisotropic materials. This approach will be based on the reference solution of Eshelby for inclusion problems [Eshelby, 1957]. Induced micro-cracks will be seen as spheroidal inclusions embedded in a solid matrix. The effective elastic properties of cracked materials will be determined using linear homogenization procedures which is combined with a irreversible thermodynamics framework for the description of damage evolution.

In this Chapter, we shall first present some theoretical backgrounds of the linear homogenization method to be used for the estimation of effective elastic properties of damaged materials, in particular some basic bounds and different homogenization schemes. Then, the emphasis will be put on the calculation of Hill's tensor for spheroidal oblate micro-cracks embedded in a transversely isotropic elastic matrix.

2 Basic homogenization schemes of cracked materials

In this section, we will recall the background of homogenization methods to estimate the effective elastic properties of random heterogeneous materials. The objective of homogenization method is to replace the heterogeneous composite material by an equivalent homogeneous one that has the same mechanical behaviours at the macroscopic level. These homogenization schemes will be used in the formulation of a damage model in Chapter IV and of a friction- damage model in Chapter V for rock-like materials.

2.1 Description of a crack-matrix system

The determination of effective properties of a heterogeneous material through a homogenization procedure is generally carried out on a representative element volume (REV), which occupies the geometric domain Ω and is limited by its external boundary surface $\partial\Omega$. In this work, the cracked material will be represented by a crack-matrix system. We consider an anisotropic elastic solid matrix which is weakened by a family of parallel penny shaped micro-cracks, as shown in Figure II .1. In such a representation, each family of micro-cracks is seen as a phase of inclusions embedded in the matrix phase. The cracked material is a two-phase composite with a crack-matrix system.

For the sake of simplicity but without loosing the generality, we assume that the solid matrix is characterized by an initially transversely isotropic elastic behaviour. We denote the elastic stiffness tensor of the transversely isotropic matrix with by $\mathbb{C}_s$ and that of the family of micro-cracks by $\mathbb{C}_{f,r}$. The elastic stiffness tensor of the solid matrix depends on five independent constants and its matrix notation is given in Chapter I .

© 2016 Tous droits réservés.

doc.univ-lille1.fr

Thèse de Mei Qi, Lille 1, 2016

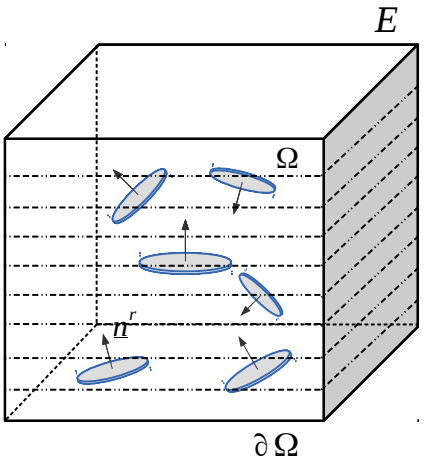

Figure II .1: Representative elementary volume (REV) of microcracked solids

On the other hand, we assume all of the micro-cracks to be penny-shaped and from geometrical point of view, each can be modelled by oblate ellipsoid with rotational symmetry around the minor axis. The orientation of each family r of micro-cracks ($r = 1$ to $\mathcal{N}$) is characterized by its normal unit vector denoted by $\underline{n}^r$, radius a and half opening c. The aspect ratio $\epsilon = c/a$ is $\ll 1$ of such penny cracks (Figure II .2).

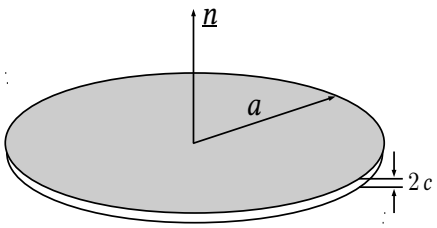

Figure II .2: Schematic representation of a penny-shaped crack

2.2 Effective elastic property of cracked materials

In order to determine the effective elastic property of the above described REV, suitable boundary conditions should be prescribed on the external boundary $\partial\Omega$. In conventional homogenization process [Ponte-Castaneda and Willis, 1995], we can adopt either

© 2016 Tous droits réservés.

doc.univ-lille1.fr

Thèse de Mei Qi, Lille 1, 2016

the uniform stress boundary condition or the uniform strain boundary condition.

a) The uniform stress boundary condition: represents the case of a REV subjected to a constant stress tensor. Let $\boldsymbol{\Sigma}$ be a constant (static) uniform stress field prescribed on $\partial\Omega$, which generates a surface force $\underline{F} = \boldsymbol{\Sigma} \cdot \underline{n}(\underline{z}), \forall \underline{z} \in \partial\Omega$. At the microscopic scale, the local stress field $\boldsymbol{\sigma}$ satisfies the following condition:

$$\boldsymbol{\sigma}(\underline{z}) \cdot \underline{n}(\underline{z}) = \boldsymbol{\Sigma} \cdot \underline{n}(\underline{z}) \qquad (\forall \underline{z} \in \partial\Omega) \tag{II .1}$$

It can be proven that $\boldsymbol{\Sigma}$ is equivalent to the volume average of the local stress $\boldsymbol{\sigma}$ in the REV for any equilibrated, which obeys:

$$\langle \boldsymbol{\sigma} \rangle_\Omega = \boldsymbol{\Sigma} \tag{II .2}$$

where $\langle \cdot \rangle_\Omega$ denotes the volumetric averaging over the domain Ω.

In this case, the average stress is given by:

$$\langle \boldsymbol{\sigma} \rangle := \frac{1}{\mid V \mid} \int_V \boldsymbol{\sigma}(\underline{z}) dz \tag{II .3}$$

b) The uniform strain boundary condition: represents the case of a REV subjected to a regular displacement condition at its boundary. Let $\boldsymbol{E}$ be the macroscopic uniform strain field on the boundary $\partial\Omega$. Correspondingly, the displacement boundary condition reads:

$$\underline{\xi}(\underline{z}) = \boldsymbol{E} \cdot \underline{z} \qquad (\forall \underline{z} \in \partial\Omega) \tag{II .4}$$

whereas $\underline{z}$ and $\underline{\xi}$ are denoted the position vector in the REV and the microscopic displacement.

It also implies the relationship between the average of local strain field $\boldsymbol{\varepsilon}$ in the REV and the macroscopic strain $\boldsymbol{E}$ as:

$$\langle \boldsymbol{\varepsilon} \rangle_\Omega = \boldsymbol{E} \tag{II .5}$$

In this case, the average strain is given by:

$$\langle \boldsymbol{\varepsilon} \rangle := \frac{1}{\mid V \mid} \int_V \boldsymbol{\varepsilon}(\underline{z}) dz \tag{II .6}$$

© 2016 Tous droits réservés.

doc.univ-lille1.fr

Thèse de Mei Qi, Lille 1, 2016

By adopting the uniform strain boundary condition, the crucial step of homogenization method consists in finding a fourth-order localization tensor $\mathbb{A}(\underline{x})$ which relates the microscopic strain field $\boldsymbol{\varepsilon}$ to the macroscopic strain $\boldsymbol{E}$.

$$\boldsymbol{\varepsilon} = \mathbb{A}(\underline{x}) : \boldsymbol{E} \qquad (\forall \underline{x} \in \Omega) \tag{II .7}$$

Note that the concentration tensor satisfies the condition $\langle \mathbb{A}(\underline{x}) \rangle = \mathbb{I}$, due to the fact that the average of microscopic strain is equal to the macroscopic strain, see II .5. $\mathbb{I}$ denotes the fourth order unit tensor: $\mathbb{I} = \frac{1}{2}(\boldsymbol{\delta}_{ik}\boldsymbol{\delta}_{jl} + \boldsymbol{\delta}_{il}\boldsymbol{\delta}_{jk})$ with $\boldsymbol{\delta}_{ij}$ the Kronecher's symbol.

Then, by using the local elastic law and making the averaging of the local stress field, one obtains the following macroscopic elastic stress-strain relation:

$$\boldsymbol{\Sigma} = \mathbb{C}^{hom} : \boldsymbol{E} \quad \text{with} \quad \mathbb{C}^{hom} = \langle \mathbb{C}_s : \mathbb{A} \rangle_\Omega \tag{II .8}$$

where $\mathbb{C}^{hom}$ denotes the effective macroscopic elastic stiffness tensor of the homogenized material. Due to the fact that the local strain field is not uniform inside each inclusion phase, the volume averaging operation in the above relation is generally difficult to perform and cannot be performed analytically. Therefore, for the sake of simplicity, it is generally assumed that the local strain field in each inclusion phase r can be represented by its constant average value. Accordingly, only the constant average of strain localization tensor $\mathbb{A}_r$ needs to be determined for each phase r. For a heterogeneous materials containing $\mathcal{N}$ phases of inclusions, the effective elastic stiffness is given by:

$$\mathbb{C}^{hom} = \sum_{r=1}^{N} \varphi_r \mathbb{C}_r : \mathbb{A}_r \tag{II .9}$$

where φ_r is the volume fraction of the phase r.

With the condition $\langle \mathbb{A}(\underline{x}) \rangle = \mathbb{I}$ and by denoting the elastic stiffness of the solid matrix by $\mathbb{C}_s$ and that of the inclusion phase r by $\mathbb{C}_{f,r}$, the effective elastic stiffness tensor can also be written in the following form:

$$\mathbb{C}^{hom} = \mathbb{C}_s + \sum_{r=1}^{N} \varphi_{f,r}(\mathbb{C}_{f,r} - \mathbb{C}_s) : \mathbb{A}_{f,r} \tag{II .10}$$

The determination of concentration tensor $\mathbb{A}_{f,r}$ for each phase r depends on the homogenization scheme used. Physically this is related to how the effects of crack interaction and spatial distribution are taken into into account. The well-known solutions to Eshelby's inclusion problem provide fundamentals for determination of such concentration tensors, [Eshelby, 1961,Eshelby, 1957,Mori and Tanaka, 1973b,Ponte Castañeda and Suquet, 1997]. The basic solution of $\mathbb{A}_{f,r}$ is written as:

© 2016 Tous droits réservés.

doc.univ-lille1.fr

Thèse de Mei Qi, Lille 1, 2016

$$\mathbb{A}_{f,r} = [\mathbb{I} + \mathbb{P}^r_\epsilon : (\mathbb{C}_{f,r} - \mathbb{C}_s)]^{-1} = [\mathbb{I} - \mathbb{S}^r_\epsilon : (\mathbb{I} - \mathbb{S}_s : \mathbb{C}_{f,r})]^{-1} \qquad \text{(II .11)}$$

which $\mathbb{S}^r_\epsilon$ is the Eshelby tensor corresponding to the rth family of micro-cracks and $\mathbb{S}^r_\epsilon$ is related to the Hill tensor $\mathbb{P}^r_\epsilon$ such as: $\mathbb{S}^r_\epsilon = \mathbb{P}^r_\epsilon : \mathbb{C}_s$. Therefore, the Hill tensor depends on the geometry of micro-cracks and the elastic properties of solid matrix. Here, it is worth to mention that for the case of initially isotropic matrix, the Eshelby tensor or Hill tensor has analytical solution for penny shaped micro-cracks [Zhu, 2006]. But for the case of spheroidal micro-cracks embedded in an initially anisotropic matrix, there is no analytical solution so far available. A suitable numerical method should be developed for computing Eshelby or Hill tensor. A detailed description of the numerical method used in this work for computing Hill tensor for arbitrarily oriented spheroidal inclusion in a transversely isotropic materials will be presented in the next section.

In this work, we will consider three widely used schemes: Dilute scheme, Mori-Tanaka (MT) scheme and Ponte-Castaneda and Willis (PCW) scheme. They will be presented in the following section.

2.3 Dilute scheme

In the case of inclusions with low concentration, we consider simply that there is no interaction between different families of micro-cracks, which implies that all families of micro-cracks are independent from each other. The effective elastic stiffness tensor is then reduced to:

$$\mathbb{C}^{hom} = \mathbb{C}_s + \sum_{r=1}^{N} \varphi_{f,r}(\mathbb{C}_{f,r} - \mathbb{C}_s) : [\mathbb{I} + \mathbb{P}^r_\epsilon : (\mathbb{C}_{f,r} - \mathbb{C}_s)]^{-1} \qquad \text{(II .12)}$$

On the other hand, the effective elastic properties of cracked materials are also dependent on opening or closure state of micro-cracks. Three situations can be distinguished. For the case of open cracks, there is the cancellation of local stress on the crack faces. The elastic tensor of cracks then vanishes, $\mathbb{C}_{f,r} = 0$. For closed frictionless cracks, the idea introduced by ([Deude et al., 2002]) consist in modelling the planar cracks as a fictitious elastic material with an elastic tensor $\mathbb{C}_{f,r} = 3k_s\mathbb{J}$, k_s being the bulk modulus of the isotropic solid matrix. This choice is justified by the need to take into account for the nullity of the tangential stress on the closed crack lips and the continuity of stress in the normal direction to cracks lips. In the last case of closed frictional cracks, we assume

© 2016 Tous droits réservés.

doc.univ-lille1.fr

Thèse de Mei Qi, Lille 1, 2016

that the friction is large enough so that the crack lips are fully glued. Therefore, one gets $\mathbb{C}_{f,r} = \mathbb{C}_s$.

a) Case of open cracks:

By putting $\mathbb{C}_{f,r} = 0$ in (II .12), one obtains:

$$\mathbb{C}^{hom} = \mathbb{C}_s : [\mathbb{I} - \sum_{r=1}^{N} \varphi_{f,r} (\mathbb{I} - \mathbb{P}^r_\epsilon : \mathbb{C}_s)^{-1}] \tag{II .13}$$

The main difficulty for the calculation of $\mathbb{C}^{hom}$ lies in the fact that $(\mathbb{I} - \mathbb{P}^r_\epsilon : \mathbb{C}_s)^{-1}$ is singular when the aspect ratio ϵ tends to 0. For this reason, the volume fraction of cracks $\varphi_{f,r}$ is expressed as:

$$\varphi_{f,r} = \frac{4}{3}\pi a^2 c \mathcal{N}_r = \frac{4}{3}\pi \epsilon d_r \tag{II .14}$$

where $\mathcal{N}_r$ denotes the number of cracks per unit volume of a family of cracks and $d_r = \mathcal{N}_r a^3$ is the crack density parameter. It is well known that when the aspect ratio ϵ tends to zero, the concentration tensor admits a limit value. The homogenized effective elasticity tensor can be also written as:

$$\mathbb{C}^{hom} = \mathbb{C}_s : [\mathbb{I} - \frac{4}{3}\pi \sum_{r=1}^{N} d_r \epsilon (\mathbb{I} - \mathbb{P}^r_\epsilon : \mathbb{C}_s)^{-1}] \tag{II .15}$$

where we denoted $\mathbb{T}^r = \epsilon(\mathbb{I} - \mathbb{P}^r_\epsilon : \mathbb{C}_s)^{-1}$. It follows that the homogenized elasticity tensor can be written as:

$$\mathbb{C}^{hom} = \mathbb{C}_s : [\mathbb{I} - \frac{4}{3}\pi \sum_{r=1}^{N} d_r \mathbb{T}^r] \ , \quad \text{with} \quad \mathbb{T}^r = \lim_{\epsilon \to 0} \epsilon (\mathbb{I} - \mathbb{P}^r_\epsilon : \mathbb{C}_s)^{-1} \tag{II .16}$$

Note that the expression II .16 of the effective elastic stiffness tensor is valid not only for isotropic but also anisotropic solid matrix. The difference lies in the calculation of Hill's tensor.

b) Case of closed frictionless cracks:

As mentioned above, it is assumed that the tangential stiffness of cracks vanishes while the normal stiffness takes the value of solid matrix, that is $k_f = k_s$ and $\mu_f = 0$. Thus, one takes for the elastic tensor of cracks $\mathbb{C}_{f,r} = 3k_s\mathbb{J}$. As a consequence, the effective elastic stiffness tensor with an initially isotropic matrix is given by:

$$\mathbb{C}^{hom} = \mathbb{C}_s : [\mathbb{I} - \frac{4}{3}\pi \sum_{r=1}^{N} d_r \epsilon \mathbb{K} : (\mathbb{I} - \mathbb{P}^r_\epsilon : \mathbb{C}_s : \mathbb{K})^{-1}] \tag{II .17}$$

where: $\mathbb{C}_{f,r} - \mathbb{C}_s = -2\mu_s\mathbb{K} = -\mathbb{C}_s : \mathbb{K}$.

© 2016 Tous droits réservés.

doc.univ-lille1.fr

Thèse de Mei Qi, Lille 1, 2016

For low cracks aspect ratio $\epsilon \to 0$, the tensor $\mathbb{T}'^r = \epsilon\mathbb{K} : (\mathbb{I} - \mathbb{P}^r_\epsilon : \mathbb{C}_s : \mathbb{K})^{-1}$ tends to its limit. It follows that:

$$\mathbb{C}^{hom} = \mathbb{C}_s : [\mathbb{I} - \frac{4}{3}\pi \sum_{r=1}^{N} d_r \mathbb{T}'^r] \ , \quad with \quad \mathbb{T}'^r = \lim_{\epsilon \to 0} \epsilon\mathbb{K} : (\mathbb{I} - \mathbb{P}^r_\epsilon : \mathbb{C}_s : \mathbb{K})^{-1} \tag{II .18}$$

2.4 Mori-Tanaka scheme estimations

To overcome the limitations of the dilute scheme, Mori and Tanaka [Mori and Tanaka, 1973a] proposed a homogenization method to deal with interactions between inclusions in composite materials. It has been applied to micro-cracked materials in [Benveniste, 1986].

The idea in Mori-Tanaka scheme to take into account interactions between cracks consists in considering an intermediate prescribed macroscopic strain $\boldsymbol{E}^0$ on the external boundary of the *REV*, instead of the remote macroscopic strain $\boldsymbol{E}$. For this new problem, the relation (II .11) is written:

$$\boldsymbol{\varepsilon}_r = [\mathbb{I} + \mathbb{P}^r_\epsilon : (\mathbb{C}_{f,r} - \mathbb{C}_s)]^{-1} : \boldsymbol{E}^0 \tag{II .19}$$

The use of the relation $\langle \boldsymbol{\varepsilon} \rangle_\Omega = \boldsymbol{E}$ leads to:

$$\boldsymbol{E}^0 = [\varphi_s \mathbb{I} + \sum_{j=1}^{N} \varphi_{f,j} [\mathbb{I} + \mathbb{P}^j_\epsilon : (\mathbb{C}_{r,j} - \mathbb{C}_s)]^{-1}]^{-1} : \boldsymbol{E} \tag{II .20}$$

from where it deduces the strain concentration rule (II .7) for the Mori-Tanaka scheme with:

$$\mathbb{A}_{f,r} = [\mathbb{I} + \mathbb{P}^r_\epsilon : (\mathbb{C}_{f,r} - \mathbb{C}_s)]^{-1} : [\varphi_s \mathbb{I} + \sum_{j=1}^{N} \varphi_{f,j} [\mathbb{I} + \mathbb{P}^j_\epsilon : (\mathbb{C}_{f,j} - \mathbb{C}_s)]^{-1}]^{-1} \tag{II .21}$$

The substitution of equation (II .21) into (V .5) allows to deduce the expression of the effective elasticity tensor corresponding to the MT scheme:

$$\begin{aligned} \mathbb{C}^{MT} \quad &= \quad \mathbb{C}_s + \sum_{r=1}^{N} \varphi_{f,r} (\mathbb{C}_{f,r} - \mathbb{C}_s) \\ &: [\mathbb{I} + \mathbb{P}^r_\epsilon : (\mathbb{C}_{f,r} - \mathbb{C}_s)]^{-1} : [\varphi_s \mathbb{I} + \sum_{j=1}^{N} \varphi_{f,j} [\mathbb{I} + \mathbb{P}^j_\epsilon : (\mathbb{C}_{f,j} - \mathbb{C}_s)]^{-1}]^{-1} \end{aligned} \tag{II .22}$$

This general result can be applied to open and closed micro-cracks.

a) Case of open cracks: $(\mathbb{C}_{f,r} = 0)$

© 2016 Tous droits réservés. doc.univ-lille1.fr

Thèse de Mei Qi, Lille 1, 2016

$$\mathbb{C}^{hom} = \mathbb{C}_s - \sum_{r=1}^{N} \varphi_{f,r}\mathbb{C}_s : (\mathbb{I} - \mathbb{S}_\epsilon^r)^{-1} : [\varphi_s\mathbb{I} + \sum_{j=1}^{N} \varphi_{f,j}(\mathbb{I} - \mathbb{S}_\epsilon^j)]^{-1} \tag{II .23}$$

We recall that $\mathbb{S}_\epsilon = \mathbb{P}_\epsilon : \mathbb{C}_s$ is the Eshelby's tensor corresponding to one family of crack. Also, (II .23) can be written as:

$$\begin{aligned} \mathbb{C}^{hom} &= \varphi_s\mathbb{C}_s : [\varphi_s\mathbb{I} + \sum_{j=1}^{N} \varphi_{f,j}(\mathbb{I} - \mathbb{S}_\epsilon^j)^{-1}]^{-1} \\ &= \mathbb{C}_s : [\mathbb{I} + \frac{4}{3}\pi \sum_{j=1}^{N} d_j\mathbb{T}^r]^{-1}, \quad with \quad \mathbb{T}^r = \lim_{\epsilon\to 0} \epsilon(\mathbb{I} - \mathbb{S}_\epsilon^j)^{-1} \end{aligned} \tag{II .24}$$

In this relation, the quantity φ_s is sensibly equal to 1 as the volume of the cracks being almost zero. The inversion of (II .24) gives the effective elastic compliance tensor $\mathbb{S}^{hom}$ of cracked media:

$$\mathbb{S}^{hom} = [\mathbb{I} + \frac{4}{3}\pi \sum_{j=1}^{N} d_j\mathbb{T}^r] : \mathbb{S}_s \tag{II .25}$$

b) Case of closed frictionless cracks: $(\mathbb{C}_{f,r} = 3k_s\mathbb{J})$

Considering $\mathbb{C}_{f,r} = 3k_s\mathbb{J}$, one gets for the MT scheme:

$$\mathbb{C}^{hom} = \mathbb{C}_s - \sum_{r=1}^{N} \varphi_{f,r}\mathbb{C}_s : \mathbb{K} : (\mathbb{I} - \mathbb{S}_\epsilon^j : \mathbb{K})^{-1} : [\varphi_s\mathbb{I} + \sum_{j=1}^{N} \varphi_{f,j}(\mathbb{I} - \mathbb{S}_\epsilon^j : \mathbb{K})^{-1}]^{-1} \tag{II .26}$$

After arrangement of the results, one obtains:

$$\begin{aligned} \mathbb{C}^{hom} &= \mathbb{C}_s : [\mathbb{I} + \frac{4}{3}\pi \sum_{j=1}^{N} d_j\epsilon(\mathbb{I} - \mathbb{S}_\epsilon^j : \mathbb{K})^{-1}]^{-1} \\ &= \mathbb{C}_s : [\mathbb{I} + \frac{4}{3}\pi \sum_{j=1}^{N} d_j\mathbb{T}'^r]^{-1}, \quad with \quad \mathbb{T}'^r = \lim_{\epsilon\to 0} \epsilon(\mathbb{I} - \mathbb{S}_\epsilon^j : \mathbb{K})^{-1} \end{aligned} \tag{II .27}$$

For the inversion of the above equation, the macroscopic compliance tensor is given by:

$$\mathbb{S}^{hom} = [\mathbb{I} + \frac{4}{3}\pi \sum_{j=1}^{N} d_j\mathbb{T}'^r]^{-1} : \mathbb{S}_s \tag{II .28}$$

Initially anisotropic cracked media

© 2016 Tous droits réservés.

doc.univ-lille1.fr

Thèse de Mei Qi, Lille 1, 2016

2.5 PCW scheme estimations

In order to take into account both interactions between cracks and effects of spatial distribution of micro-cracks, the idea in the Ponte-Castaneda and Willis scheme is to consider two independent functions, one associated with the shape of inclusions, the other one associated with the spatial distribution form of inclusions. In the case of considering the same spatial distribution for all of inclusions, the strain concentration tensor can be taken into the form:

$$\mathbb{A}^{f,r} = [\mathbb{I} + \mathbb{P}^r_\epsilon : (\mathbb{C}_{f,r} - \mathbb{C}_s)]^{-1} : \tag{II .29}$$
$$[\mathbb{I} + \sum_{j=1}^{N} \varphi_{f,j}[\mathbb{I} + (\mathbb{P}^j_\epsilon - \mathbb{P}_d) : (\mathbb{C}_{f,j} - \mathbb{C}_s)] : [\mathbb{I} + \mathbb{P}^j_\epsilon : (\mathbb{C}_{f,j} - \mathbb{C}_s)]^{-1}]^{-1}$$

where the tensor $\mathbb{P}^r_\epsilon$ is related to the shape of the r^{th} family of cracks while $\mathbb{P}_d$ is the function associated with the spatial distribution of cracks. According to [Ponte-Castañeda and Willis, 1995], the general expression of macroscopic elasticity tensor for the *PCW* scheme can be written as:

$$\mathbb{C}^{PCW} = \mathbb{C}^s + (\mathbb{I} - \sum_{r=1}^{N} \varphi_{f,r}[(\mathbb{C}_{f,r} - \mathbb{C}_s)^{-1} + \mathbb{P}^r_\epsilon]^{-1} : \mathbb{P}_d)^{-1} : \sum_{r=1}^{N} \varphi_{f,r}[(\mathbb{C}_{f,r} - \mathbb{C}_s)^{-1} + \mathbb{P}^r_\epsilon]^{-1} \tag{II .30}$$

This result can be applied to open and closed micro-cracks by considering different elastic tensor of inclusion phase, as that already discussed for the *Dilute* and *MT* schemes.

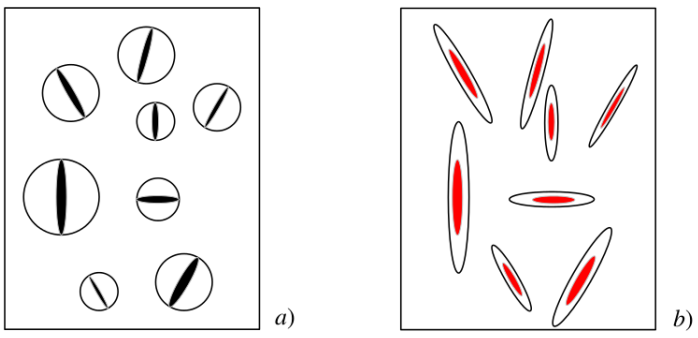

Figure II .3: Comparison of microstructure: a) spherical distribution adopted for the PCW scheme; b) ellipsoidal distribution of type MT, $\mathbb{P}_d = \mathbb{P}^r_\epsilon$.

© 2016 Tous droits réservés.

doc.univ-lille1.fr

Thèse de Mei Qi, Lille 1, 2016

3 Eshelby problem

In the previous section, it has been shown that most linear homogenization schemes for the determination of effective elastic properties of cracked materials are based on the application of Eshelby solution to an eigenstrain problem to an equivalent inclusion problem. In case of isotropic solid matrix, it is possible to obtain analytical expressions of Eshelby tensor for spheroidal inclusions. However, for materials with an initially anisotropic solid matrix, such analytical solutions are no more available and suitable numerical methods should be developed for computing Eshelby tensor. In this section, we present a short summary of the formulation of Green's function method which is used to solve Eshelby and Hill polarization tensors in general case. This presentation will serve as the theoretical background for numerical computing of Hill's tensor in the next section.

3.1 Eshelby's equivalent eigenstrain method

The principle of this method is to replace the initial heterogeneous body with a homogeneous body, within which an eigenstrain field is prescribed. Consider here an infinite homogeneous elastic solid Ω, with elasticity tensor $\mathbb{C}^0$, and compliance tensor $\mathbb{S}^0$. Inside the elastic solid, there is an inhomogeneity, a subdomain I. This inhomogeneity can be presented by an ordinary eigenstrain field $\boldsymbol{\varepsilon}^t$ or an polarization tensor σ^I equivalently. Eigenstrain or polarization equals to zero besides the subdomain I, and the displacement $\underline{u}$ tends to zero in infinity (Figure II .32 (a)).

The eigenstrain field $\boldsymbol{\varepsilon}^t$ has been introduced by [Mura, 1987]. It is a fictitious strain to describe a transformation strain field that can equivalently represent induced strain due to the presence of inhomogeneities.

Now, an eigenstress field also called polarization tensor is created by the incompatibility of the eigenstrain field $\boldsymbol{\varepsilon}^t$, which can be written as:

$$\boldsymbol{\sigma}^I = -\mathbb{C}^0 : \boldsymbol{\varepsilon}^t \tag{II .31}$$

When there is an eigenstrain in the subdomain I, the solution of the problem satisfies the

© 2016 Tous droits réservés.

doc.univ-lille1.fr

Thèse de Mei Qi, Lille 1, 2016

following system of equations:

$$\begin{cases} \boldsymbol{\sigma}^* = \mathbb{C}^0 : (\boldsymbol{\varepsilon}^* - \boldsymbol{\varepsilon}^t) & \underline{x} \in I \\ \boldsymbol{\sigma}^* = \mathbb{C}^0 : \boldsymbol{\varepsilon}^* & \underline{x} \in (\Omega - I) \\ \underline{u} \to 0 & \underline{x} \to \infty \\ \underline{div}\boldsymbol{\sigma}^* = 0 & \underline{x} \in \Omega \\ \|\boldsymbol{\sigma}^*\| = 0, \|\underline{u}\| = 0 & \underline{x} \in \partial I \end{cases} \tag{II .32}$$

It is obvious that the polarization is an ordinary tensor, its divergence is zero excluding the boundary surface of the subdomain ∂I. So, we can obtain:

$$\begin{aligned} \underline{f} &= -\boldsymbol{\sigma}^I \cdot \underline{n}\delta(\partial I) \\ &= \mathbb{C}^0 : \boldsymbol{\varepsilon}^t \cdot \underline{n}(\partial I) \end{aligned} \tag{II .33}$$

where the $\underline{n}$ is the unit vector, the $\delta(\partial I)$ and the surface ∂I are the associated Dirac delta functions.

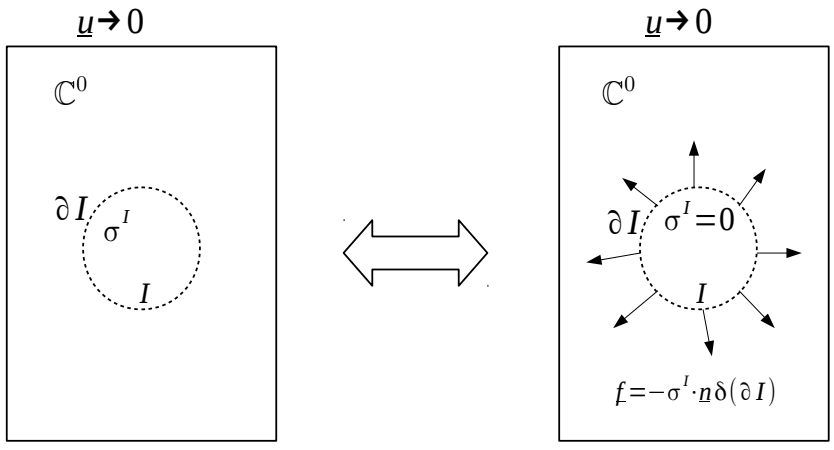

(a) Eshelby's problem (b) equivalent problem

Figure II .4: (a) Eshelby's problem and (b) equivalent problem in infinite medium

The previous problem can be explained with Figure II .4 (b): in the infinite homogeneous elastic medium Ω, we apply a force $-\boldsymbol{\sigma}^I \cdot \underline{n}$ in the boundary surface of the subdomain

© 2016 Tous droits réservés. doc.univ-lille1.fr

Thèse de Mei Qi, Lille 1, 2016

∂I, the strain $\mathbf{E} = 0$ in infinity, it should find the displacement $\underline{u}'(\underline{x})$ for the eigenstrain field. If we can find the displacement field with the superposition method, the problem can be solved. In order to solve the displacement field, the Green's function is proposed and presented in the following subsection.

3.2 Green's function for Eshelby's problem

It is well known that the solutions of many elasticity problems can be obtained from the elastic Green's function solutions. The concept of Green's function can be effectively used to obtain general results for linear problems, using the superposition method. Now we will introduce briefly the method to solve Eshelby's problem using the Green's function.

For the Eshelby's problem, it presents the infinite linear elasticity medium, when the inclusion is ellipsoidal, if the eigenstrain (initial transformation strain) $\boldsymbol{\varepsilon}^t$ is an ordinary tensor, that means it is uniform according to the variation the position of the inclusion in the domain I, so the strain in the inclusion $\boldsymbol{\varepsilon}^I$ is also an ordinary tensor, expressed as (see [Eshelby, 1957], [Eshelby, 1961]):

$$\boldsymbol{\varepsilon}^I = \mathbb{S}^0_{Esh} : \boldsymbol{\varepsilon}^t \quad \text{with} \quad \mathbb{S}^0_{Esh} = \mathbb{P}^0 : \mathbb{C}^0 \tag{II .34}$$

The Eshelby's tensor depends on the form and orientation of ellipsoid (inclusion), and the elastic property of matrix.

In order to solve this inclusion problem with Green's function, a general linear-elastic heterogeneous infinite medium with elasticity tensor $\mathbb{C}^0$ is considered. At the point $\underline{x}'$, we apply a unit force $\underline{F}(\underline{x}')$, the related displacement field can be expressed:

$$u'_i(\underline{x}) = \mathbf{G}^0_{ij}(\underline{x}, \underline{x}') \cdot \underline{F}(\underline{x}') \tag{II .35}$$

In this equation, the $\mathbf{G}^0_{ij}$ is Green's function associated with the infinite elasticity medium $\mathbb{C}^0$. The Green's function is a second-order tensor with components $\mathbf{G}_{ij}(\underline{x}, \underline{x}')$, representing the displacement components $u_i(\underline{x})$ at a point x, due to the unit concentration force applied at a point x' in the j direction.

The Green's function $\mathbf{G}_{ij}(\underline{x}, \underline{x}')$ has two important properties:

- In the infinite elastic medium, the Green's tensor can be expressed as:

$$\mathbf{G}_{ij}(\underline{x}, \underline{x}') = \mathbf{G}_{ij}(\underline{x} - \underline{x}') \tag{II .36}$$

- According to the Betti's reciprocal theorem, the Green's function has the following symmetry property:

$$\mathbf{G}_{ij}(\underline{x} - \underline{x}') = \mathbf{G}_{ij}(\underline{x}' - \underline{x}) \tag{II .37}$$

© 2016 Tous droits réservés.

doc.univ-lille1.fr

Thèse de Mei Qi, Lille 1, 2016

With this property, we can also obtain:

$$\mathbf{G}_{ij}(\underline{x},\underline{x}') = \frac{1}{\mid \underline{x}-\underline{x}' \mid}\mathbf{G}_{ij}(\frac{\underline{x}-\underline{x}'}{\mid \underline{x}-\underline{x}' \mid}) = \frac{1}{\mid \underline{x}-\underline{x}' \mid}\mathbf{G}_{ij}[-(\frac{\underline{x}-\underline{x}'}{\mid \underline{x}-\underline{x}' \mid})] \qquad \text{(II .38)}$$

If we know the solution of the Green's function $\mathbf{G}_{ij}(\underline{x},\underline{x}')$, with the Green's function and the integrate of the force at the boundary surface $-\boldsymbol{\sigma}^I \cdot \underline{n}da'$, the displacement u_i' at the point $\underline{x}'$ can be obtained (see [Mura, 1987]):

$$\begin{aligned} u_i'(\underline{x}) &= -\int_{\partial I} \mathbf{G}_{ij}(\underline{x},\underline{x}')\boldsymbol{\sigma}^I \underline{n}_k(\underline{x}')da' \\ &= \int_{\partial I} \mathbf{G}_{ij}(\underline{x},\underline{x}')\mathbb{C}^0_{jklm}\varepsilon^t_{lm}\underline{n}_k(\underline{x}')da' \qquad \text{(II .39)} \\ &= -(\int_I \mathbf{G}_{ij}(\underline{x},\underline{x}')d\Omega')_{,k}\mathbb{C}^0_{jklm}\varepsilon^t_{lm} \end{aligned}$$

with,

$$\begin{aligned} \frac{\partial}{\partial \underline{x}'}\mathbf{G}_{ij}(\underline{x}-\underline{x}') &= -\frac{\partial}{\partial \underline{x}}\mathbf{G}_{ij}(\underline{x}-\underline{x}') \qquad \text{(II .40)} \\ \mathbf{G}_{ij,k'} &= \frac{\partial}{\partial \underline{x}'}\mathbf{G}_{ij} = -\mathbf{G}_{ij,k} \end{aligned}$$

a' is the integrate surface on the boundary surface of the inclusion ∂I. So the strain field in the inclusion can be obtained:

$$\boldsymbol{\varepsilon}^I_{in}(\underline{x}) = -(\int_I \mathbf{G}_{ij}(\underline{x},\underline{x}')d\Omega'_{,kn(in)(jk)})\mathbb{C}^0_{jklm}\boldsymbol{\varepsilon}^t_{lm} \qquad \text{(II .41)}$$

where $(in)(jk)$ indicate the symmetry of i,n and j,k.

According to II .41, the general Hill's tensor can be expressed with the Green's function as follows:

$$\mathbb{P}^0_{injk} = -(\int_I \mathbf{G}_{ij}(\underline{x},\underline{x}')d\Omega')_{,kn(in)(jk)}) \quad \underline{x} \in I \qquad \text{(II .42)}$$

3.3 Hill tensor for arbitrarily oriented spheroidal inclusion in a transversely isotropic matrix

As mentioned above, the Hill tensor $\mathbb{P}$ captures the morphology and orientation of inclusion phases and is necessary for the estimation of strain concentration tensors in

© 2016 Tous droits réservés.

doc.univ-lille1.fr

Thèse de Mei Qi, Lille 1, 2016

homogenization methods. When the solid matrix is an isotropic elastic material and weakened by a family of spheroidal cracks, it is possible to obtain an analytical form of the Hill's tensor or Eshelby's tensor ([Zhu et al., 2008a]). Many authors, for instance ([Eshelby, 1957], [Eshelby, 1961], [Mura, 1987], [Nemat-Nasser and Hori, 1993]), have used the Hill tensor $\mathbb{P}$ and Eshelby tensor $\mathbb{S}_\epsilon$ for ellipsoidal inclusions in an isotropic matrix in different homogenization schemes. Both preferentially oriented or randomly distributed ellipsoidal inclusions have been considered.

In the case of anisotropic matrix, exact solutions are restricted to the simplest case of aligned inclusions with the directions of anisotropy. See [Withers, 1989] solution for an oblate spheroidal inclusion aligned with the direction of symmetry of a transversely isotropic matrix. The computation of Eshelby and Hill tensors in general case is generally based upon Fourier transform method and elastic Green functions, for instance [Ghahremani, 1977], [Mura, 1987], [Gavazzi and Lagoudas, 1990], [Suvorov and Dvorak, 2002].

More recently [Masson, 2008] presented a review of existing elastic solutions and new expressions of the Hill polarization tensor by applying the Cauchy theory of residues. His important result is that when the body is three-dimensional the double integral [Mura, 1987] can be reduced to a simple one. [Barthélémy, 2009] developed a similar approach to derive solutions for the case of cracks modeled as a flat ellipsoid embedded in fully anisotropic three dimensional matrix (see also [Huang and Liu, 1998]). He presented solutions for the Hill polarization tensors and for the crack compliance tensor, by using the method of residues ($1D$ numerical integration) on the one hand and a numerical integration method ($2D$ numerical integration) on the other hand.

Theoretically, the solutions developed using the Cauchy theory of residues are general and cover the complete set of fully anisotropic three dimensional body. However some difficulties are met in practical complex situations: multiple poles are sources of difficulty and they may be encountered depending on:

- ellipsoidal inclusion aspect ratios
- orientation of inclusions compared to the directions of symmetry of the anisotropic medium

These difficulties are encountered in the present study. $3D$ circular cracks are modelled as oblate spheroidal inclusions and are randomly distributed in orientation in a transversely isotropic matrix. A robust and $2D$ numerical integration method has been chosen instead of the previously cited $1D$ residue method. We will use a solution based on the numerical

© 2016 Tous droits réservés.

doc.univ-lille1.fr

Thèse de Mei Qi, Lille 1, 2016

integration of the exact Green's function of the transversely isotropic medium presented by [Pan and Chou, 1976]. The fundamental problem is to solve one of the isolated ellipsoidal inclusion with arbitrarily orientation in an infinite transversely isotropic medium. No analytical results have been provided in the general case of the ellipsoidal inclusion with arbitrary orientation in a anisotropic solid so semi-analytical methods have been proposed to evaluated $\mathbb{S}_\epsilon$ and $\mathbb{P}$ tensors by ([Giraud et al., 2007]). The semi-analytical method to obtain the Hill tensor of the isolated arbitrarily oriented ellipsoidal inclusion in a transversely isotropic matrix is based on numerical integration of the exact Green's function provided by ([Pan and Chou, 1976]) for the transversely isotropic media. ([Giraud et al., 2007]) proposed an intermediate coordinate system attached to the inhomogeneity. This choice of coordinate system can simplify numerical calculation because one axis equal to the symmetry axis of the transversely isotropic matrix. By performing the numerical integration in an intermediate system, the Hill tensor depends only one angle which is the angle between the symmetry axis of the inclusion and the symmetry axis of the matrix.

We will summary the method proposed by [Giraud et al., 2007] for computing Hill tensor for arbitrarily oriented spheroidal cracks in a transversely isotropic material, using numerical integration of the exact Green's function based on the coordinates system transformation.

3.3.1 Local and global coordinates systems

In what follows, the global coordinates system associated with the matrix is defined by (e_1, e_2, e_3), ($\underline{e}_3$ being the symmetry axis of the transversely isotropic matrix) while $\underline{e}_i^\alpha$ is defining the local coordinates system associated with an arbitrarily orientated inclusion, with ($\underline{e}_3^\alpha$ being the symmetry axis of the inclusion). Here, all quantities related to the inclusion α are denoted by the subscript α.

We deal with oblate or prolate spheroidal inclusions whose half-lengths (centred at the origin $\mathcal{O}$) are denoted respectively a in the plane $\underline{e}_1^\alpha - \underline{e}_2^\alpha$ and $c = a\epsilon$. We recall that ϵ defines the aspect ratio of the spheroidal inclusion as shown in Figure (II .5).

The characteristic equation to describe the particle geometry of an spheroidal inclusion, occupying the domain Ω_α, aligned in the principal directions of the local coordinate system $(e_1^\alpha, e_2^\alpha, e_3^\alpha)$ is given as follows:

$$\begin{aligned} &\underline{e}^\alpha \in \Omega_\alpha \Leftrightarrow \|\underline{\underline{\zeta}}^\alpha.\underline{e}^\alpha\| \leq 1 \quad , \quad \underline{\underline{\zeta}}^\alpha = \frac{1}{a}\left(\underline{u}_1^\alpha \otimes \underline{u}_1^\alpha + \underline{u}_2^\alpha \otimes \underline{u}_2^\alpha\right) + \frac{1}{a\,\epsilon}\underline{u}_3^\alpha \otimes \underline{u}_3^\alpha \\ &\frac{(e_1^\alpha)^2 + (e_2^\alpha)^2}{a^2} + \frac{(e_3^\alpha)^2}{a^2\,\epsilon^2} \leq 1 \end{aligned} \qquad \text{(II .43)}$$

The key point is that this method takes benefit of two symmetries of revolution:

© 2016 Tous droits réservés.

doc.univ-lille1.fr

Thèse de Mei Qi, Lille 1, 2016

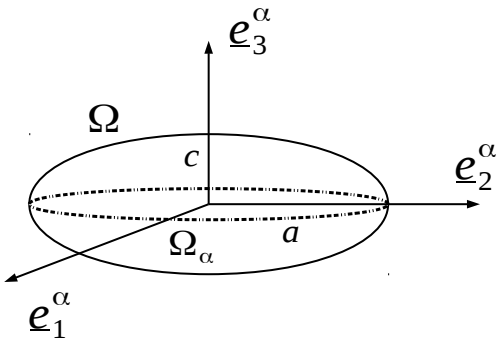

Figure II .5: A spheroidal inclusion to take into account principal directions of the local coordinate system

- the oblate spheroidal inclusion verifies a symmetry of revolution around its central unit normal direction $\underline{n} = \underline{e}_3^\alpha$
- the transversely isotropic material surrounding the inclusions verifies a symmetry of revolution around its symmetry axis $\underline{e}_3$

As a consequence, only one angle is needed for the calculation of the Hill tensor of an arbitrarily oriented spheroidal inclusion. This angle characterizes the inclination of the normal vector $\underline{n} = \underline{e}_3^\alpha$ of the inclusion with respect to the symmetry axis of the material ($\underline{e}_3$). An intermediate local frame is then defined for the calculation of Hill polarization tensor. This intermediate coordinates system (denoted e^{φ_α}) is chosen such that one axis ($\underline{e}_3^{\varphi_\alpha}$) coincides with the symmetry axis of the surrounding material ($\underline{e}_3^{\varphi_\alpha} = \underline{e}_3$). Once the Hill polarization tensor is calculated in the intermediate coordinate system, a coordinate transformation is then performed to characterize the rotation between intermediate coordinate system e^{φ_α} and the fix coordinate system corresponding to the transversely isotropic surrounding material.

The second order orthogonal tensor $\boldsymbol{Q}^\alpha$ helps to transfer the components of the global frame (e_1, e_2, e_3) in the α-coordinates. The unit vector in the e_i^α direction is denoted by $\underline{u}_i^\alpha$, so it can be stated:

$$\underline{u}_i^\alpha = \boldsymbol{Q}_{ij}^\alpha \, \underline{u}_j \quad , (j, i = 1, 2, 3) \qquad , \qquad \underline{u}_k = \boldsymbol{R}_{kl}^\alpha \, \underline{u}_l^\alpha \quad , (k, l = 1, 2, 3) \tag{II .44}$$

where $\boldsymbol{Q}^\alpha$ represents the rotation matrix and it's inverse $\boldsymbol{R}^\alpha$ is expressed as (only orthogonal matrix rotations are considered),

$$\boldsymbol{R}_{kl}^\alpha = \boldsymbol{Q}_{lk}^\alpha \tag{II .45}$$

© 2016 Tous droits réservés.

doc.univ-lille1.fr

Thèse de Mei Qi, Lille 1, 2016

The rotation matrix $\boldsymbol{Q}^{\alpha}$ is expressed as a product of two rotations matrices $\boldsymbol{Q}^{\alpha} = \boldsymbol{Q}^{\theta_\alpha}.\boldsymbol{Q}^{\varphi_\alpha}$, the angle between the e_1 and the $e_1^{\varphi_\alpha}$ axis is φ_α $(0 \leq \varphi_\alpha \leq 2\pi)$ and the angle between the e_3 and the $e_3^{\theta_\alpha}$ axis is θ_α $(0 \leq \theta_\alpha \leq \pi)$, see figure (II .6). The non zero components of matrices $\boldsymbol{Q}^{\alpha}$, $\boldsymbol{Q}^{\theta_\alpha}$ and $\boldsymbol{Q}^{\varphi_\alpha}$ write:

$$\begin{aligned} &Q_{11}^{\theta_\alpha} = 1, \quad Q_{22}^{\theta_\alpha} = Q_{33}^{\theta_\alpha} = \cos(\theta_\alpha), \quad -Q_{23}^{\theta_\alpha} = Q_{32}^{\theta_\alpha} = \sin(\theta_\alpha) \\ &Q_{33}^{\varphi_\alpha} = 1, \quad Q_{11}^{\varphi_\alpha} = Q_{22}^{\varphi_\alpha} = \cos(\varphi_\alpha), \quad Q_{12}^{\varphi_\alpha} = -Q_{21}^{\varphi_\alpha} = \sin(\varphi_\alpha) \end{aligned} \tag{II .46}$$

and

$$\begin{aligned} &\boldsymbol{Q}_{ij}^{\alpha} = \boldsymbol{Q}_{ik}^{\theta_\alpha}\boldsymbol{Q}_{kj}^{\varphi_\alpha} \\ &Q_{11}^{\alpha} = \cos(\varphi_\alpha), \qquad Q_{12}^{\alpha} = \sin(\varphi_\alpha) \\ &Q_{21}^{\alpha} = -\cos(\theta_\alpha)\sin(\varphi_\alpha), \quad Q_{22}^{\alpha} = \cos(\theta_\alpha)\cos(\varphi_\alpha), \quad Q_{23}^{\alpha} = -\sin(\theta_\alpha) \\ &Q_{31}^{\alpha} = -\sin(\theta_\alpha)\sin(\varphi_\alpha), \quad Q_{32}^{\alpha} = \sin(\theta_\alpha)\cos(\varphi_\alpha), \quad Q_{33}^{\alpha} = \cos(\theta_\alpha) \end{aligned} \tag{II .47}$$

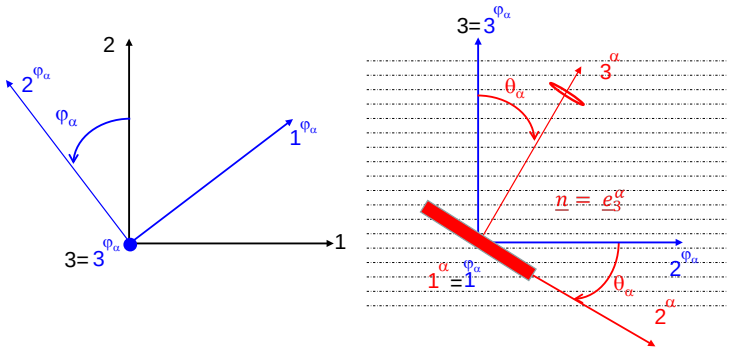

Figure II .6: Local and global system coordinates for an oblate spheroidal inclusion embedded in a transversely isotropic matrix

The exact Green's function obtained by [Pan and Chou, 1976] for the transversely isotropic material is given in the coordinate system of the material (e_3 axis is the symmetry axis of the material). The calculation of the Hill tensor based on the Green's function obtained by [Pan and Chou, 1976] can be easily performed in a coordinate system with one axis equal to the symmetry axis of the transversely isotropic material. This is the case

© 2016 Tous droits réservés.

doc.univ-lille1.fr

Thèse de Mei Qi, Lille 1, 2016

of the e^{φ_α} intermediate system coordinate:

$$\begin{aligned}\underline{u}_1^{\varphi_\alpha} &= \cos(\varphi_\alpha)\underline{u}_1 + \sin(\varphi_\alpha)\underline{u}_2 \\ \underline{u}_2^{\varphi_\alpha} &= -\sin(\varphi_\alpha)\underline{u}_1 + \cos(\varphi_\alpha)\underline{u}_2 \\ \underline{u}_3^{\varphi_\alpha} &= \underline{u}_3\end{aligned} \tag{II .48}$$

In what follows it will be useful to express the local coordinates e_i^α in terms of the *intermediate*, or *local* (as it is attached to the ellipsoid orientation) system coordinates $e_i^{\varphi_\alpha}$:

$$\begin{aligned}\underline{u}_1^{\alpha} &= \underline{u}_1^{\varphi_\alpha} \\ \underline{u}_2^{\alpha} &= \cos(\theta_\alpha)\underline{u}_2^{\varphi_\alpha} - \sin(\theta_\alpha)\,\underline{u}_3^{\varphi_\alpha} \\ \underline{u}_3^{\alpha} &= \sin(\theta_\alpha)\underline{u}_2^{\varphi_\alpha} + \cos(\theta_\alpha)\underline{u}_3^{\varphi_\alpha}\end{aligned} \tag{II .49}$$

which can expressed also as:

$$\mathbf{Q}_{ij}^{\theta_\alpha} = \begin{bmatrix} 1 & 0 & 0 \\ 0 & cos(\theta_\alpha) & -sin(\theta_\alpha) \\ 0 & sin(\theta_\alpha) & cos(\theta_\alpha) \end{bmatrix} \quad \mathbf{Q}_{ij}^{\varphi_\alpha} = \begin{bmatrix} cos(\varphi_\alpha) & sin(\varphi_\alpha) & 0 \\ -sin(\varphi_\alpha) & cos(\varphi_\alpha) & 0 \\ 0 & 0 & 1 \end{bmatrix} \tag{II .50}$$

By using the transformation rules (II .44) and (II .45) it can also be stated:

$$\underline{e} = e_i\underline{u}_i^\alpha = e_i\boldsymbol{R}_{ij}^\alpha\underline{u}_j^\alpha = \boldsymbol{Q}_{ji}^\alpha e_i\underline{u}_j^\alpha = e_j^\alpha\underline{u}_j^\alpha \quad , \quad e_i^\alpha = \boldsymbol{Q}_{ij}^\alpha e_j \tag{II .51}$$

As the rotation matrices $\boldsymbol{Q}^\alpha$, $\boldsymbol{Q}^{\theta_\alpha}$, $\boldsymbol{Q}^{\varphi_\alpha}$, are orthogonal. It may be noticed that transformation rules are identical between base vectors (relation II .44) and vector coordinates (relation II .51):

$$\underline{u}_i^\alpha = \boldsymbol{Q}_{ij}^{\theta_\alpha}\underline{u}_j^{\varphi_\alpha} \quad , \quad e_i^\alpha = \boldsymbol{Q}_{ij}^{\theta_\alpha}e_j^{\varphi_\alpha} \quad , \quad \underline{u}_i^{\varphi_\alpha} = \boldsymbol{Q}_{ij}^{\varphi_\alpha}\underline{u}_j \quad , \quad e_i^{\varphi_\alpha} = \boldsymbol{Q}_{ij}^{\varphi_\alpha}e_j \tag{II .52}$$

As the same transformation rules of the second-order matrix, the fourth-order tensor $\mathbb{P}$ can be transferred in form:

$$\mathbb{P}_{ijkl}^\alpha = \mathbf{Q}_{ip}^\alpha\mathbf{Q}_{jq}^\alpha\mathbf{Q}_{kr}^\alpha\mathbf{Q}_{ls}^\alpha\mathbb{P}_{pqrs} \tag{II .53}$$

$$\mathbb{P}_{ijkl} = \mathbf{Q}_{pi}^\alpha\mathbf{Q}_{qj}^\alpha\mathbf{Q}_{rk}^\alpha\mathbf{Q}_{sl}^\alpha\mathbb{P}_{pqrs}^\alpha$$

© 2016 Tous droits réservés.

doc.univ-lille1.fr

Thèse de Mei Qi, Lille 1, 2016

3.3.2 Formulation of Hill tensor in the intermediate coordinates system

In this subsection, we present the calculation of the Hill tensor for an arbitrarily oriented spheroidal inclusion in a transversely isotropic matrix in the intermediate coordinates. According to the intermediate system (φ_α coordinates), it allows to simplify numerical calculation because there is only one angle to consider: the angle between the symmetry axis of the spheroid $\underline{e}_3^{\alpha}$ and the symmetry axis of the material ($\underline{e}_3 = \underline{e}_3^{\varphi_\alpha}$).

The fourth-order Hill tensor of the ellipsoidal inhomogeneity can be expressed classically by ([Mura, 1987], [Nemat-Nasser and Hori, 1993]) from the second-order derivatives of Green's function, such as:

$$\mathbb{P}_{ijkl}^{\varphi_\alpha}(\underline{e}^{\varphi_\alpha}) = \frac{1}{4}\left(\mathbb{M}_{kijl}^{\varphi_\alpha}(\underline{e}^{\varphi_\alpha}) + \mathbb{M}_{kjil}^{\varphi_\alpha}(\underline{e}^{\varphi_\alpha}) + \mathbb{M}_{lijk}^{\varphi_\alpha}(\underline{e}^{\varphi_\alpha}) + \mathbb{M}_{ljik}^{\varphi_\alpha}(\underline{e}^{\varphi_\alpha})\right) \tag{II .54}$$

with

$$\mathbb{M}_{ijkl}^{\varphi_\alpha}(\underline{e}^{\varphi_\alpha}) = -\int_\Omega \mathbf{G}_{ij,kl}^{\varphi_\alpha}(\underline{e}^{\varphi_\alpha} - \underline{e}'^{\varphi_\alpha}) d\Omega_{e'}, \quad \underline{e}^{\varphi_\alpha} \in \Omega \tag{II .55}$$

By using the property of the Green's function:

$$\mathbf{G}_{ij,kl}^{\varphi_\alpha}(\underline{e}^{\varphi_\alpha} - \underline{e}'^{\varphi_\alpha}) = \frac{\partial^2}{\partial \underline{e}_k^{\varphi_\alpha} \partial \underline{e}_l^{\varphi_\alpha}} \mathbf{G}_{ij}^{\varphi_\alpha}(\underline{e}^{\varphi_\alpha} - \underline{e}'^{\varphi_\alpha}) \tag{II .56}$$

The equation (II .55) can be expressed:

$$\mathbb{M}_{ijkl}^{\varphi_\alpha}(\underline{e}^{\varphi_\alpha}) = -\frac{\partial}{\partial \underline{e}_l^{\varphi_\alpha}} \int_\Omega \frac{\partial \mathbf{G}_{ij}^{\varphi_\alpha}(\underline{e}^{\varphi_\alpha} - \underline{e}'^{\varphi_\alpha})}{\partial \underline{e}_k^{\varphi_\alpha}} d\Omega_{e'}, \quad \underline{e}^{\varphi_\alpha} \in \Omega \tag{II .57}$$

The second-order Green function $\mathbf{G}_{ij,kl}^{\varphi_\alpha}(\underline{e}^{\varphi_\alpha} - \underline{e}'^{\varphi_\alpha})$ expresses the displacement at point $\underline{e}^{\varphi_\alpha}$ in linear elastic solid medium of stiffness $\mathbb{C}_s$ resulting from a unit concentrated force applied at a point $\underline{e}'^{\varphi_\alpha}$ in the medium.

As discussed in the previous works ([Eshelby, 1957]), ([Mura, 1987]), ([Withers, 1989]) and ([Giraud et al., 2007]), the volume element can be defined as(see Figure II .7):

$$d\Omega_{e'} = d\Omega(\underline{r}^{\varphi_\alpha}) = dr^{\varphi_\alpha} \tag{II .58}$$

with $\underline{r}^{\varphi_\alpha} = \underline{e}'^{\varphi_\alpha} - \underline{e}^{\varphi_\alpha}$, $r^{\varphi_\alpha} = \mid \underline{e}'^{\varphi_\alpha} - \underline{e}^{\varphi_\alpha} \mid$.

The volume integral (II .57) can be written as a surface integral in terms of the solid angle $d\omega$:

$$dS = (r^{\varphi_\alpha})^2 dr^{\varphi_\alpha} d\omega \tag{II .59}$$

© 2016 Tous droits réservés.

doc.univ-lille1.fr

Thèse de Mei Qi, Lille 1, 2016

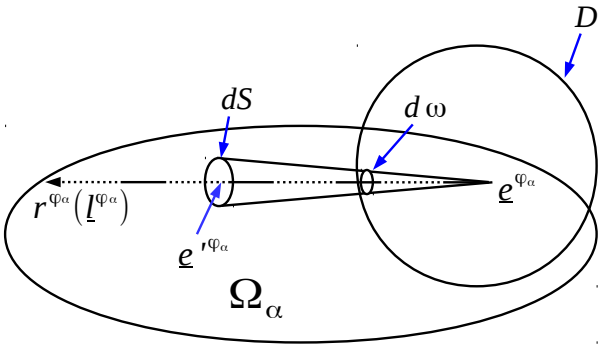

Figure II .7: The domain of the spheroidal inclusion and a unit sphere centred at the origin $\underline{e}'^{\varphi_\alpha}$ in the $r^{\varphi_\alpha}(\underline{l}^{\varphi_\alpha})$-space Green's function.

We define the unit vector $\underline{l}^{\varphi_\alpha}$ drawn from the point of interest $\underline{e}^{\varphi_\alpha}$:

$$\underline{l}^{\varphi_\alpha} = \frac{\underline{e}'^{\varphi_\alpha} - \underline{e}^{\varphi_\alpha}}{\mid \underline{e}'^{\varphi_\alpha} - \underline{e}^{\varphi_\alpha} \mid} = (\underline{l}_1^{\varphi_\alpha}, \underline{l}_2^{\varphi_\alpha}, \underline{l}_3^{\varphi_\alpha}) \tag{II .60}$$

The derivatives of the Green's functions $\mathbf{G}_{ij}^{\varphi_\alpha}$ are expressed thanks to the $g_{ijk}^{\varphi_\alpha}$ components:

$$\begin{aligned} g_{ijk}^{\varphi_\alpha}(\underline{l}^{\varphi_\alpha}) &= (r^{\varphi_\alpha})^2 \mathbf{G}_{ij,k}^{\varphi_\alpha}(\underline{e}^{\varphi_\alpha} - \underline{e}'^{\varphi_\alpha}) \\ &= -(r^{\varphi_\alpha})^2 \mathbf{G}_{ij,k}^{\varphi_\alpha}(\underline{r}^{\varphi_\alpha}) \end{aligned} \tag{II .61}$$

with the property of the Green's function $\mathbf{G}_{ij,k}^{\varphi_\alpha}(\underline{e}^{\varphi_\alpha} - \underline{e}'^{\varphi_\alpha}) = -\mathbf{G}_{ij,k}^{\varphi_\alpha}(\underline{e}'^{\varphi_\alpha} - \underline{e}^{\varphi_\alpha})$.

The components $g_{ijk}^{\varphi_\alpha}$ are given in the (Appendix: B). By using (II .61), (II .57) it becomes:

$$\mathbb{M}_{ijkl}^{\varphi_\alpha}(\underline{e}^{\varphi_\alpha}) = -\frac{\partial}{\partial \underline{e}_l^{\varphi_\alpha}} \int_D r^{\varphi_\alpha}(\underline{l}^{\varphi_\alpha}) g_{ijk}^{\varphi_\alpha}(\underline{l}^{\varphi_\alpha}) d\omega \tag{II .62}$$

D denotes the surface of an unit sphere centred at the point $\underline{e}^{\varphi_\alpha}$ ([Mura, 1987]) and $r^{\varphi_\alpha}(\underline{l}^{\varphi_\alpha})$ defines the boundary of the oblate or prolate spheroid and is given by the positive root equation:

$$\frac{(\underline{e}_1^\alpha + r^{\varphi_\alpha}\underline{l}_1^\alpha)^2 + (\underline{e}_2^\alpha + r^{\varphi_\alpha}\underline{l}_2^\alpha)^2}{a^2} + \frac{(\underline{e}_3^\alpha + r^{\varphi_\alpha}\underline{l}_3^\alpha)^2}{a^2\epsilon^2} = 1 \tag{II .63}$$

© 2016 Tous droits réservés.

doc.univ-lille1.fr

Thèse de Mei Qi, Lille 1, 2016

which is given by:

$$r^{\varphi_\alpha}(\underline{l}^{\varphi_\alpha}) = -\frac{f_\alpha}{g_\alpha} + (\frac{f_\alpha^2}{g_\alpha^2} + \frac{\mathsf{e}_\alpha}{g_\alpha})^{1/2} \tag{II .64}$$

with,

$$\mathsf{e}_\alpha = 1 - (\frac{(\underline{e}_1^\alpha)^2 + (\underline{e}_2^\alpha)^2}{a^2} + \frac{(\underline{e}_3^\alpha)^2}{a^2\epsilon^2}) \tag{II .65}$$

$$f_\alpha = \frac{\underline{e}_1^\alpha \underline{l}_1^\alpha + \underline{e}_2^\alpha \underline{l}_2^\alpha}{a^2} + \frac{\underline{e}_3^\alpha \underline{l}_3^\alpha}{a^2\epsilon^2} \tag{II .66}$$

$$g_\alpha = \frac{(\underline{l}_1^\alpha)^2 + (\underline{l}_2^\alpha)^2}{a^2} + \frac{(\underline{l}_3^\alpha)^2}{a^2\epsilon^2} \tag{II .67}$$

By using the transformation rules (II .50-II .52), e_α, f_α, g_α can be written as functions of $\underline{e}_i^{\varphi_\alpha}$ and $\underline{l}_i^{\varphi_\alpha}$ coordinates:

$$\begin{aligned}
a^2\epsilon^2\mathsf{e}_\alpha &= a^2\epsilon^2 - \epsilon^2(\underline{e}_1^{\varphi_\alpha})^2 - (\underline{e}_3^{\varphi_\alpha} cos(\theta_\alpha) + \underline{e}_2^{\varphi_\alpha} sin(\theta_\alpha))^2 \\
&\quad -\epsilon^2(\underline{e}_2^{\varphi_\alpha} cos(\theta_\alpha) - \underline{e}_3^{\varphi_\alpha} sin(\theta_\alpha))^2 \\
a^2\epsilon^2 f_\alpha &= \epsilon^2 \underline{e}_1^{\varphi_\alpha} \underline{l}_1^{\varphi_\alpha} + (\underline{l}_3^{\varphi_\alpha} cos(\theta_\alpha) + \underline{l}_2^{\varphi_\alpha} sin(\theta_\alpha))(\underline{e}_3^{\varphi_\alpha} cos(\theta_\alpha) + \underline{e}_2^{\varphi_\alpha} sin(\theta_\alpha)) \\
&\quad +(\epsilon^2(\underline{l}_2^{\varphi_\alpha} cos(\theta_\alpha) - \underline{l}_3^{\varphi_\alpha} sin(\theta_\alpha)(\underline{e}_2^{\varphi_\alpha} cos(\theta_\alpha) - \underline{e}_3^{\varphi_\alpha} sin(\theta_\alpha)) \\
a^2\epsilon^2 g_\alpha &= \epsilon^2(\underline{l}_1^{\varphi_\alpha})^2 + (\underline{l}_3^{\varphi_\alpha} cos(\theta_\alpha) + \underline{l}_2^{\varphi_\alpha} sin(\theta_\alpha))^2 \\
&\quad +\epsilon^2(\underline{l}_2^{\varphi_\alpha} cos(\theta_\alpha) - \underline{l}_3^{\varphi_\alpha} sin(\theta_\alpha))^2
\end{aligned} \tag{II .68}$$

When we take equation (II .64) into equation (II .62), we obtain:

© 2016 Tous droits réservés.

doc.univ-lille1.fr

Thèse de Mei Qi, Lille 1, 2016

$$\mathbb{M}^{\varphi_\alpha}_{ijkl}(\underline{e}^{\varphi_\alpha}) = \frac{\partial}{\partial \underline{e}^{\varphi_\alpha}_l}\int_D (\frac{f_\alpha}{g_\alpha}) g^{\varphi_\alpha}_{ijk}(\underline{l}^{\varphi_\alpha})d\omega - \frac{\partial}{\partial \underline{e}^{\varphi_\alpha}_l}\int_D (\frac{f^2_\alpha}{g^2_\alpha} + \frac{\mathsf{e}_\alpha}{g_\alpha})^{1/2} g^{\varphi_\alpha}_{ijk}(\underline{l}^{\varphi_\alpha})d\omega \qquad \text{(II .69)}$$

In this relation, we can verify that:

$$\int_D (\frac{f^2_\alpha}{g^2_\alpha} + \frac{\mathsf{e}_\alpha}{g_\alpha})^{1/2} g^{\varphi_\alpha}_{ijk}(\underline{l}^{\varphi_\alpha})d\omega = 0 \qquad \text{(II .70)}$$

Because $(\frac{f^2_\alpha}{g^2_\alpha} + \frac{\mathsf{e}_\alpha}{g_\alpha})^{1/2}$ is even in $\underline{l}^{\varphi_\alpha}$ and $g^{\varphi_\alpha}_{ijk}$ and is odd in $\underline{l}^{\varphi_\alpha}$ according to the relations (II .68). So equation (II .62) can be written as follows:

$$\mathbb{M}^{\varphi_\alpha}_{ijkl}(\underline{e}^{\varphi_\alpha}) = \frac{\partial}{\partial \underline{e}^{\varphi_\alpha}_l}\int_D \frac{f_\alpha}{g_\alpha} g^{\varphi_\alpha}_{ijk}(\underline{l}^{\varphi_\alpha})d\omega \qquad \text{(II .71)}$$

As in the reference of ([Eshelby, 1957]) for the isotropic matrix and ([Withers, 1989]) for the transversely isotropic matrix with an ellipsoidal inclusion aligned in the direction of the material, the ratio f_α/g_α is linear function of the coordinates $\underline{e}^{\varphi_\alpha}_i$, which can be developed in the relations (II .68) to (as [Giraud et al., 2007]):

$$\begin{aligned}
a^2\epsilon^2 \frac{\partial f_\alpha}{\partial \underline{e}^{\varphi_\alpha}_1} &= \epsilon^2 \underline{l}^{\varphi_\alpha}_1 \\
a^2\epsilon^2 \frac{\partial f_\alpha}{\partial \underline{e}^{\varphi_\alpha}_2} &= \tfrac{1}{2}((1+\epsilon^2)\underline{l}^{\varphi_\alpha}_2 + (1-\epsilon^2)(\underline{l}^{\varphi_\alpha}_3 sin(2\theta_\alpha) - \underline{l}^{\varphi_\alpha}_2 cos(2\theta_\alpha))) \qquad \text{(II .72)} \\
a^2\epsilon^2 \frac{\partial f_\alpha}{\partial \underline{e}^{\varphi_\alpha}_3} &= \tfrac{1}{2}((1+\epsilon^2)\underline{l}^{\varphi_\alpha}_3 + (1-\epsilon^2)(\underline{l}^{\varphi_\alpha}_3 sin(2\theta_\alpha) + \underline{l}^{\varphi_\alpha}_2 cos(2\theta_\alpha)))
\end{aligned}$$

Here, we can notice that the limiting case of the penny shaped inclusion can be reduced by setting the $\epsilon \to 0$ in the relations (II .72), ones can obtain the simple relations:

$$\begin{cases}
\underline{p}^{\varphi_\alpha}_1 = 0 \\
\underline{p}^{\varphi_\alpha}_2 = 1/(\underline{l}^{\varphi_\alpha}_2 + \underline{l}^{\varphi_\alpha}_3 cot(\theta_\alpha)) \\
\underline{p}^{\varphi_\alpha}_3 = 1/(\underline{l}^{\varphi_\alpha}_3 + \underline{l}^{\varphi_\alpha}_2 tan(\theta_\alpha))
\end{cases} \qquad \text{(II .73)}$$

By taking into account relations (II .68) and (II .72), it can reduce the coefficients $\underline{p}^{\varphi_\alpha}_i$ such as:

$$\underline{p}^{\varphi_\alpha}_i = \underline{p}^{\varphi_\alpha}_i(\theta_\alpha, \underline{l}^{\varphi_\alpha}) = \frac{1}{g_\alpha}\frac{\partial f_\alpha}{\partial \underline{e}^{\varphi_\alpha}_i} \qquad \text{(II .74)}$$

© 2016 Tous droits réservés.

doc.univ-lille1.fr

Thèse de Mei Qi, Lille 1, 2016

The detail of the coefficients $\underline{p}_i^{\varphi_\alpha}$ can be find in (Appendix B).

Taking into account the coefficients $\underline{p}_i^{\varphi_\alpha}$ into (II .71) one obtains:

$$\mathbb{M}_{ijkl}^{\varphi_\alpha}(\theta_\alpha) = \int_D \underline{p}_l^{\varphi_\alpha}(\theta_\alpha, \underline{l}^{\varphi_\alpha}) g_{ijk}^{\varphi_\alpha}(\underline{l}^{\varphi_\alpha}) d\omega \tag{II .75}$$

The $\mathbb{M}$ tensor respects the symmetry (36 components are independent):

$$\mathbb{M}_{ijkl}^{\varphi_\alpha} = \mathbb{M}_{jikl}^{\varphi_\alpha} = \mathbb{M}_{ijlk}^{\varphi_\alpha} \tag{II .76}$$

and

$$\begin{aligned}
\mathbb{M}_{ij11}^{\varphi_\alpha}(\theta_\alpha) &= \int_D \underline{p}_1^{\varphi_\alpha}(\theta_\alpha, \underline{l}^{\varphi_\alpha}) g_{ij1}^{\varphi_\alpha}(\underline{l}^{\varphi_\alpha}) d\omega \\
\mathbb{M}_{ij22}^{\varphi_\alpha}(\theta_\alpha) &= \int_D \underline{p}_2^{\varphi_\alpha}(\theta_\alpha, \underline{l}^{\varphi_\alpha}) g_{ij2}^{\varphi_\alpha}(\underline{l}^{\varphi_\alpha}) d\omega \\
\mathbb{M}_{ij33}^{\varphi_\alpha}(\theta_\alpha) &= \int_D \underline{p}_3^{\varphi_\alpha}(\theta_\alpha, \underline{l}^{\varphi_\alpha}) g_{ij3}^{\varphi_\alpha}(\underline{l}^{\varphi_\alpha}) d\omega \\
\mathbb{M}_{ij12}^{\varphi_\alpha}(\theta_\alpha) &= \int_D \underline{p}_2^{\varphi_\alpha}(\theta_\alpha, \underline{l}^{\varphi_\alpha}) g_{ij1}^{\varphi_\alpha}(\underline{l}^{\varphi_\alpha}) d\omega \\
\mathbb{M}_{ij23}^{\varphi_\alpha}(\theta_\alpha) &= \int_D \underline{p}_3^{\varphi_\alpha}(\theta_\alpha, \underline{l}^{\varphi_\alpha}) g_{ij2}^{\varphi_\alpha}(\underline{l}^{\varphi_\alpha}) d\omega \\
\mathbb{M}_{ij31}^{\varphi_\alpha}(\theta_\alpha) &= \int_D \underline{p}_1^{\varphi_\alpha}(\theta_\alpha, \underline{l}^{\varphi_\alpha}) g_{ij3}^{\varphi_\alpha}(\underline{l}^{\varphi_\alpha}) d\omega \\
(m,n) &= (11, 22, 33, 12, 23, 31)
\end{aligned} \tag{II .77}$$

After the mathematical manipulations, the general form of the Hill tensor in intermediate coordinates and in terms of the arguments θ_α and $\underline{l}_i^{\varphi_\alpha}$ can be written as ([Giraud et al., 2007]) :

$$\mathbb{P}_{ijkl}^{\varphi_\alpha} = \int_D (\underline{p}_l^{\varphi_\alpha} g_{kij}^{\varphi_\alpha} + \underline{p}_l^{\varphi_\alpha} g_{kji}^{\varphi_\alpha} + \underline{p}_k^{\varphi_\alpha} g_{lij}^{\varphi_\alpha} + \underline{p}_k^{\varphi_\alpha} g_{lji}^{\varphi_\alpha}) d\omega \tag{II .78}$$

© 2016 Tous droits réservés.

doc.univ-lille1.fr

Thèse de Mei Qi, Lille 1, 2016

where the expression for $\underline{p}_i^{\varphi_\alpha} = \underline{p}_i^{\varphi_\alpha}(\theta_\alpha, \underline{l}^{\varphi_\alpha}, \epsilon)$ and $g_{ijk}^{\varphi_\alpha} = g_{ijk}^{\varphi_\alpha}(l^{\varphi_\alpha}, \mathbb{C}_s)$, (see Appendix B for detailed expression of $\underline{p}_i$ and derivatives of Green functions g_{ijk}).

The components of $\mathbb{P}$ tensor has the major and minor symmetries, there are 21 independent components:

$$\mathbb{P}_{ijkl}^{\varphi_\alpha} = \mathbb{P}_{jikl}^{\varphi_\alpha} = \mathbb{P}_{ijlk}^{\varphi_\alpha}\ , \quad \mathbb{P}_{ijkl}^{\varphi_\alpha} = \mathbb{P}_{klij}^{\varphi_\alpha} \tag{II .79}$$

The 21 independent components of the Hill tensor $\mathbb{P}$ can be defined as a 6×6 matrix ([Walpole, 1984]):

$$\mathbb{P}_{ijkl}^{\varphi_\alpha} = \begin{bmatrix} P_{1111}^{\varphi_\alpha} & P_{1122}^{\varphi_\alpha} & P_{1133}^{\varphi_\alpha} & \sqrt{2}P_{1123}^{\varphi_\alpha} & \sqrt{2}P_{1131}^{\varphi_\alpha} & \sqrt{2}P_{1112}^{\varphi_\alpha} \\ P_{2211}^{\varphi_\alpha} & P_{2222}^{\varphi_\alpha} & P_{2233}^{\varphi_\alpha} & \sqrt{2}P_{2223}^{\varphi_\alpha} & \sqrt{2}P_{2231}^{\varphi_\alpha} & \sqrt{2}P_{2212}^{\varphi_\alpha} \\ P_{3311}^{\varphi_\alpha} & P_{3322}^{\varphi_\alpha} & P_{3333}^{\varphi_\alpha} & \sqrt{2}P_{3323}^{\varphi_\alpha} & \sqrt{2}P_{3331}^{\varphi_\alpha} & \sqrt{2}P_{3312}^{\varphi_\alpha} \\ \sqrt{2}P_{2311}^{\varphi_\alpha} & \sqrt{2}P_{2322}^{\varphi_\alpha} & \sqrt{2}P_{2333}^{\varphi_\alpha} & 2P_{2323}^{\varphi_\alpha} & 2P_{2331}^{\varphi_\alpha} & 2P_{2312}^{\varphi_\alpha} \\ \sqrt{2}P_{3111}^{\varphi_\alpha} & \sqrt{2}P_{3122}^{\varphi_\alpha} & \sqrt{2}P_{3133}^{\varphi_\alpha} & 2P_{3123}^{\varphi_\alpha} & 2P_{3131}^{\varphi_\alpha} & 2P_{3112}^{\varphi_\alpha} \\ \sqrt{2}P_{1211}^{\varphi_\alpha} & \sqrt{2}P_{1222}^{\varphi_\alpha} & \sqrt{2}P_{1233}^{\varphi_\alpha} & 2P_{1223}^{\varphi_\alpha} & 2P_{1231}^{\varphi_\alpha} & 2P_{1212}^{\varphi_\alpha} \end{bmatrix} \tag{II .80}$$

It is interesting to notice that the Hill tensor $\mathbb{P}$ is symmetry about a plane with the relation II .79. That means that it is monoclinic . And then it can be characterized by 13 independent components in $\underline{e}_i^{\varphi_\alpha}$ system coordinates:

$$\mathbb{P}_{ijkl}^{\varphi_\alpha} = \begin{bmatrix} P_{1111}^{\varphi_\alpha} & P_{1122}^{\varphi_\alpha} & P_{1133}^{\varphi_\alpha} & \sqrt{2}P_{1123}^{\varphi_\alpha} & 0 & 0 \\ P_{2211}^{\varphi_\alpha} & P_{2222}^{\varphi_\alpha} & P_{2233}^{\varphi_\alpha} & \sqrt{2}P_{2223}^{\varphi_\alpha} & 0 & 0 \\ P_{3311}^{\varphi_\alpha} & P_{3322}^{\varphi_\alpha} & P_{3333}^{\varphi_\alpha} & \sqrt{2}P_{3323}^{\varphi_\alpha} & 0 & 0 \\ \sqrt{2}P_{2311}^{\varphi_\alpha} & \sqrt{2}P_{2322}^{\varphi_\alpha} & \sqrt{2}P_{2333}^{\varphi_\alpha} & 2P_{2323}^{\varphi_\alpha} & 0 & 0 \\ 0 & 0 & 0 & 0 & 2P_{3131}^{\varphi_\alpha} & 2P_{3112}^{\varphi_\alpha} \\ 0 & 0 & 0 & 0 & 2P_{1231}^{\varphi_\alpha} & 2P_{1212}^{\varphi_\alpha} \end{bmatrix} \tag{II .81}$$

By taking into account the relation (II .73) into (II .71), it can be shown that Hill tensor $\mathbb{P}$ of an arbitrary oriented penny shaped inclusion by nine independent components:

© 2016 Tous droits réservés.

doc.univ-lille1.fr

Thèse de Mei Qi, Lille 1, 2016

$$\mathbb{P}^{\varphi_\alpha}_{ijkl} = \begin{bmatrix} 0 & 0 & 0 & 0 & 0 & 0 \\ 0 & P^{\varphi_\alpha}_{2222} & P^{\varphi_\alpha}_{2233} & \sqrt{2}P^{\varphi_\alpha}_{2223} & 0 & 0 \\ 0 & P^{\varphi_\alpha}_{3322} & P^{\varphi_\alpha}_{3333} & \sqrt{2}P^{\varphi_\alpha}_{3323} & 0 & 0 \\ 0 & \sqrt{2}P^{\varphi_\alpha}_{2322} & \sqrt{2}P^{\varphi_\alpha}_{2333} & 2P^{\varphi_\alpha}_{2323} & 0 & 0 \\ 0 & 0 & 0 & 0 & 2P^{\varphi_\alpha}_{3131} & 2P^{\varphi_\alpha}_{3112} \\ 0 & 0 & 0 & 0 & 2P^{\varphi_\alpha}_{1231} & 2P^{\varphi_\alpha}_{1212} \end{bmatrix} \tag{II .82}$$

For the aim to solve the equation (V .20), the unit vector $\underline{l}^{\varphi_\alpha}_i$ can be expressed in terms of two angles characterizing spherical coordinates:

$$\begin{cases} \underline{l}^{\varphi_\alpha}_1 = sin(\psi)cos(\zeta) \\ \underline{l}^{\varphi_\alpha}_2 = sin(\psi)sin(\zeta) \\ \underline{l}^{\varphi_\alpha}_3 = cos(\psi) \end{cases} \tag{II .83}$$

and the integral on the surface of an unit sphere D can be expressed as:

$$\int_D \mathbb{F}(\theta_\alpha, \underline{l}^{\varphi_\alpha})d\omega = \int_{\zeta=0}^{2\pi}\int_{\psi=0}^{\pi} \mathbb{F}(\theta_\alpha, \psi, \zeta)sin(\psi)d\psi d\zeta \tag{II .84}$$

Finally, the Hill tensor can be evaluated numerically using Gauss-Legendre quadrature method in terms of the integration angles ζ in the intervals $[0, 2\pi]$ and ψ in the intervals $[0, \pi]$. The evaluation of the Hill tensor in the intermediate coordinate system depends on the aspect ratio of the inclusion ϵ, the angle θ^α of the inclusion, and the elastic properties of the matrix:

$$\mathbb{P}^{\varphi_\alpha}_{ijkl} = \mathbb{P}^{\varphi_\alpha}_{ijkl}(\epsilon, \theta_\alpha, \mathbb{C}_s) \tag{II .85}$$

3.3.3 Numerical calculations

In order to use Gauss-Legendre quadrature method which is an approximation of the definite integral of a function to evaluate the Hill tensor in the intermediate system, the formulation (V .22) which is the double integral on the surface of an unit sphere D can be stated as a weighted sum of function values at specified points within the domain of integration. By using the spheroidal coordinates, we obtain:

$$\mathbb{P}^{\varphi_\alpha}_{ijkl}(\theta_\alpha) \approx \sum_{k=1}^{N^G_\zeta}\sum_{l=1}^{N^G_\psi} w^\zeta_k w^\psi_l \mathbb{G}^{\varphi_\alpha}_{ijkl}(\theta_\alpha, \zeta^G_l, \psi^G_k)sin(\psi^G_k) \tag{II .86}$$

© 2016 Tous droits réservés. doc.univ-lille1.fr

Thèse de Mei Qi, Lille 1, 2016

where w_k^{ζ}, w_l^{ψ}, ζ_l^G, ψ_k^G denote perspectively the Gauss-Legendre weights and coordinates corresponding to the N_{ζ}^G and N_{ψ}^G integrating points which are comprised in the intervals $[0, 2\pi]$ (ζ angle) and $[0, \pi]$ (ψ angle) as previously mentioned. The $\mathbb{G}_{ijkl}^{\varphi_\alpha}$ coefficients can be given by the relation (II .78). The unit vector components $\underline{l}^{\varphi_\alpha}$ in the $\mathbb{G}_{ijkl}^{\varphi_\alpha}$ coefficients defined by relations (II .83) as the functions of angles ψ and ζ, are introduced into the relations (II .65)-(II .72) and also in the relations presented in the (Appendix B) which are necessary to compute $\mathbb{G}_{ijkl}^{\varphi_\alpha}$ coefficients in the relation (II .78).

Finally, the numerical values of $\mathbb{P}_{ijkl}^{\varphi_\alpha}$ components are computed by using the Gaussian quadrature method (see: (II .86)). The numerical calculations have been achieved by using Fortran software. 5 integrations points of Gaussian quadrature in each subinterval were adopted, and we take the relation $N_{\zeta}^G = 2N_{\psi}^G$ in all cases in a division of intervals $[0, 2\pi]$ and $[0, \pi]$ respectively.

3.3.4 Hill tensor in global coordinates

Now, we consider the Hill tensor in global coordinates. The transformation rules between $\underline{e}_i$ and $\underline{e}^{\varphi_\alpha}$ coordinates are used to express the components of a fourth-order tensor $\mathbb{P}_{ijkl}$. It can be written in the following form:

$$\mathbb{P} = \mathbb{P}_{pqrs}\underline{n}_p \otimes \underline{n}_q \otimes \underline{n}_r \otimes \underline{n}_s = \mathbb{P}_{ijkl}^{\varphi_\alpha}\underline{n}_i^{\varphi_\alpha} \otimes \underline{n}_j^{\varphi_\alpha} \otimes \underline{n}_k^{\varphi_\alpha} \otimes \underline{n}_l^{\varphi_\alpha} \tag{II .87}$$

$$\mathbb{P}_{ijkl}(\theta_\alpha, \varphi_\alpha) = \mathbf{Q}_{p,i}^{\varphi_\alpha}(\varphi_\alpha)\mathbf{Q}_{q,j}^{\varphi_\alpha}(\varphi_\alpha)\mathbf{Q}_{r,k}^{\varphi_\alpha}(\varphi_\alpha)\mathbf{Q}_{s,l}^{\varphi_\alpha}(\varphi_\alpha)\mathbb{P}_{pqrs}^{\theta_\alpha} \tag{II .88}$$

It is interesting to notice that due to this operation of transformation rules, we achieved to evaluate the Hill tensor in 3D conditions in the case of random distributions of spheroidal inclusion in a transversely isotropic matrix. Two angles θ_α, φ_α are taken into account to calculation the Hill tensor in the global coordinates. The advantage to separate these two variables of functions of angles θ_α and φ_α allows to simplify the numerical calculate based on integrate of Hill tensor. It means only numerical integration on θ_α is needed.

Finally, after all these mathematical and numerical manipulations, we can conclude that there are six parameters to be determined in order to calculate numerically the Hill tensor in the case of random distributions of spheroidal inclusions in a transversely isotropic materials as shown in equation (II .89). These parameters have main influences of the calculations of the Hill tensor components. They are respectively integrating points N_{ζ}^G and N_{ψ}^G of the Gauss-Legendre method; the aspect ratio ϵ of the inclusion; two angles of the inclusion (θ_α is the angle in the local coordinates and φ_α is the angle in the global coordinates); and the elastic property of the matrix $\mathbb{C}_s$.

© 2016 Tous droits réservés.

doc.univ-lille1.fr

Thèse de Mei Qi, Lille 1, 2016

$$\mathbb{P}_{ijkl} = \mathbb{P}_{ijkl}(N_\zeta^G, N_\psi^G, \epsilon, \theta^\alpha, \varphi_\alpha, \mathbb{C}_s) \tag{II .89}$$

The influences of these parameters have been discussed in ([Giraud et al., 2007]).

4 Conclusion

This Chapter has been dedicated to present the theoretical background of homogenization methods applied to modeling micro-cracked materials. The formulations of the three different homogenization schemes, respectively the dilute scheme, MT scheme and PCW scheme, have been reviewed for the estimation of effective elastic properties of cracked materials for both open and closed cracks The key step of the homogenization procedure is to determine the strain concentration law which is based on the Hill's tensor and Eshelby's tensor. These tensors should be evaluated by suitable numerical methods in the case of initially anisotropic solid matrix. Therefore, we have adopted an efficient numerical method based on an analytical solution of Green function for three-dimensional ellipsoidal micro-cracks embedded in a transversely isotropic solid matrix. Using this method, the effective elastic properties of cracked material can be investigated by considering interactions between the initial anisotropy and induced cracks and some numerical examples will be presented in the Chapter III . A specific damage evolution criterion will be proposed to describe the progressive growth of induced cracks based on the irreversible thermodynamics framework in Chapter IV . Also, coupling between micro-crack growth and frictional sliding will taken into account in Chapter V .

© 2016 Tous droits réservés.

doc.univ-lille1.fr

Chapter III

Numerical study of effective elastic properties of initially transversely isotropic materials

Contents

1 Introduction 61

2 An approximation of limit case of tensor $\mathbb{T}$ for penny-shaped crack in a transversely isotropic material 62

3 Sensitivity study of effective elastic properties 64

3.1 Effect of crack orientation on effective elastic properties 65

3.2 Effects of micro-cracks on elastic properties in arbitrary direction . . . 70

4 Conclusion 73

1 Introduction

In this Chapter, we will investigate effects of interaction between the initial anisotropy and induced oriented micro-cracks on elastic properties of transversely isotropic materials. With the numerical method that we presented in Chapter II , the effective macroscopic elastic stiffness tensor $\mathbb{C}^{hom}$ or compliance tensor $\mathbb{S}^{hom}$ of the homogenized material will be determined through a rigorous up-scaling procedure. Three different homogenization schemes will be used and compared. In particular, a series of sensitivity studies will be presented to study influences of micro-cracks orientation and aspect ratio as well as initial anisotropy degree of matrix on macroscopic properties of cracked materials.

© 2016 Tous droits réservés.

doc.univ-lille1.fr

Thèse de Mei Qi, Lille 1, 2016

2 An approximation of limit case of tensor $\mathbb{T}$ for penny-shaped crack in a transversely isotropic material

In order to determine effective elastic properties of cracked materials using Eshelby solution based homogenization methods, micro-cracks are seen as a penny-shaped inclusion embedded in a transversely isotropic matrix. According to the homogenization procedure presented in section 2.3, the main step is to evaluate the tensor $\mathbb{T}^r = \lim_{\epsilon\to 0} \epsilon(\mathbb{I}-\mathbb{S}_\epsilon)^{-1}$ which contains the aspect ratio $\epsilon = a/c$. The aspect ratio of penny shaped cracks is generally very small. The objective here is to consider the limit case of the tensor $\mathbb{T}$ when the aspect ratio tends towards to zero. When the solid matrix is isotropic, it is possible to analytically eliminate the aspect ratio in the tensor $\mathbb{T}^r$. For the case of micro-cracks in a transversely isotropic matrix, there is no analytical solution and it is needed to find a numerical approximation for the tensor $\mathbb{T}$.

As a reference case of the numerical approximation, a simple example has been considered by [Zhu, 2006]. One family of parallel penny-shaped open cracks, with the normal vector $\underline{n} = \underline{e}_3$, is embedded in an initially isotropic elastic matrix. The non-zero components of the Eshelby tensor are given in the Walpole notation by ([Mura, 1987], [Nemat-Nasser and Hori, 1993], [Hori and Nemat-Nasser, 1983]) (more detail see I):

$$\mathbb{S}_\epsilon = (S_{1111}+S_{1122}, S_{3333}, S_{1111}-S_{1122}, 2S_{1313}, S_{3311}, S_{1133}) \qquad \text{(III .1)}$$

with

$$S_{1111} = S_{2222} = \frac{13-8\nu^s}{32(1-\nu^s)}\pi\epsilon, \qquad S_{3333} = 1-\frac{1-2\nu^s}{1-\nu^s}\frac{\pi}{4}\epsilon,$$

$$S_{1122} = S_{2211} = \frac{8\nu^s-1}{32(1-\nu^s)}\pi\epsilon, \qquad S_{1133} = S_{2233} = \frac{2\nu^s-1}{8(1-\nu^s)}\pi\epsilon, \qquad \text{(III .2)}$$

$$S_{3311} = S_{3322} = \frac{\nu^s}{1-\nu^s}(1-\frac{4\nu^s+1}{8\nu^s}\pi\epsilon), \quad S_{1212} = \frac{7-8\nu^s}{32(1-\nu^s)}\pi\epsilon,$$

$$S_{1313} = S_{2323} = \frac{1}{2}(1+\frac{\nu^s-2}{1-\nu^s}\frac{\pi}{4}\epsilon)$$

When the aspect ratio tends to 0, the limit case of the Eshelby tensor is given:

$$\lim_{\epsilon\to 0}\mathbb{S}_\epsilon = (0,1,0,1,\frac{\nu^s}{1-\nu^s},0) \qquad \text{(III .3)}$$

© 2016 Tous droits réservés. doc.univ-lille1.fr

Thèse de Mei Qi, Lille 1, 2016

According to the calculation rules of the Walpole notation, we can obtain the tensor $\mathbb{T}$ (for open cracks):

$$\begin{aligned} \mathbb{T} &= \lim_{\epsilon\to 0} \epsilon(\mathbb{I}-\mathbb{S}_\epsilon)^{-1} \\ &= \lim_{\epsilon\to 0} \epsilon(\mathbb{I}-\mathbb{S}_\epsilon)^{-1} : \mathbb{S}_\epsilon = \frac{4}{\pi}(0, \frac{(1-\nu^s)^2}{1-2\nu^s}, 0, \frac{1-\nu^s}{2-\nu^s}, \frac{\nu^s(1-\nu^s)}{1-2\nu^s}, 0) \end{aligned} \tag{III .4}$$

Now, we perform the numerical calculation of Hill tensor with the numerical method presented previously. The expression of the tensor $\mathbb{T}$ is written:

$$\mathbb{T} = \epsilon(\mathbb{I}-\mathbb{P}:\mathbb{C}^s)^{-1} \tag{III .5}$$

Numerical calculations of the tensor $\mathbb{T}$ have been realized for three different values of the aspect ratio: 10^{-1}, 10^{-2}, 10^{-3}. The two elastic constants defining the isotropic stiffness tensor $\mathbb{C}^s$ of the solid matrix are respectively $E^s = 38000MPa$ and $\nu^s = 0.2$. The comparison of the tensor $\mathbb{T}$ between numerical calculations and analytical solutions is shown in the Walpole base (we assumed that all values are smaller than $10^{-10} \approx 0$):

Table III .1: Comparison of the components of tensor $\mathbb{T}$ between the analytical solution and the numerical solutions

$\mathbb{T} = \epsilon(\mathbb{I}-\mathbb{P}:\mathbb{C}^s)^{-1}$	$T_{1111}+T_{1122}$	T_{3333}	$T_{1111}-T_{1122}$	$2T_{1313}$	T_{3311}	T_{1133}
Analytical solution $\epsilon \to 0$	0	1.356	0	0.56	0.34	0
$\epsilon = 10^{-1}$	0.106	1.414	0.106	0.682	0.2857	0
$\epsilon = 10^{-2}$	9.17×10^{-3}	1.364	9.17×10^{-3}	0.577	0.334	0
$\epsilon = 10^{-3}$	9.17×10^{-4}	1.359	9.17×10^{-4}	0.567	0.339	0

In Table III .1, the accuracy of the numerical solution in the case of $\epsilon = 10^{-2}$ and $\epsilon = 10^{-3}$ are pretty close with the analytical solution. In order to reach the needed accuracy for a lower aspect ratio, higher Gauss integration points are needed. For instance, for the aspect ratio $\epsilon = 10^{-3}$, the numerical integral method has to be optimized to increase calculation accuracy. It is 10 times longer than the aspect ratio 10^{-2}. For these reasons,

© 2016 Tous droits réservés.

doc.univ-lille1.fr

Thèse de Mei Qi, Lille 1, 2016

in the rest part of this thesis, the value $\epsilon = 10^{-2}$ with the Gauss integration points $N_\zeta^G = 200$, $N_\psi^G = 100$ will be considered for a penny-shaped inclusion in a transversely isotropic material.

3 Sensitivity study of effective elastic properties

In order to show the calculation of effective elastic properties in cracked materials using the numerical method proposed above, some numerical examples are presented here. We consider a family of parallel cracks which are embedded in a transversely isotropic solid matrix (see Fig: III .1). The global coordinates corresponding to the matrix is characterized by (e_1, e_2, e_3). $\underline{e}_3$ is the symmetry axis and the plane $\underline{e}_1 - \underline{e}_2$ is the isotropic plane of the transversely isotropic matrix. The normal vector of the micro-cracks is denoted by $\underline{n}$. The angle between the axis $\underline{e}_3$ and the normal $\underline{n}(\underline{e}_2, \underline{e}_3)$ is θ_α and the angle between the normal $\underline{n}(\underline{e}_2, \underline{e}_3)$ and the axis $\underline{e}_1$ is φ_α as shown in Fig: III .1. The effective elastic properties are evaluated as functions of the crack density parameter using three different homogenization schemes mentioned above. The five initially elastic parameters for undamaged material are respectively two principal elastic modulus (E_3, E_1), related to the axes $(\underline{e}_1, \underline{e}_2)$, two Poisson's ratios (ν_{12}, ν_{31}) and shear modulus (G_{13}). In all calculations, the initial anisotropy ratio of elastic modulus of the solid matrix is taken as $E_3/E_1 = 0.5$.

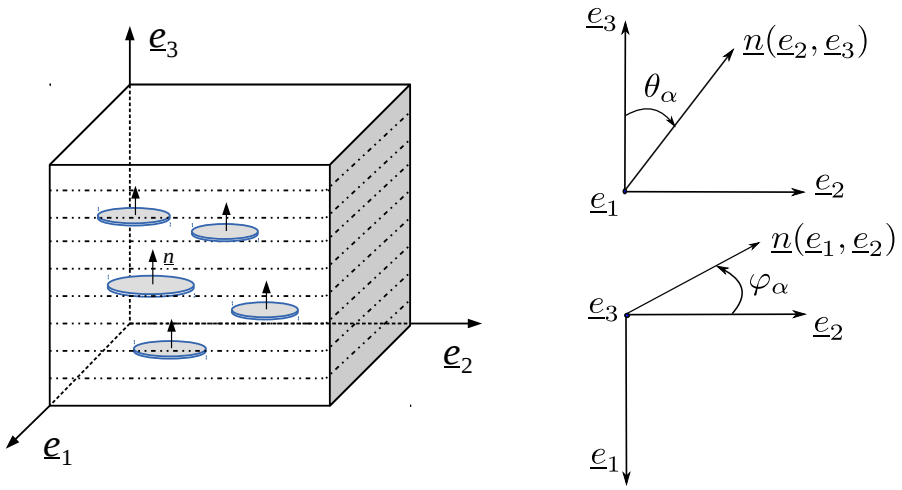

Figure III .1: One family of penny-shaped cracks in initially transversely isotropic system

© 2016 Tous droits réservés.

doc.univ-lille1.fr

Thèse de Mei Qi, Lille 1, 2016

3.1 Effect of crack orientation on effective elastic properties

In order to study effects of the crack orientation with respect to the symmetry axis of solid matrix, three different orientations are considered here (see Figure III .1). According to the different orientation of cracks, the effective elastic property of cracked material may exhibit different kinds of behaviours, such as transversely isotropic, orthotropic.

- **(1)** $\theta_\alpha = 0°, \varphi_\alpha = 0°$**:**

In this case, the presence of micro-cracks (Figure III .1) generates a transversely isotropy behavior in cracked material. This is characterized by the modification of Young modulus and shear modulus in the plan of crack. A comparison between the different homogenization schemes is shown in Figure III .2 for the longitudinal Young modulus and in Figure III .3 for the shear modulus in the plan of cracks. In these calculations, a spherical spatial distribution has been used for the PCW scheme.

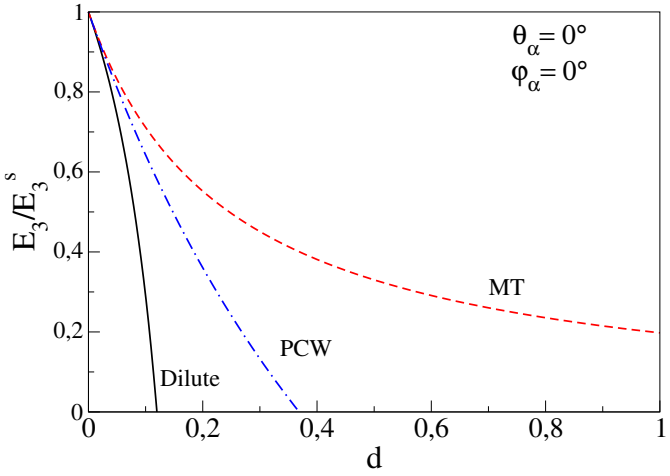

Figure III .2: Parallel cracks : Comparison of the predictions of the different schemes for the Young modulus with transversely isotropic material

In Figures III .2 and III .3, the evolutions of axial elastic modulus and shear modulus are presented as functions of crack density parameter for three different homogenization schemes. It is found that the effective elastic properties are clearly dependent on the homogenization scheme used. Physically, when the crack interaction is neglected in the dilute scheme, the degradation of elastic modulus due to crack growth is the faster than the two other schemes. The MT scheme, which partially takes into account the crack interaction, seems to lead to a stationary residual value of elastic modulus when the crack density become high. When the crack interaction and spatial distribution effects are both

© 2016 Tous droits réservés.

doc.univ-lille1.fr

Thèse de Mei Qi, Lille 1, 2016

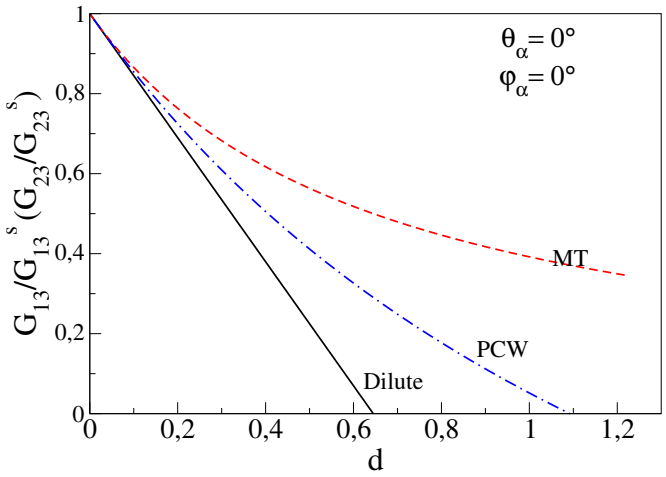

Figure III .3: Parallel cracks : Comparison of the predictions of the different schemes for the shear modulus with transversely isotropic material

considered in the PCW scheme, the elastic modulus is progressively degraded to zero when the crack density reaches some critical value.

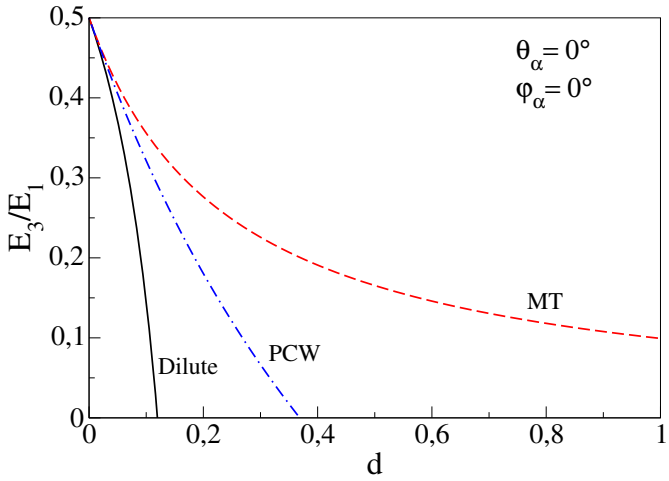

Figure III .4: Influence of cracking on the anisotropic ratio

In Figure III .4, the variation of anisotropy ratio of the elastic modulus is presented for the case of induced crack family oriented in $\theta_\alpha = 0°, \varphi_\alpha = 0°$. In this case, the induced cracks are parallel to the initial bedding planes of the solid matrix. Therefore, the induced damage does not modify the anisotropy nature of the material which remains transversely isotropic one. However, with the growth of induced cracks, the anisotropic degree is significantly increased (the ratio between the perpendicular elastic modulus E_3

© 2016 Tous droits réservés.

doc.univ-lille1.fr

Thèse de Mei Qi, Lille 1, 2016

and the parallel on E_1 or E_2 is significantly reduced). This means that the induced damage enhances the initial anisotropy of material. Further as shown in this figure III .4, the variation of material anisotropy degree is also affected by the homogenization scheme used.

Now, we will show the variations of 9 independent coefficients (respectively 3 Young's moduli E_i, 3 shear moduli G_i, and 3 Poisson ratios ν_i) as functions of the crack density parameter d. The analyse is done for the case of open cracks with the PCW estimation scheme with a spherical spatial distribution. The results are normalized with the initial values of the elastic moduli. We can see that the effective elastic properties of the cracked material keeps the transversely isotropic character as the induced crack set is parallel to the isotropic plan as shown in Figure III .5. The longitudinal Young's moduli, the shear moduli and the Poisson ratios decrease with the crack density parameter.

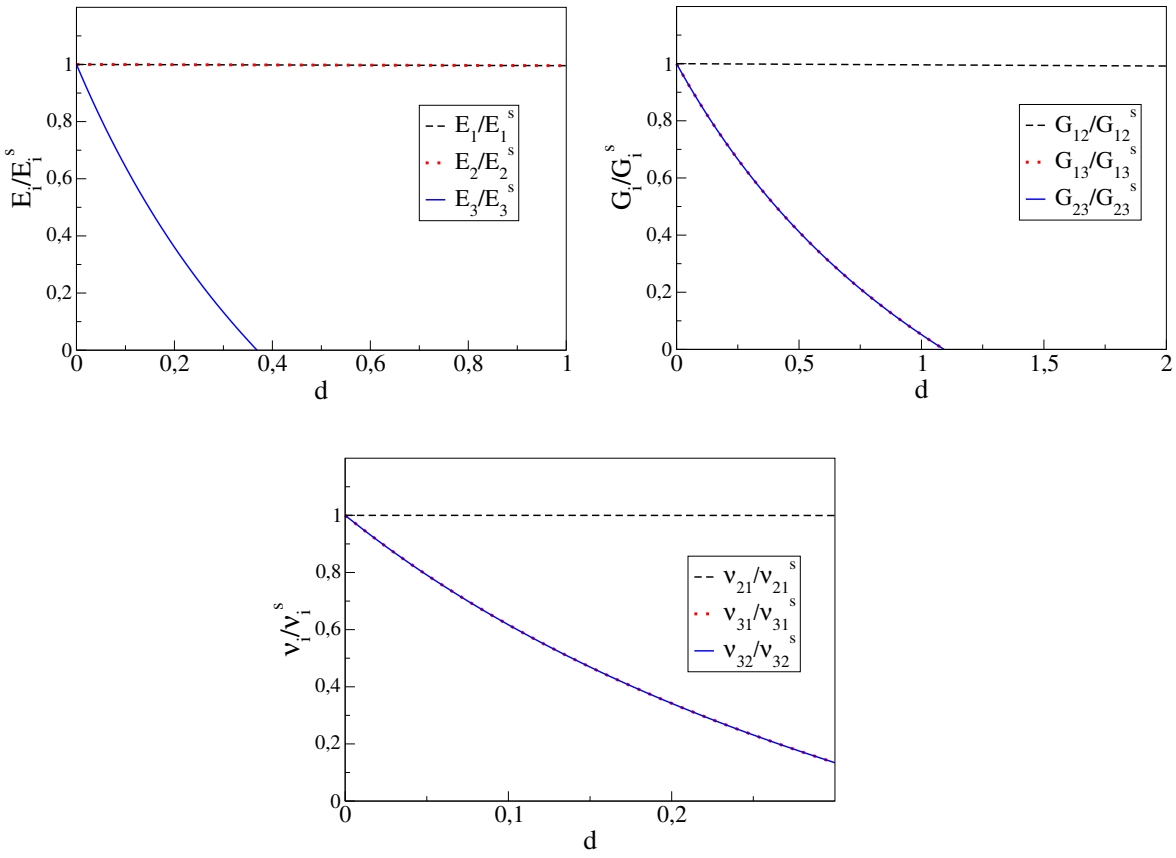

Figure III .5: Comparison of the variations of the 9 independent coefficients with the evaluation of the crack density ($\theta_\alpha = 0°, \varphi_\alpha = 0°$)

© 2016 Tous droits réservés.

doc.univ-lille1.fr

Thèse de Mei Qi, Lille 1, 2016

- **(2)** $\theta_\alpha = 45°, \varphi_\alpha = 0°$**:**

In Figure III .6, it is also shown the evolution of elastic coefficients as functions of induced crack density for the case of $\theta_\alpha = 45°, \varphi_\alpha = 0°$, obtained with the PCW scheme. In this case, as the induced crack set is inclined with respect to the initial bedding plane (see Figure III .2), the transversely isotropic property of material is changed. One can see that both axial moduli E_2 and E_3, and three shear moduli as well as one Poisson's ratio are affected by the induced cracks.

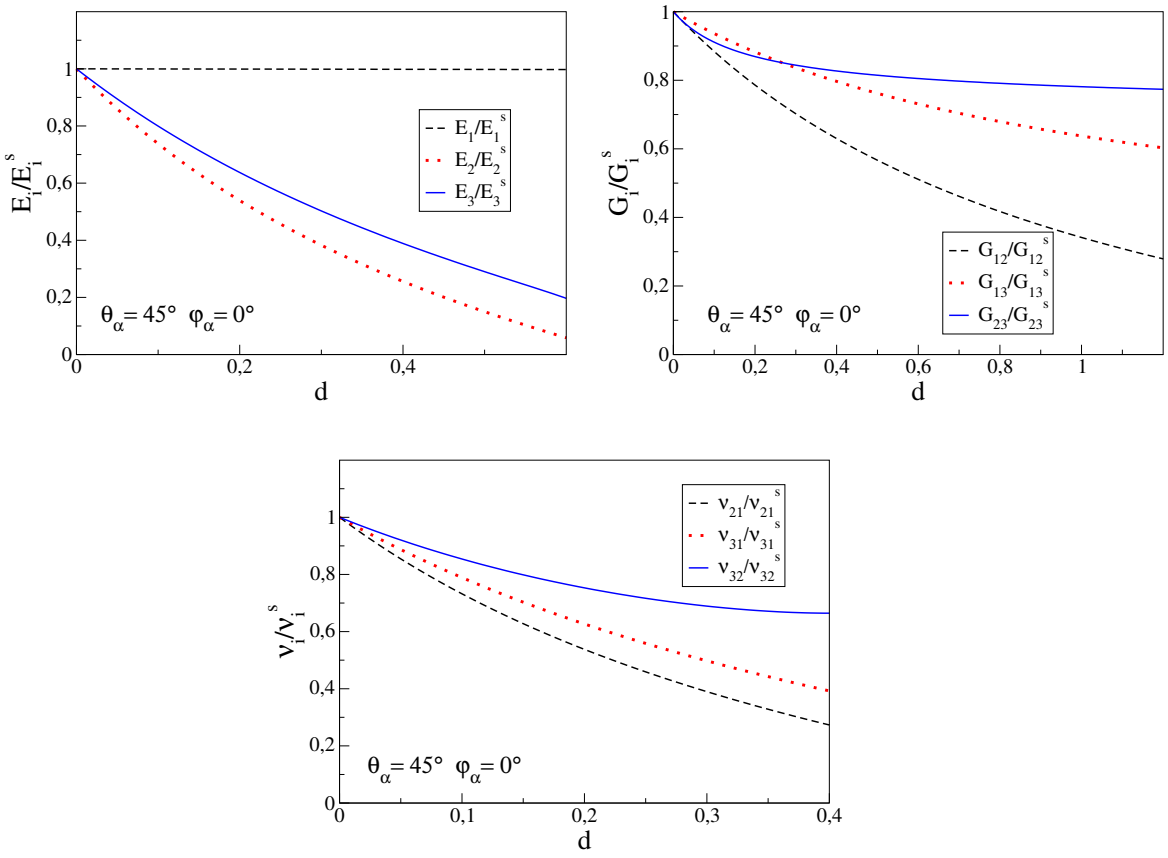

Figure III .6: Comparison of the variations of the 9 independent coefficients with the evaluation of the crack density ($\theta_\alpha = 45°, \varphi_\alpha = 0°$)

- **(3)** $\theta_\alpha = 90°, \varphi_\alpha = 0°$**:**

Consider now the crack set oriented at an angle $\pi/2$ and its unit normal vector of the cracks $\underline{n}$ coinciding with the principal direction $\underline{e}_2$. The transversely isotropic material becomes an orthotropic one due to the induced micro-cracks. We can also see that with

© 2016 Tous droits réservés.

doc.univ-lille1.fr

Thèse de Mei Qi, Lille 1, 2016

different orientations of induced micro-cracks, different elastic moduli are affected by the induced cracks III .7.

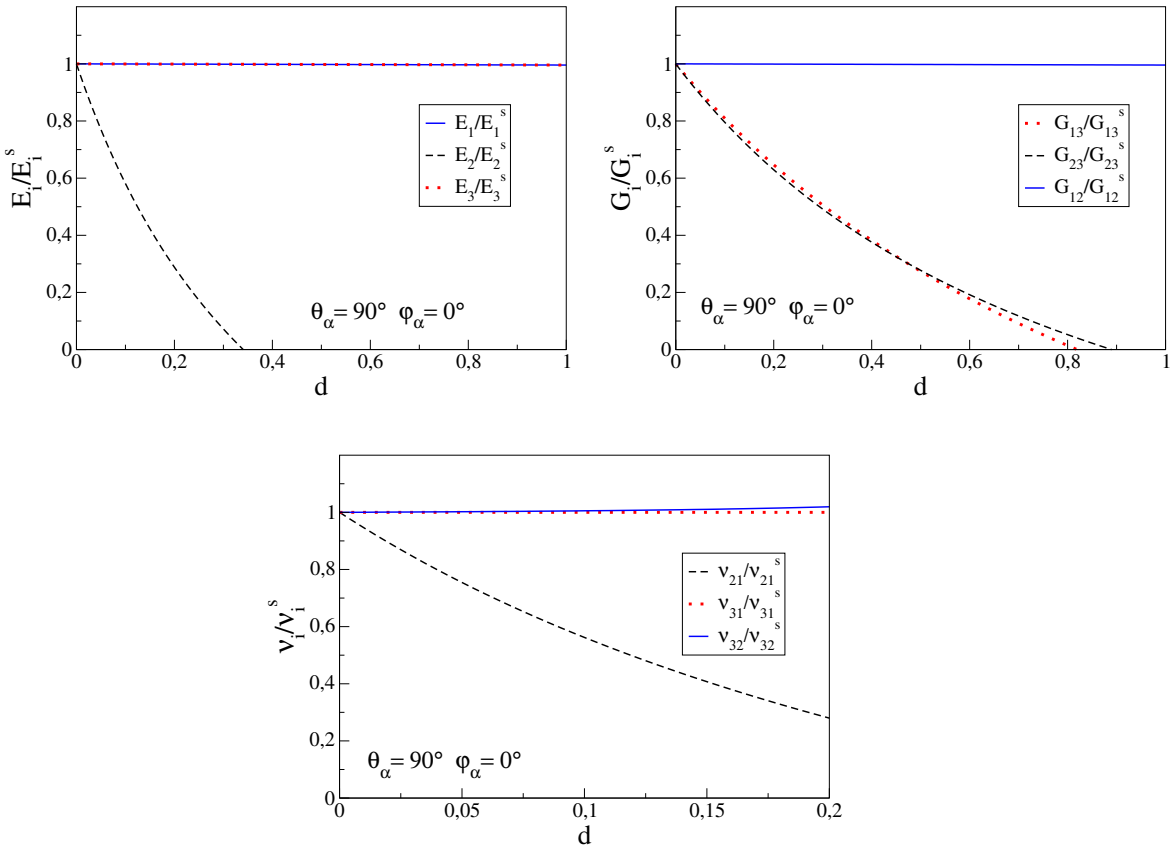

Figure III .7: Comparison of the variations of the 9 independent coefficients with the evaluation of the crack density ($\theta_\alpha = 90°, \varphi_\alpha = 0°$)

- **(4)** $\theta_\alpha = 90°, \varphi_\alpha = 90°$**:**

The same observation can be done for cracks oriented with $\pi/2$ around to the axis $\underline{e}_1$, then $\pi/2$ around to the axis $\underline{e}_3$. It is interesting to notice that the results presented in Figure III .8 can be obtained by a simple rotation of those shown in Figure III .7.

© 2016 Tous droits réservés.

doc.univ-lille1.fr

Thèse de Mei Qi, Lille 1, 2016

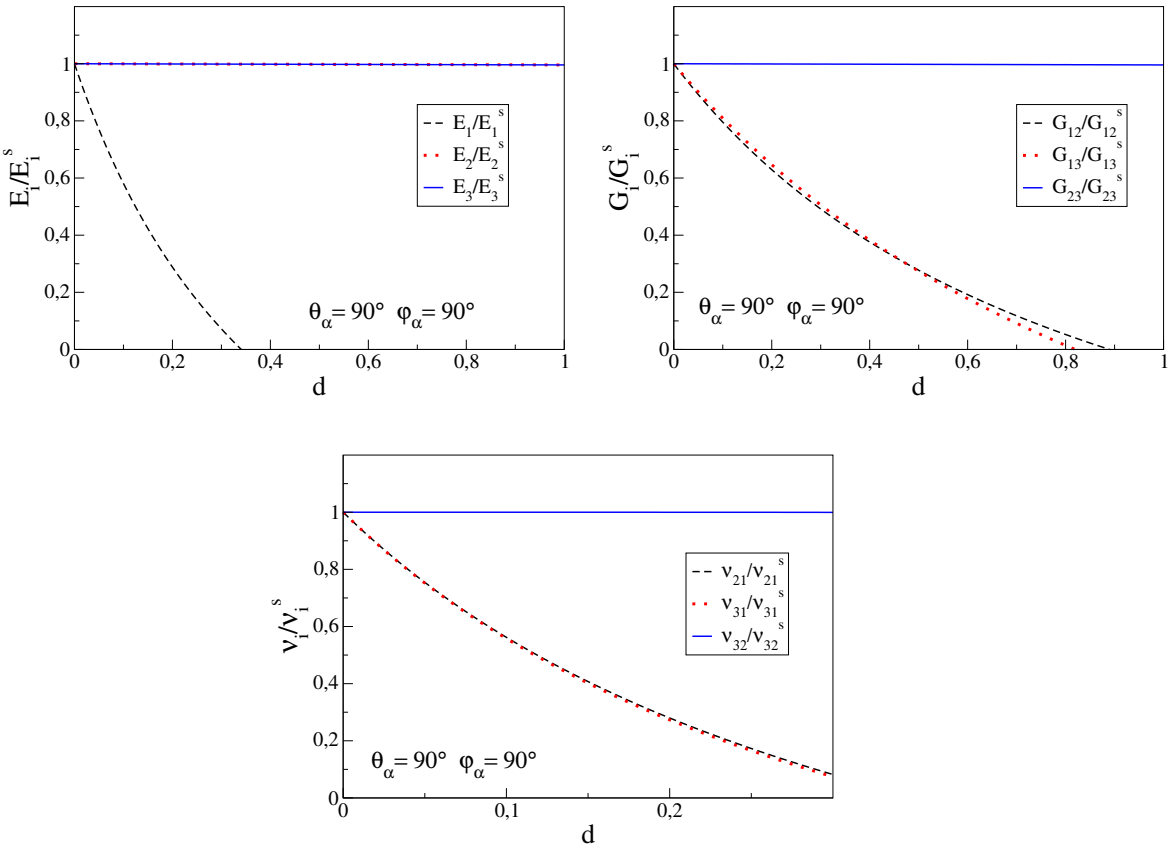

Figure III .8: Comparison of the variations of the 9 independent coefficients with the evaluation of the crack density ($\theta_\alpha = 90°, \varphi_\alpha = 90°$)

3.2 Effects of micro-cracks on elastic properties in arbitrary direction

In the previous section, we have investigated effects of induced micro-cracks on elastic properties in some privileged direction, for instance the principal directions of orthotropic materials. In some situations, it is also interesting to examine effects of induced micro-cracks on elastic properties in an arbitrary orientation. For instance, consider the effective Young's modulus $E_i^{hom}(\underline{m})$ in the direction defined by a unit vector $\underline{m}$, the Poisson ratio $\nu_i^{hom}(\underline{m},\underline{t})$ and the shear modulus $\mu_i^{hom}(\underline{m},\underline{t})$, associated to two orthogonal directions defined respectively by two unit vectors $\underline{m}$ and $\underline{t}$. These elastic properties in anisotropic materials have been previously defined by [Monchiet and Bonnet, 2012], [He and Curnier,

© 2016 Tous droits réservés.

doc.univ-lille1.fr

Thèse de Mei Qi, Lille 1, 2016

1995], [Hayes, 1972]:

$$\begin{cases} E_i^{hom}(\underline{m}) = [(\underline{m}\otimes\underline{m}) : \mathbb{S}^{hom} : (\underline{m}\otimes\underline{m})]^{-1} \\ \nu_i^{hom}(\underline{m},\underline{t}) = -\frac{(\underline{m}\otimes\underline{m}):\mathbb{S}^{hom}:(\underline{t}\otimes\underline{t})}{(\underline{m}\otimes\underline{m}):\mathbb{S}^{hom}:(\underline{m}\otimes\underline{m})} \\ \mu_i^{hom}(\underline{m},\underline{t}) = [4(\underline{m}\otimes\underline{t}) : \mathbb{S}^{hom} : (\underline{m}\otimes\underline{t})]^{-1} \end{cases} \quad \text{(III .6)}$$

As an illustration, we consider here a new system which is weakened by a set of parallel cracks, whose the unit normal $\underline{n}(\underline{e}_2,\underline{e}_3)$ associated with the angle θ_α with respect to the symmetry axis $\underline{e}_3$ of the matrix. The second angle φ_α between the unit normal $\underline{n}(\underline{e}_1,\underline{e}_2)$ and the axis $\underline{e}_2$ is always taken as zero (see Figure III .1). For each spatial direction given by a vector $\underline{m}$, taken in the plane $(\underline{e}_2,\underline{e}_3)$, values of the elastic moduli are normalized by the corresponding values of the solid matrix and presented by an unit circle.

The analyse is done for the case of open and closed cracks with 3 different schemes. We here used the cracks density $d = 0.1$.

As a simple example, only the effect of cracks on the generalized Young's modulus $E_i^{hom}(\underline{m})$ will be presented here. The results shown in Figures III .9 and III .10 represent the variation of Young's modulus $E_3^{hom}(\underline{m})$ and $E_2^{hom}(\underline{m})$ in the plane $\underline{e}_2\underline{e}_3$ for both open and closed cracks with 3 different schemes corresponding to $\theta_\alpha = 0°$. Here, a spherical distribution of the PCW scheme is considered.

The results also show that the effective elastic properties are clearly dependent on the homogenization scheme. In Fig: III .9, the results show a significant degradation of the Young modulus E_3 in the normal direction to the crack. It is interesting to note that we cannot obtain the results in Fig: III .10 with a simple rotation of the result given in Fig: III .9. It means that the degradation of elastic properties differs from one direction to the other due to the anisotropy of material and damage induced anisotropy. Further, comparisons of the Young modulus between initially isotropic and transversely isotropic matrix are shown in Appendix C.

© 2016 Tous droits réservés.

doc.univ-lille1.fr

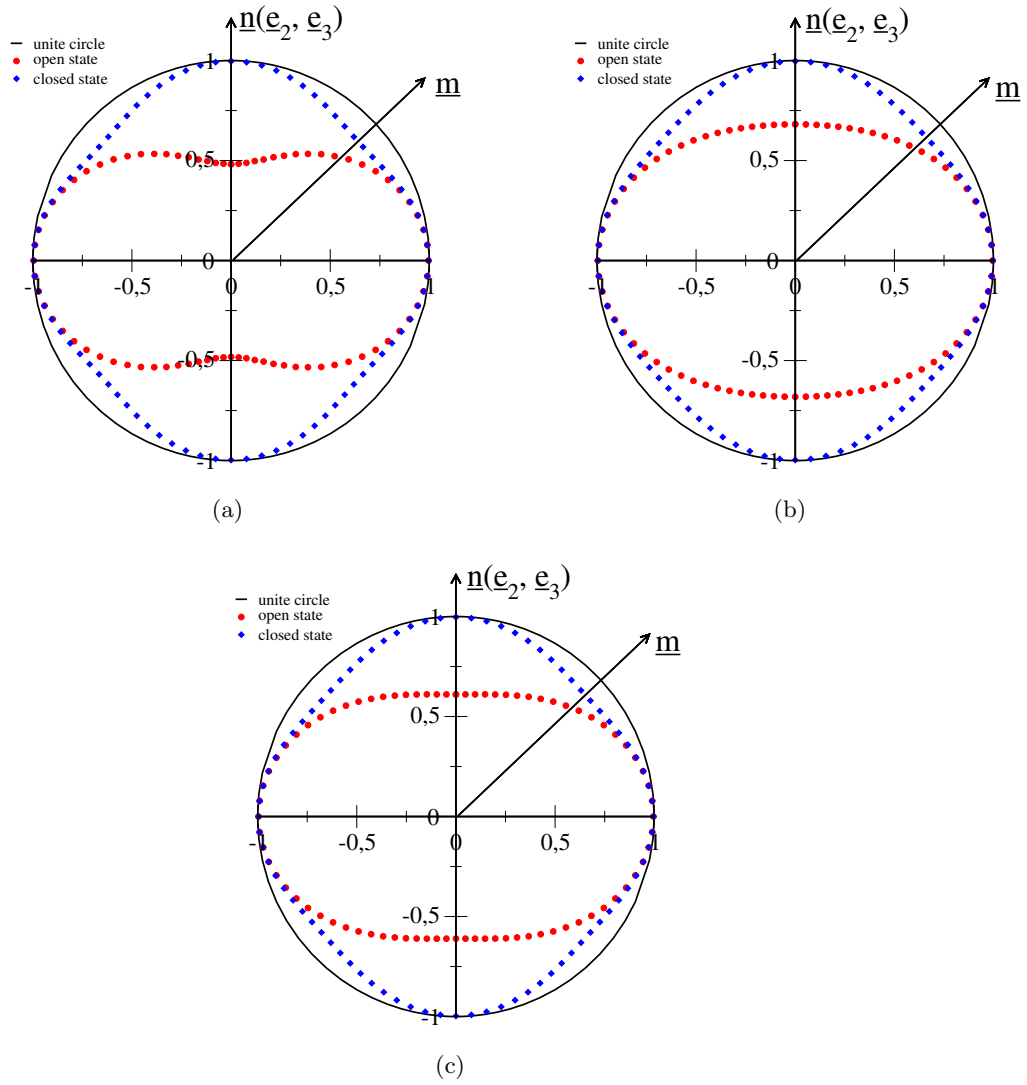

Figure III .9: Variation of the Young's moduli E_3 produced by parallel open/closed cracks media for $\theta_\alpha = 0°$: (a) Dilute scheme, (b) Mori-Tanaka scheme, (c) Ponte-Castaneda et Willis scheme.

© 2016 Tous droits réservés.

doc.univ-lille1.fr

Thèse de Mei Qi, Lille 1, 2016

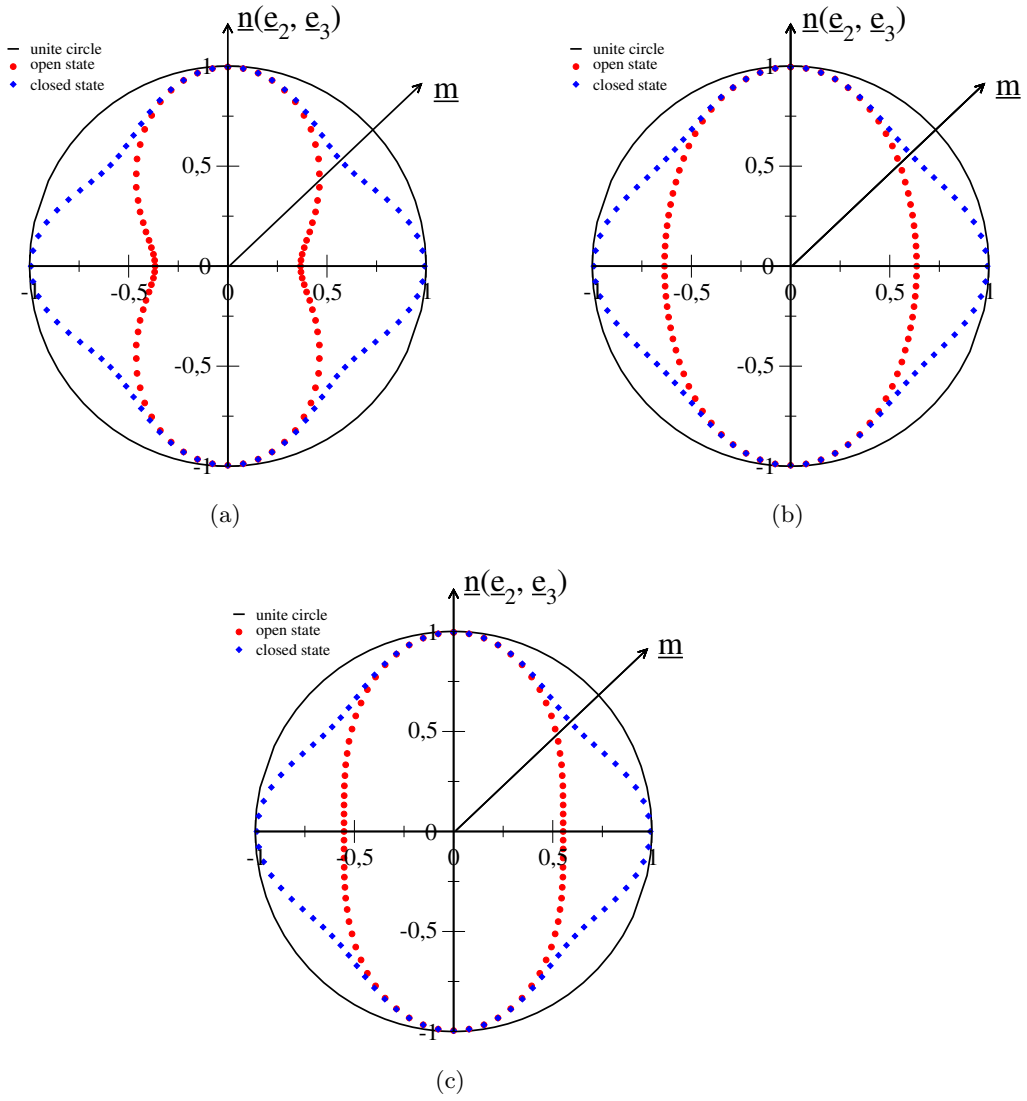

Figure III .10: Variation of the Young's moduli E_2 produced by parallel open/closed cracks media for $\theta_\alpha = 0°$: (a) Dilute scheme, (b) Mori-Tanaka scheme, (c) Ponte-Castaneda et Willis scheme.

4 Conclusion

In this Chapter, we have presented a series of numerical simulations in view of investigating effective elastic properties of cracked materials using three different homogenization schemes. The validity of numerical method used for the computation of Hill's tensor has first been checked by the comparison with analytical solution for the case of isotropic

© 2016 Tous droits réservés.

doc.univ-lille1.fr

Thèse de Mei Qi, Lille 1, 2016

matrix. Its validity for initially anisotropic matrix still needs to be verified when corresponding analytical solutions are available or with other numerical results. The numerical results obtained have clearly shown that the effective elastic properties of cracked materials are strongly influenced by homogenization schemes, then influenced by interactions between micro-cracks and spatial distribution of micro-cracks. The effective elastic properties are also effected by the initial anisotropy degree of solid matrix. Therefore, there is an interaction between the initial material anisotropy and induced anisotropy by micro-cracks. Based on these results, micro-mechanics based damage models will be developed in next Chapters after the proposition of suitable criteria for crack propagation and frictional sliding.

© 2016 Tous droits réservés.

doc.univ-lille1.fr

Chapter IV

Micromecanical damage model of transversely isotropic materials with unilateral effects

Contents

1 Introduction 75

2 Formulation of anisotropic damage model 77

2.1 Free energy and state equations 78

2.2 Damage criterion and evolution law 78

2.3 Computational aspect 79

3 Numerical application 81

3.1 Modelling pre-existing cracks 81

3.2 Uniaxial tension test 84

3.3 Uniaxial compression test 85

3.4 Simple shear test 87

4 Conclusion 88

1 Introduction

During the last decades, a large number of experimental investigations and modeling works have been archived for the characterization and description of material damage process. Based on the irreversible thermodynamics framework, phenomenological damage

© 2016 Tous droits réservés.

doc.univ-lille1.fr

Thèse de Mei Qi, Lille 1, 2016

model have been first developed and it is not the intention to give here an exhaustive list of such models. In these models, the spatial distribution of cracks is generally represented by either scalar or tensorial variables. By postulating a suitable free energy function of cracked materials, the elastic-damage constitutive relations can be deduced and the thermodynamic conjugate damage forces are defined. Some damage criteria based on experimental are then formulated in terms of the conjugate damage forces. These models are generally able to well reproduce overall responses of brittle materials and used in engineering applications. However, it is not easy to properly describe some specific phenomena related to damage process such as unilateral effects due to crack opening-closure and coupling between crack propagation and frictional sliding. Also it is also desired to get a deeper insight on spatial distribution of cracks at microscopic scales during loading process.

Therefore, in order to complete phenomenological models and provide an alternative way to model damage process, important efforts have been provided by various authors on the development of micro-mechanical damage models. Directly relied on the basic results established in the linear fracture mechanics, some isotropic and anisotropic micro-mechanical damage models have first been proposed, for instance [Kachanov, 1982],[Andrieux et al., 1986],[Gambarotta and Lagomarsino, 1993],[Prat and Bazant, 1997],[Pensee et al., 2002b],[Jefferson and Bennett, 2007]. These models do not use rigorous up-scaling methods. Their extension to general conditions, for example three dimensional loading paths, multiple interacting cracks, multi-physical coupling can meet more or less theoretical difficulties. Alternatively, inspired by different linear homogenization techniques developed for heterogeneous materials, micro-mechanical damage models based on the use of the Eshelby's reference solution for inclusion problems have recently been proposed [Eshelby, 1957]. The cracked materials are seen as a matrix inclusion system composed of a solid matrix and embedded cracks. Using a rigorous up-scaling procedure, the effective elastic properties of cracked materials can be determined. This kind of approach has also been applied to model poroelastic behaviours of fluid saturated materials [Barthelemy et al., 2003],[Dormieux et al., 2006]. Along this line, [Zhu et al., 2008a] incorporated the linear homogenization procedure into the standard framework of irreversible thermodynamics and formulated a complete micro-mechanical damage model with unilateral effects. This homogenization-based approach has significantly facilitated the formulation of damage models and also their numerical implementation into computer codes for engineering applications [Zhu et al., 2008b]. Later various extensions have proposed different aspects related to damage process. For example, the unilateral damage-friction coupling has been

© 2016 Tous droits réservés.

doc.univ-lille1.fr

Thèse de Mei Qi, Lille 1, 2016

properly described in both dry materials [Zhu et al., 2011] and applied to brittle rocks [Xie et al., 2011] and fluid saturated porous materials [Xie et al., 2012]. On the other hand, some multi-physical coupling phenomena have been taken into account in the same framework, for instance, damage-permeability coupling by [Jiang et al., 2010] and [Chen et al., 2012b], damage-induced thermo-mechanical coupling by [Chen et al., 2014].

However, in most damage models developed so far, induced cracks are generally embedded in an isotropic solid matrix. The material is then assumed initially isotropic in nature and only the induced anisotropy due to crack propagation in some preferential orientations is investigated. In many brittle materials like rocks and concrete, due to tectonic loading history or fabrication process, there is an initial anisotropy related to the presence of oriented microstructural morphology. For example, most sedimentary rocks exhibit a transversely isotropic behaviour due to the presence of parallel bedding planes. Therefore, in such materials, the induced anisotropic crack propagation should be take into account the interaction with the initial material anisotropic. It is then needed to develop damage models for initially anisotropic materials.

In the present chapter, a numerical micro-mechanical damage will be developed for initially anisotropic brittle materials. The formulation will be based on the extension of the homogenization method used the micro-mechanical damage model by [Zhu et al., 2008a]. To this end, the representative element volume (REV) of cracked materials will be represented by different families of parallel cracks which are embedded in an initially transversely isotropic elastic solid matrix (see figure III .1 in the Chapter III). Based on the theories presented in the previous chapters, a specific damage criterion is defied in the framework of irreversible thermodynamics to describe the progressive growth of cracks. More precisely, the idea of this model is to combine the results from homogenization methods (*Dilute* scheme, *MT* scheme, *PCW* scheme) with the thermodynamic reasoning based on the energy released rate, and the assumption of normality rule will be employed to build the evolution law of damage. And then, the proposed model is implemented in a computer code and applied to study elastic-damage behaviours of brittle materials respectively under uniaxial tension and compression as well as simple shear tests.

2 Formulation of anisotropic damage model

Based on the estimation of effective elastic properties of cracked material, a micro-mechanical damage model is now proposed for initially transversely isotropic materials.

© 2016 Tous droits réservés.

doc.univ-lille1.fr

Thèse de Mei Qi, Lille 1, 2016

To this end, an appropriate damage criterion should be determined in order to describe the growth of induced cracks.

2.1 Free energy and state equations

The damage evolution law is formulated in the framework of irreversible thermodynamics. Note the effective elastic stiffness tensor of cracked material by $\mathbb{C}^{hom}(d_r)$ presented in the previous section, which is a function of the induced crack density parameter d_r. The free energy function of cracked material is written by:

$$W(\boldsymbol{E}) = \frac{1}{2}\boldsymbol{E} : \mathbb{C}^{hom}(d_r) : \boldsymbol{E} \tag{IV .1}$$

In this relation, $\boldsymbol{\Sigma}$ is the macroscopic stress tensor, and $\boldsymbol{E}$ the macroscopic strain tensor. The effective elastic stress-strain relations are deduced from the free energy function:

$$\boldsymbol{\Sigma} = \frac{\partial W}{\partial \boldsymbol{E}} = \mathbb{C}^{hom}(d_r) : \boldsymbol{E} \tag{IV .2}$$

It is also possible to define the thermodynamic force F^{d_r} conjugated with each family of induced cracks d_r, from the free energy function:

$$F^{d_r} = -\frac{\partial W}{\partial d_r} = -\frac{1}{2}\boldsymbol{E} : \frac{\partial \mathbb{C}^{hom}}{\partial d_r} : \boldsymbol{E} \tag{IV .3}$$

F^{d_r} is the thermodynamic force associated to damage variable d_r. From the point of view of thermodynamics, F^{d_r} can be interpreted as a kind of energy release rate associated with microcracks, which will be used as the driving force for damage evolution as usually performed in various macroscopic models.

It should be pointed out that in both equations (IV .2) and (IV .3), the effective elastic tensor $\mathbb{C}^{hom}(d_r)$ is expressed in its general form for closed microcracks of initially anisotropic materials. For the open microcracks, we can choose the expression of $\mathbb{C}^{hom}(d_r)$ as previously mentioned in the section (2.3), without special distinguishing between initially isotropic and anisotropic materials.

2.2 Damage criterion and evolution law

Based on the above thermodynamic arguments, there are two important issues for the implementation of damage models, the damage criterion and its evolution law respectively, are discussed in this section. The implied mission is to present the evolution of the propagation of damage. For complete consistency of a micro-macro approach, the macroscopic

© 2016 Tous droits réservés. doc.univ-lille1.fr

Thèse de Mei Qi, Lille 1, 2016

damage criterion and the dissipation potential should be deducted from microscopic considerations. The approach adopted here is to combine the results from micromechanics with the thermodynamic approach which is usually seen in macroscopic formulations. According to the general thermodynamic framework and limited to the time-independent behaviours, a damage criterion in the form of a function of the conjugated damage force F^{d_r} can be put in form:

$$f(F^{d_r}, d_r) = F^{d_r} - \mathcal{R}(d_r) \leqslant 0 \tag{IV .4}$$

In (IV .4), the function $\mathcal{R}(d_r)$ describes the crack resistance to damage propagation of the material whose physical significance is similar to that of the material Crack Resistance Curve (R-curve) in fracture mechanics. Correspondingly, it is reasonable to assume that the damage resistance $\mathcal{R}(d_r)$ should not be a constant but vary with the damage level. It should be emphasized that the choice of $\mathcal{R}(d_r)$ is essentially phenomenological since the R-curve, determined from the investigations of cracking experiments (see [Ouyang et al., 1997]), is used to reflect the effect of possible microstructural heterogeneities. Attempts have been made by ([Dormieux and Kondo, 2005]) to build a connection between the linear elastic fracture mechanics (LEFM) and micromechanical approach. Theoretically, the specific form of damage resistance function $\mathcal{R}(d_r)$ should be determined based on appropriate experimental observations at suitable material scale. For simplicity, the linear form is used in the most of situation, for example, $\mathcal{R}(d_r) = c_0 + c_1 d_r$ is chosen in ([Zhu, 2006]).

Here, a non linear form is used:

$$\mathcal{R}(d_r) = c_0 + (c_m - c_0)\frac{d_r}{c_1 + d_r} \tag{IV .5}$$

which c_0 is defining the initial damage threshold, c_1 is controlling kinetics of the damage evolution, c_m defining the maxi damage threshold.

The damage evolution is obtained by the following form:

$$\begin{cases} \text{if} \quad f < 0, \ \dot{d}_r = 0 & \text{(Elastic domain)} \\ \text{if} \quad f = 0 \quad and \quad \dot{f} < 0 \ \ \dot{d}_r = 0 & \text{(Elastic unloading)} \\ \text{if} \quad f = 0 \quad and \quad \dot{f} = 0 \ \ \dot{d}_r \geqslant 0 & \text{(Damage growth)} \end{cases} \tag{IV .6}$$

2.3 Computational aspect

The proposed micro-mechanical damage model is now implemented in a computer code in order to predict macroscopic mechanical behaviours under general loading paths. Due

© 2016 Tous droits réservés.

doc.univ-lille1.fr

Thèse de Mei Qi, Lille 1, 2016

to the nonlinear character of the constitutive model, the loading path is divided into a limit number of steps. Starting from given initial conditions, at the end of loading step j, the macroscopic stresses $\boldsymbol{\Sigma}_j$ and strains $\boldsymbol{E}_j$ as well all internal variables (cracks density parameters $d_{i,j}$) are known. The problem to be solved here is stated as follows. Given a macroscopic strain increment $\Delta\boldsymbol{E}_{j+1}$, it consists in determining the corresponding macroscopic stress increment $\Delta\boldsymbol{\Sigma}_{j+1}$ and crack density evolutions Δd_i for the loading step $j+1$. The numerical algorithm used is based on the classical operator splitting method which is composed of the elastic predictor and damage corrector. The flowchart of numerical algorithm can be summarized as follows.

a) Elastic prediction:

For each i^{th} family of cracks, the crack density is assumed unchanged:

$$d_{i,(j+1)} = d_{i,j} \tag{IV .7}$$

Update the macroscopic strain for the step $j+1$ as:

$$\boldsymbol{E}_{j+1} = \boldsymbol{E}_j + \Delta\boldsymbol{E}_{j+1} \tag{IV .8}$$

Calculate the damage conjugate force to each family of cracks F_{d_i} by;

$$F_{d_{i,j}} = -\frac{1}{2}\boldsymbol{E}_{j+1} : \frac{\partial\mathbb{C}^{hom}(d_{i,j})}{\partial d_i} : \boldsymbol{E}_{j+1} \tag{IV .9}$$

Check the corresponding damage criterion. If $f(F_{d_{i,(j+1)}}, d_{i,j}) \leq 0$, for all of crack families, the macroscopic stress for the step $j+1$ is calculated by:

$$\boldsymbol{\Sigma}_{j+1} = \mathbb{C}^{hom}(d_{i,j}) : \boldsymbol{E}_{j+1} \tag{IV .10}$$

Else, it is needed to proceed with damage correction for all families of cracks where the damage growth condition is met, say $f(F_{d_{i,(j+1)}}, d_{i,j}) > 0$ for $i \in N$.

b) Damage correction:

1) Solving a linear system of equations to determine the increments of damage density parameters for all activated families of cracks, $\Delta d_{i,j+1}$ for $i \in [1, N]$, and update the corresponding values $d_{i,j+1} = d_{i,j} + \Delta d_{i,j+1}$.

2) Updating of the Hill tensor $\mathbb{P}_{i,j+1}$ and of the strain concentration tensor $\mathbb{A}_{i,j+1}$ for each family of cracks.

3) Calculate the current effective elastic stiffness tensor $\mathbb{C}^{hom}(d_{i,j+1})$.

© 2016 Tous droits réservés.

doc.univ-lille1.fr

Thèse de Mei Qi, Lille 1, 2016

4) Update the macroscopic stress for the step $j+1$ according to the stress-strain relation:

$$\boldsymbol{\Sigma}_{j+1} = \mathbb{C}^{hom}(d_{i,j+1}) : \boldsymbol{E}_{j+1} \tag{IV .11}$$

3 Numerical application

We consider the same REV who is a family of parallel cracks which are embedded in a transverse isotropic solid matrix (see Fig: III .1). The global coordinates corresponding to the matrix is characterized by (e_1, e_2, e_3). $\underline{e}_3$ is the symmetry axis and the plane $\underline{e}_1 - \underline{e}_2$ is the isotropic plane of the transversely isotropic matrix. The normal of the microcrack is denoted by $\underline{n}$. The angle between the axis $\underline{e}_3$ and the normal $\underline{n}(\underline{e}_2, \underline{e}_3)$ is θ_α and the angle between the normal $\underline{n}(\underline{e}_2, \underline{e}_3)$ and the axis $\underline{e}_1$ is φ_α as shown in the (Fig: III .1) in Chapter III .

The effective mechanical behaviours of cracked material under various loading paths are investigated using the proposed numerical damage model. The emphasis is put on the study of initial anisotropy effects, on the comparison of the different homogenization schemes and also on the result to modelling pre-existing cracks. For the sake of simplicity, the present investigation is limited to materials with one family of cracks. For this purpose, both initially isotropic and anisotropic materials are considered. The typical values of elastic parameters are given in Table IV .1 while those for damage evolution in Table IV .2.

3.1 Modelling pre-existing cracks

As we presented in the Chapter I , there is usually pre-existing cracks in rocks. Some experimental results show that the closure of pre-existing cracks is observed in a very low stress level at beginning of loading process. We can observe clearly in the Fig. IV .1, there is a tightening phase at beginning of loading process due to the closure of pre-existing cracks [NIANDOU, 1994].

In order to predictive this mechanical behaviour, we consider an uniaxial compression test. The boundary conditions of macroscopic stresses are given by $\boldsymbol{\Sigma} = \Sigma_{33}\underline{e}_3 \otimes \underline{e}_3$ and the loading path is driven by a prescribed compressive strain E_{33} along the axis $\underline{e}_3$. All pre-existing cracks are assumed to be closed and oriented in the direction $\theta_\alpha = 0°$, $\varphi_\alpha = 0°$.

© 2016 Tous droits réservés.

doc.univ-lille1.fr

Thèse de Mei Qi, Lille 1, 2016

Table IV .1: Initial elastic parameters

Isotropic material	E_m	38000 MPa
	ν_m	0.19
Anisotropic material	E_1	38000 MPa
	E_3	19000 MPa
	G_{13}	8000 MPa
	ν_{12}	0.19
	ν_{31}	0.19

Table IV .2: Damage criterion parameters

$c_0(Jm^{-2})$	$c_1(Jm^{-2})$	$c_m(Jm^{-2})$	d_0
0.74×10^{-3}	0.5	5.81×10^{-2}	0

A linear empirical criterion is proposed to describe the variation of the aspect ratio of the pre-existing cracks as a function of the macroscopic strain:

$$\epsilon = k_1 E_{33} + k_2 \tag{IV .12}$$

which k_1 is defining the initial aspect ratio, k_2 is constant parameter which controlling kinetics of the aspect ratio evolution.

In the Fig. IV .2, the numerical results of axial stress-strain curves are presented with PCW scheme. We take the empirical value $k_1 = 200$ and $k_2 = 0.21$ and the initial crack density $d_0 = 2$. The elastic parameter of anisotropic material is shown in IV .1. The aspect ratio value varies between $0.2 - 0.01$. We can observe that the elastic modulus becomes more rigid because of closure of pre-existing cracks.

© 2016 Tous droits réservés.

doc.univ-lille1.fr

Thèse de Mei Qi, Lille 1, 2016

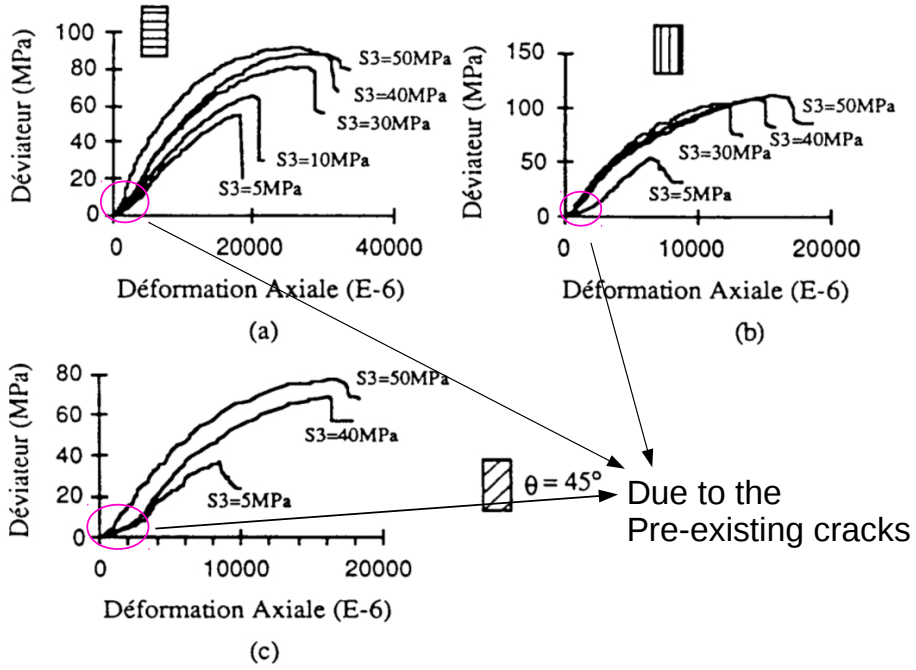

Figure IV .1: Axial strains during triaxial tests with various confining pressure and different loading orientations [NIANDOU, 1994].

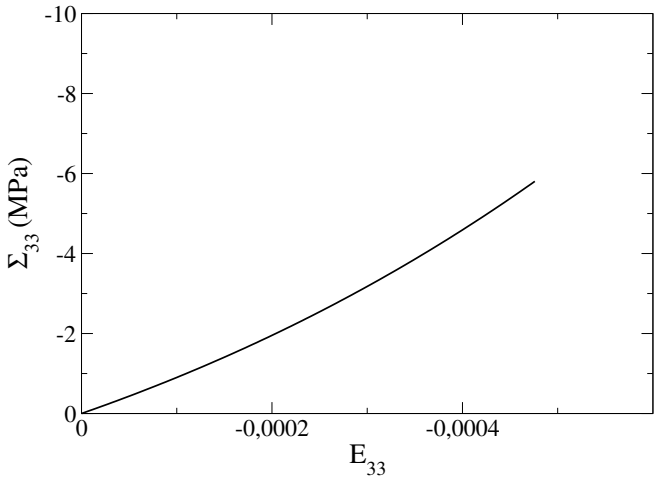

Figure IV .2: Stress-strain curve in uniaxial compression test: modelling the tightening phase due to pre-existing cracks.

© 2016 Tous droits réservés.

doc.univ-lille1.fr

Thèse de Mei Qi, Lille 1, 2016

3.2 Uniaxial tension test

Then, an uniaxial tension test is considered. An initially transversely isotropic solid material is weakened by a family of penny-shaped cracks whose normal is parallel to the symmetry axis of material $\underline{e}_3$. The boundary conditions of macroscopic stresses are given by $\mathbf{\Sigma} = \Sigma_{33}\underline{e}_3 \otimes \underline{e}_3$. The loading is driven by the prescribed tensile strain ($E_{33} > 0$) along the axis $\underline{e}_3$. Note that in this loading condition, all induced cracks are opened. Both the normal and tangential elastic stiffness on the crack surfaces are vanished.

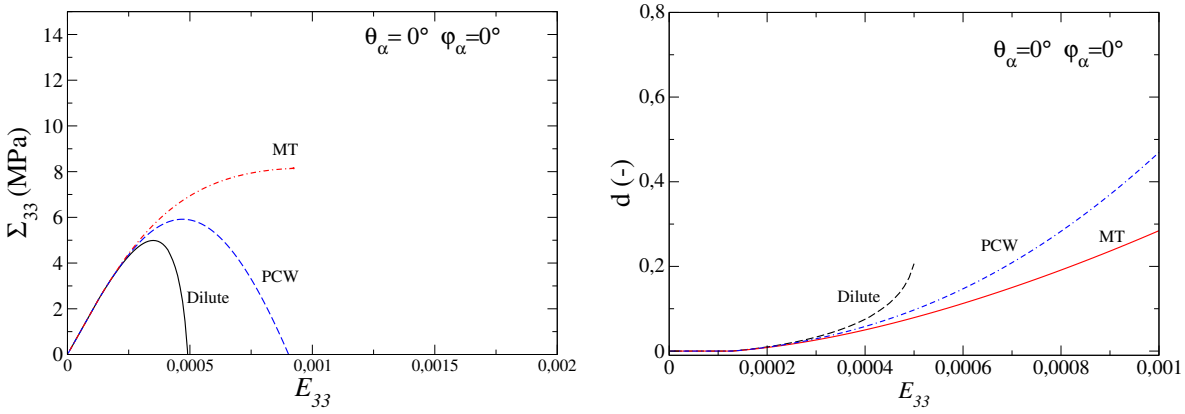

Figure IV .3: Stress-strain curves and damage evolution curves in uniaxial tension test: comparison between three different homogenization schemes

In Figure IV .3, the numerical results of axial stress-strain curves and damage evolution curves are presented and compared between three different homogenization schemes. It is clear that the macroscopic mechanical response of cracked material is strongly affected by the homogenization scheme used. With the dilute scheme, without considering crack interaction, a quasi elastic-brittle behaviour is obtained. There is a sharp drop of stress after the peak strength. In the case of MT scheme, the crack interaction is taken into account by a simplified way, a much ductile behaviour than that by the dilute scheme is found. The material softening is limited even for a large value of applied strain. With the PCW scheme in which both the crack interaction and spatial distribution effect are accounted for, one obtains a typical elastic-damage behaviour with a progressive decrease of axial stress with damage growth. Such a behaviour is quite representative for a large class of brittle materials such as rocks and concrete.

In order to study effects of the initial material anisotropy on the macroscopic behaviour of cracked material, different degrees of initial anisotropy are considered. In Figure IV .4, it is presented the stress-strain and damage evolutions curves in uniaxial tension tests

© 2016 Tous droits réservés.

doc.univ-lille1.fr

Thèse de Mei Qi, Lille 1, 2016

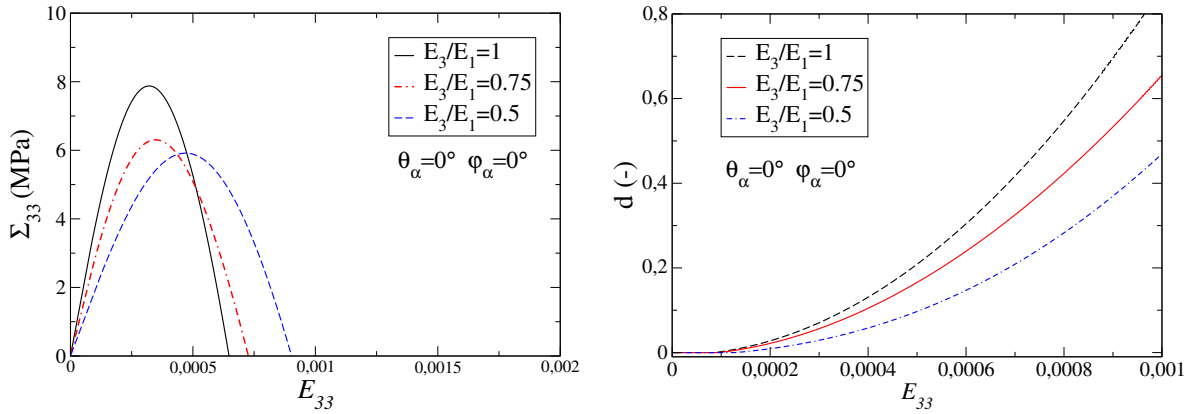

Figure IV .4: Influences of initial anisotropy of solid matrix on macroscopic mechanical behaviour in uniaxial tension test using *PCW* scheme

obtained using *PCW* scheme and respectively for three different anisotropy degrees of the solid matrix. It is found that the macroscopic behaviour of cracked material is significantly affected by the initial anisotropy of the solid matrix. The damage evolution is faster in the isotropic solid than in anisotropic ones. There is therefore an interaction between the initial anisotropy and induced crack growth.

3.3 Uniaxial compression test

Consider now an uniaxial compression test. The boundary conditions of macroscopic stresses are still given by $\boldsymbol{\Sigma} = \Sigma_{33}\underline{e}_3 \otimes \underline{e}_3$. However, the loading path is driven by a prescribed compressive strain ($E_{33} < 0$) along the axis $\underline{e}_3$. The family of induced cracks is assumed to be oriented in the direction $\theta_\alpha = 45°$. Under the compressive stress, all induced cracks are closed. As mentioned above, in the present work, only smooth cracks without friction are considered. Therefore, the tangential stiffness along crack surfaces is vanished while the normal one is equal to the average value of the solid matrix.

In Figure IV .5, the stress-strain and damage evolution curves are presented by using three different homogenization schemes. Again, the macroscopic mechanical behaviour of cracked material is affected by the homogenization scheme, and then by the crack interaction and spatial distribution effect. By comparing with the uniaxial tension test, it is found that the peak compression strength is higher than the peak tensile strength. There is dissymmetry of response between tension and compression loading. This is due to the fact that the local behaviour of cracks is different between the open and closed states. Such a dissymmetrical behaviour is a typical feature of most brittle materials like rocks

© 2016 Tous droits réservés.

doc.univ-lille1.fr

Thèse de Mei Qi, Lille 1, 2016

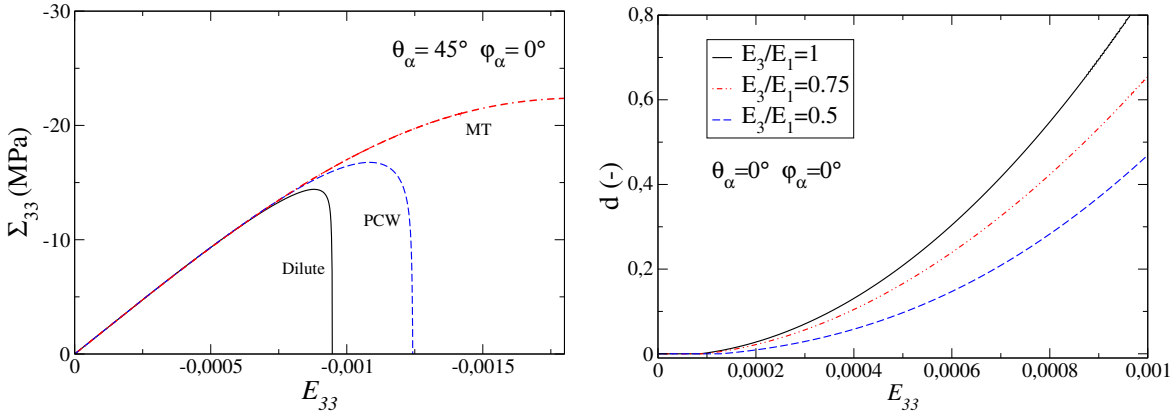

Figure IV .5: Stress-strain curves and damage evolution curves in uniaxial compression test and comparison between three different homogenization schemes

and concrete. However, the ratio between the uniaxial compression and tension strength obtained in the present model is about 2.5. This is much lower that that generally observed in such class of materials, for instance about 20. This difference is due to the fact that only smooth cracks are considered in the present study. By considering friction sliding in closed cracks, the compression mechanical strength will be significantly increased. This feature will be performed in future works.

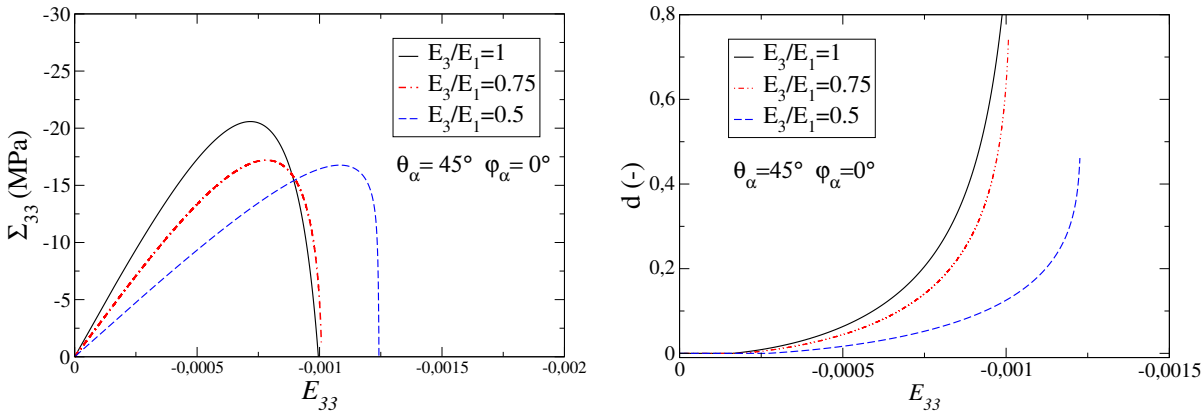

Figure IV .6: Stress-strain curves and damage evolution curves in uniaxial compression test obtained with *PCW* scheme for different initial anisotropy degrees

As for the uniaxial tension test, the effects of the initial anisotropy of solid matrix on the macroscopic behaviour of cracked material are also investigated for the uniaxial compression test. As shown in Figure IV .6, the induced damage evolution is again coupled with the initial anisotropy degree and higher in the isotropic matrix than in the anisotropic

© 2016 Tous droits réservés.

doc.univ-lille1.fr

Thèse de Mei Qi, Lille 1, 2016

ones.

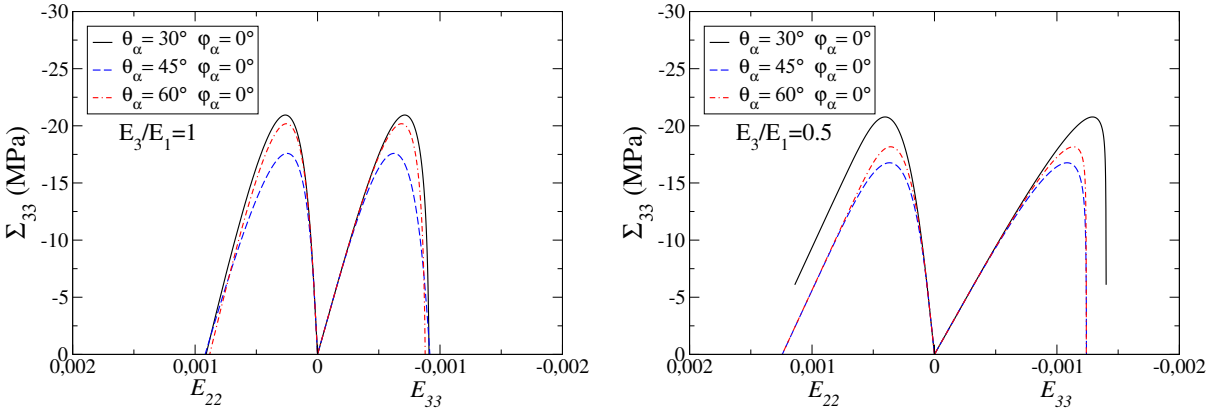

Figure IV .7: Stress-strain curves and damage evolution curves in uniaxial compression test obtained with PCW scheme for different orientations of induced cracks

Further, the orientation effect of the induced crack family is also studied. In Figure IV .7, the stress-strain relations obtained with PCW scheme in a uniaxial compression test are presented for three different orientations of the induced cracks and for two different initial anisotropy degrees. It is found that the macroscopic stress-strain relations are clearly dependent on the orientation of induced cracks for both isotropic and anisotropic materials. It seems that the smallest compression strength is obtained for the crack family with $\theta_\alpha = 45°$.

3.4 Simple shear test

Another example studied is the simple shear test. In this test, a macroscopic shear strain, for instance E_{13} is prescribed and the corresponding macroscopic shear stress Σ_{13} is computed with the proposed micro-mechanical damage model. Two different configurations are considered. In the first case, the induced crack family is parallel to the initial bedding planes of solid matrix, say $\theta_\alpha = 0°$. The shear test is performed in the plane $\underline{e}_3\underline{e}_1$ (or equivalently in the plane $\underline{e}_2\underline{e}_3$). The stress-strain curves obtained are presented in Figure IV .8. In the second case, the induced crack family is perpendicular to the initial bedding planes, say $\theta_\alpha = 90°$. The cracked material exhibits an orthotropic behavior. The shear strain is prescribed respectively in the planes $\underline{e}_1\underline{e}_2$ and $\underline{e}_2\underline{e}_3$. The obtained stress-strain curves are shown in Figure IV .9. It is first found that the macroscopic mechanical behavior is again dependent on the homogenization scheme used, and thus affected by the crack interaction and spatial distribution effect. Further, the stress-strain behavior

© 2016 Tous droits réservés.

doc.univ-lille1.fr

Thèse de Mei Qi, Lille 1, 2016

is also dependent on the orientation of induced cracks and there is an interaction effect between the initial anisotropy and induced cracks. Comparing the results obtained with *PCW* scheme, it seems that the smallest shear strength is obtained for the shear test in the plane $\underline{e}_2\underline{e}_3$ and when the induced crack family is perpendicular to the initial bedding planes.

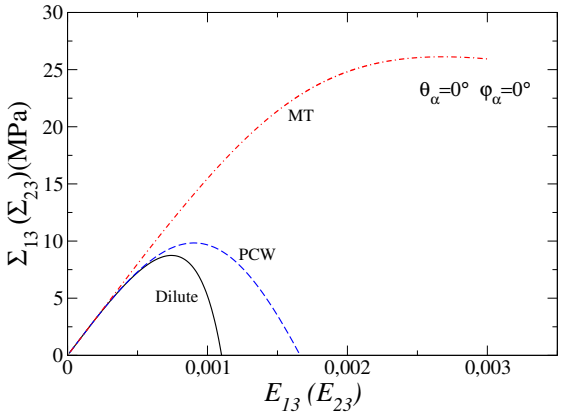

Figure IV .8: Stress-strain curves in simple shear test in plane $\underline{e}_3\underline{e}_1$ and comparisons between different homogenization schemes

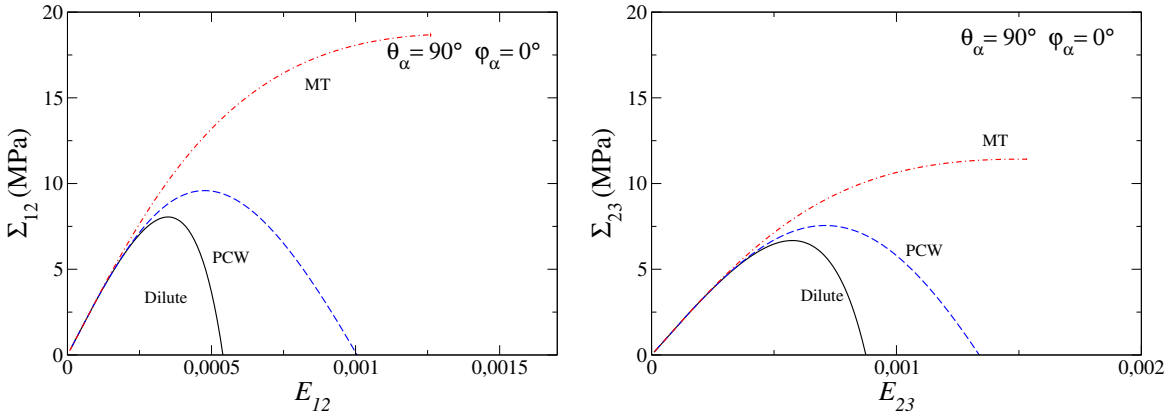

Figure IV .9: Stress-strain curves in simple shear tests respectively in planes $\underline{e}_1\underline{e}_2$ and $\underline{e}_2\underline{e}_3$ and comparisons between different homogenization schemes

4 Conclusion

In this chapter, a numerical micro-mechanical damage model has been proposed for a class of brittle materials. Compared with existing models, the proposed model is able

© 2016 Tous droits réservés.

doc.univ-lille1.fr

Thèse de Mei Qi, Lille 1, 2016

to account for interactions between initial material anisotropy and induced growth of cracks. To this end, based on the irreversible thermodynamics framework, a specific damage evolution criterion has been proposed to describe the progressive growth of induced cracks. The proposed numerical damage model was implemented in a computer code and applied to study mechanical behaviours of cracked materials under different loading paths. Uniaxial tension and compression as well as simple shear tests have been considered. For all cases, the macroscopic stress-strain relations and damage evolutions have been investigated. It was found that the overall mechanical behaviour of cracked material was significantly dependent on the homogenization scheme. With the *dilute* scheme without considering crack interactions, a too fast damage evolution kinetics was obtained and leading a too sharp material softening after the peak strength. In the case of MT scheme which consider the crack interaction in a simplified way, one generally obtained a too ductile behaviour with a small decrease of stress in the post-peak regime. The PCW scheme, considering both the crack interaction and spatial distribution effects, provided the most typical results compared with a number of experimental evidences observed in a class of brittle materials such as rocks and concrete. The macroscopic behaviour was also affected by the orientation of induced cracks and their interactions with the initial materials anisotropy. Further, the proposed model was able to describe the dissymmetric behaviour between compression and tension due to the different local behaviour in open and closed cracks. However, this feature should be improved in future works by considering the coupling between the frictional sliding in closed cracks and crack propagation. The present work can also be extended to brittle materials with a general initial anisotropy.

© 2016 Tous droits réservés.

doc.univ-lille1.fr

Thèse de Mei Qi, Lille 1, 2016

© 2016 Tous droits réservés.

doc.univ-lille1.fr

Chapter V

Coupling between damage evolution and frictional sliding in an initially anisotropic material

Contents

1 Introduction 92

2 Description of cracked material 94

2.1 Deformation of cracked material 94

2.2 Effective properties of cracked materials 95

2.3 Free enthalpy with damage-friction 97

3 Hill tensor for arbitrarily oriented spheroidal cracks in a transversely isotropic material 98

4 Description of friction-damage evolutions 102

4.1 Friction criterion 103

4.2 Damage criterion 104

4.3 Damage-friction coupling 105

4.4 Numerical implementation 106

5 Numerical assessment and experimental verification 107

5.1 Parameters identification 108

5.2 Simulation of triaxial compression test 110

5.3 Direct shear tests 115

6 Conclusion 115

Initially anisotropic cracked media

© 2016 Tous droits réservés.

doc.univ-lille1.fr

Thèse de Mei Qi, Lille 1, 2016

1 Introduction

Damage due to growth of micro-cracks is an essential mechanism of inelastic deformation and failure in quasi brittle materials. The induced damage affects not only mechanical properties but also other physical properties such as permeability and conductivity. Significant efforts have been made during the last decades on modelling of induced damage in different engineering materials. Without giving an exhaustive list, a number of macroscopic damage models have been developed in the framework of irreversible thermodynamics. In these models, spatial distribution of micro-cracks is mathematically represented by scalar or tensorial variables. Effective properties of cracked materials are determined by postulating specific forms of thermodynamic potential. Damage evolution is evaluated through definition of a specific damage criterion. Directly calibrated from experimental data, most of such models are able to capture main features of macroscopic behaviours of brittle materials. However, macroscopic approaches are not able to consider physical mechanisms at relevant materials scales and usually meet difficulties in dealing with some specific features such as unilateral effects, damage-friction coupling, etc.

Micro-mechanical approaches provide an efficient alternative to deal with damage-friction problems and obtained important advances in recent years. The main objective of micro-mechanical approaches is to consider growth and friction of micro-cracks at appropriate scales and determine effective properties of cracked materials by a up-scaling method. Two categories of micro-mechanical damage models have been so far formulated. In the first category, the formulation of micro-mechanical models is directly based on results issued from Linear Fracture Mechanics. Different feature have been discussed, for instance, loaded induced anisotropy [Hori and Nemat-Nasser, 1983], frictional sliding of closed cracks [Kachanov, 1982, Lawn and Marshall, 1998], interaction between cracks [Gambarotta and Lagomarsino, 1993, Paliwal and Ramesh, 2008], and unilateral effects [Prat and Bazant, 1997, Pensee et al., 2002b]. In general, these models are not based on rigorous up-scaling procedure to determine effective properties of cracked materials. To complete this kind of models, the second category of micro-mechanical models is formulated using rigorous linear homogenization procedures for heterogeneous materials. In this context, cracks are considered as inclusions embedded in an elastic matrix. Effective elastic properties of cracked materials are estimated using an Eshelby solution homogenization method, for instance [Barthelemy et al., 2003, Dormieux et al., 2006]. [Zhu et al., 2008a, Zhu et al., 2011] have proposed micro-mechanical models for brittle materials with closed frictional micro-cracks by considering coupling between crack growth and frictional sliding. Further, micro-mechanical models have also been extended to saturate brittle

© 2016 Tous droits réservés.

doc.univ-lille1.fr

Thèse de Mei Qi, Lille 1, 2016

materials by taking into account effects of fluid pressure [Xie et al., 2012]. More recently, [Zhu and Shao, 2015] proposed an refined micro-mechanical damage-friction model based on an original strain decomposition of cracked materials. On the other hand, asymptotic homogenization methods have also been proposed for damage modelling of brittle materials with interacting micro-cracks [Markenscoff and Dascalu, 2012].

Most micro-mechanical models mentioned above deal with crack growth and frictional sliding in initially isotropic solid matrix. However, for many engineering materials, there is a inherent anisotropy due to oriented micro-structures such as bedding planes, preferential orientations of mineral grains or pores, etc. It is therefore an important issue to consider effects of the initial structural anisotropy on induced crack growth. Recently, the micro-mechanical models take into account the initially anisotropic materials is proposed by [Levassseur et al., 2015]. This work have been formulated a full 2D anisotropic damage model for initially anisotropic materials, and accounted for the coupling between the damage induced anisotropy and the orthotropy of the solid matrix. In our work, in the context of Eshelby solution based micro-mechanical approach, an essential step of homogenization procedure is to establish a suitable relation between prescribed macroscopic strain (or stress) and local strain field inside crack phases using a specific strain concentration (or stress localization) tensor. Such a concentration tensor is directly related to the so-called Eshelby tensor or equivalently Hill's tensor and depends on homogenization schemes considering or not cracks interaction and spatial distribution. In the case of ellipsoidal micro-cracks embedded in an isotropic elastic solid matrix, it is possible to obtain a closed-form of such a tensor. However, when cracked materials with inherent anisotropy are concerned, it is no more possible to get such closed-form solutions. Suitable numerical procedure have to be developed to computer Hill's tensor. In this chapter, we propose an efficient numerical method for three-dimensional ellipsoidal micro-cracks embedded in a transversely isotropic solid matrix. This method is based on the numerical integration technique of the exact Green function presented by [Pan and Chou, 1976] and a frame transformation technique presented in [Giraud et al., 2007]. Using this method, the micro-mechanical damage model initially proposed in [Zhu and Shao, 2015] is extended to initially anisotropic brittle materials. The proposed approach also open the perspective to deal with damage-friction problems in brittle materials with arbitrary inherent anisotropy.

The proposed micro-mechanical model is implemented as a used defined material model subroutine and can be used for numerical analysis of damage in engineering structures. A series of numerical assessments are presented for different loading paths such as triaxial compression and shear. The efficiency of the proposed model is also verified through

© 2016 Tous droits réservés.

doc.univ-lille1.fr

Thèse de Mei Qi, Lille 1, 2016

experimental validation for a typical shale that was extensively investigated in the context of geological disposal of radioactive waste and shale gas exploration. In particular, interactions between the initial anisotropy and induced damage are analysed. Coupling between damage by crack growth and frictional sliding is also studied through numerical examples.

2 Description of cracked material

Micro-mechanical analyses are performed on a representative elementary volume (REV) that is assumed to occupy a geometric domain Ω limited by its external boundary surface $\partial\Omega$. In the present study, the REV is composed of a transversely isotropic linearly elastic solid matrix with stiffness tensor $\mathbb{C}^m$ and a number of oblate ellipsoidal micro-cracks (see Figure V .1). The presence of micro-cracks weakens the solid matrix and affects macroscopic behaviours of cracked materials. The crack growth in some preferential directions usually induces a material anisotropy and this induced anisotropy is coupled with the material initial anisotropy. The present study proposes to develop a micro-mechanical model based on the Eshelby's solution to the well-known equivalent inclusion problem. The REV of cracked materials is thus viewed as a matrix-inclusion system. More precisely, micro-cracks are seen as ellipsoidal inclusions embedded in the solid matrix and assumed to potentially propagate in a self-similar manner. Further, all micro-cracks with the same normal vector are put into the same family. Therefore, a family of oblate ellipsoidal cracks can be sufficiently characterized by its normal $\underline{n}$, mean radius a and mean half opening c (see Figure V .1). The volume fraction of cracks in this family is then given by $\varphi_f = \frac{4}{3}\pi a^2 c\mathcal{N} = \frac{4}{3}\pi\epsilon d$ where $\epsilon = \frac{c}{a}$ represents the aspect ratio of cracks, $\mathcal{N}$ denotes the number of cracks per unit volume, and $d = \mathcal{N}a^3$ is the well-known crack density parameter which is usually used as an internal damage variable.

2.1 Deformation of cracked material

In order to study deformation of cracked material, we consider here a uniform macroscopic strain $\boldsymbol{E}$ prescribed on the external boundary surface of the REV $\partial\Omega$. Due to the presence of micro-cracks, the local strain field inside the REV is not uniform and denoted as $\boldsymbol{\varepsilon}$. The macroscopic strain $\boldsymbol{E}$ is equal to the volume average of local strain field, such as:

$$\boldsymbol{E} = \frac{1}{\Omega}\int_{\Omega_m} \boldsymbol{\varepsilon}(\underline{x})d\Omega + \frac{1}{\Omega}\int_{\Omega_c} \boldsymbol{\varepsilon}(\underline{x})d\Omega \qquad \text{(V .1)}$$

© 2016 Tous droits réservés.

doc.univ-lille1.fr

Thèse de Mei Qi, Lille 1, 2016

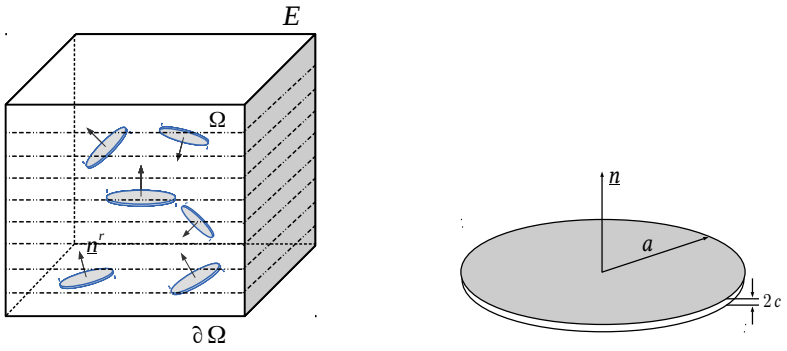

Figure V .1: Oblate ellipsoidal cracks embedded in a transversely isotropic solid matrix

where Ω_m and Ω_c denotes respectively the volume occupied by the solid matrix and micro-cracks. Therefore, the macroscopic strain can be decomposed as:

$$\boldsymbol{E} = \boldsymbol{E}^m + \boldsymbol{E}^c \tag{V .2}$$

where the $\boldsymbol{E}^m$ denotes the part of the strain due to deformation of the matrix phase and the $\boldsymbol{E}^c$ denotes the strain due to micro-cracks. By applying the divergence theorem, the strain due to micro-cracks can be related to displacement jumps on crack surfaces.

$$\boldsymbol{E}^c = \mathcal{N} \int_{\omega^+} (\underline{n} \otimes^s [\underline{u}]) dS \tag{V .3}$$

where ω^+ denotes the crack surface and $[\underline{u}]$ the displacement jump on crack surface. In the case of multiple families of micro-cracks, as each crack induces an isolated discontinuity in the solid matrix, the contribution of all families of micro-cracks to the macroscopic strain can be taken into account separately by the following simple summation:

$$\boldsymbol{E}^c = \sum_{r=1}^{N} \boldsymbol{E}^{c,r} \tag{V .4}$$

where $\boldsymbol{E}^{c,r}$ denotes the part of strain caused by the rth family of micro-cracks.

2.2 Effective properties of cracked materials

When the crack propagation is the unique energy dissipation mechanism, the determination of the effective elastic stiffness tensor of the homogenized equivalent medium $\mathbb{C}^{hom}$ leads to the free enthalpy of crack-matrix system $W^* = \frac{1}{2}\boldsymbol{\Sigma} : \mathbb{S}^{hom} : \boldsymbol{\Sigma}$, with

© 2016 Tous droits réservés.

doc.univ-lille1.fr

Thèse de Mei Qi, Lille 1, 2016

$\mathbb{S}^{hom} = (\mathbb{C}^{hom})^{-1}$ being the effective compliance tensor and $\boldsymbol{\Sigma}$ the macroscopic stress. Based on previous works [Zaoui, 2002, Dormieux et al., 2006, Zhu et al., 2008a], using a standard linear homogenization framework, the effective elastic stiffness of a cracked solid medium can be written in the following general form:

$$\mathbb{C}^{hom} = \mathbb{C}^m + \sum_{r=1}^{N} \varphi^{c,r}(\mathbb{C}^{c,r} - \mathbb{C}^m) : \mathbb{A}^{c,r} \qquad (V.5)$$

The fourth order tensor $\mathbb{C}^{c,r}$ denotes the elastic stiffness of the constituent phase corresponding to the rth family of micro-cracks. Three different cases can be considered: (i) for open cracks, the cancellation of the locale stress on cracks surfaces leads to $\mathbb{C}^{c,r} = 0$; (ii) for closed cracks without friction (smooth cracks), one takes $\mathbb{C}^{c,r} = \eta \underline{n} \otimes \underline{n} \otimes \underline{n} \otimes \underline{n}$ in order to describe the recovery of the elastic stiffness of cracked medium in the normal direction of micro-cracks; (iii) for closed frictional cracks, assuming a static friction along crack surfaces so that cracks are sufficiently blocked, one takes $\mathbb{C}^{c,r} = \mathbb{C}^m$.

The strain concentration tensor $\mathbb{A}^{c,r}$ for the rth family of micro-cracks plays an essential role in homogenization procedure. It defines a linear relation between the local strain field inside the rth crack phase and the macroscopic strain prescribed on the external boundary of REV such that $\boldsymbol{\varepsilon}^{c,r}(\underline{x}) = \mathbb{A}^{c,r}(\underline{x}) : \boldsymbol{E}$. The expression of $\mathbb{A}^{c,r}$ depends on the choice of homogenization scheme. In the literature, various homogenization schemes have been developed for different heterogeneous materials. Among these, the Mori-Tanaka scheme [Mori and Tanaka, 1973c, Benveniste, 1986]) is particularly suitable for matrix-inclusion systems and has been found to provide a close link with the results established from the linear fracture mechanics in the context of damage modeling of elastic brittle materials [Pensee et al., 2002b, Dormieux and Kondo, 2005, Zhu et al., 2008b, Zhu et al., 2008a]. Therefore, this scheme is adopted here and applied to ellipsoidal micro-cracks with small aspect ratios:

$$\mathbb{A}^{c,r} = [\mathbb{I} + \mathbb{P}_e^r : (\mathbb{C}^{c,r} - \mathbb{C}^m)]^{-1} : \{\mathbb{I} + \sum_{j=1}^{N} \varphi^{c,j}[\mathbb{I} + \mathbb{P}_e^j : (\mathbb{C}^{c,j} - \mathbb{C}^m)]^{-1}\}^{-1} \qquad (V.6)$$

where $\mathbb{I}$ is the fourth order unit tensor and $\mathbb{P}_e^r$ is the so-called fourth order Hill's tensor than can be related to the Eshelby's tensor $\mathbb{S}_e^r$ such that $\mathbb{S}_e^r = \mathbb{P}_e^r : \mathbb{C}^m$. Applying now the strain concentration tensor to open cracks, one obtains the following effective elastic stiffness tensor:

$$\mathbb{C}^{hom} = \mathbb{C}^m : [\mathbb{I} + \frac{4}{3}\pi \sum_{r=1}^{N} d_r \mathbb{T}^r]^{-1} \quad \text{with} \quad \mathbb{T}^r = \lim_{\epsilon \to 0} \epsilon(\mathbb{I} - \mathbb{S}_\epsilon^r)^{-1} \qquad (V.7)$$

© 2016 Tous droits réservés.

doc.univ-lille1.fr

Thèse de Mei Qi, Lille 1, 2016

The inversion of $\mathbb{C}^{hom}$ leads to the following effective elastic compliance tensor:

$$\mathbb{S}^{hom} = \mathbb{S}^m + \frac{4}{3}\pi \sum_{r=1}^{N} d^r \mathbb{T}^r : \mathbb{S}^m \tag{V .8}$$

As mention in [Zhu and Shao, 2015], although $\mathbb{C}^{hom}$ has a non-linear form, $\mathbb{S}^{hom}$ is a linear function of crack density parameters d^r. This interesting feature provides great facilities for the model's formulation in the stress space. Further, for the convenience of model's formulation in the following sections, the following two fourth order operators are introduced:

$$\mathbb{S}^n = \frac{4}{3}\pi \mathbb{T}^r : \mathbb{S}^m \quad , \ \mathbb{C}^n = \frac{3}{4\pi}\mathbb{C}^m : (\mathbb{T}^r)^{-1} \tag{V .9}$$

Accordingly, the effective elastic compliance tensor can be rewritten as:

$$\mathbb{S}^{hom} = \mathbb{S}^m + \sum_{r=1}^{N} d_r \mathbb{S}^{n,r} \tag{V .10}$$

The macroscopic strain is related to the macroscopic stress by:

$$\boldsymbol{E} = \boldsymbol{E}^m + \boldsymbol{E}^c = \mathbb{S}^{hom} : \boldsymbol{\Sigma} = \mathbb{S}^m : \boldsymbol{\Sigma} + \sum_{r=1}^{N} d_r \mathbb{S}^{n,r} : \boldsymbol{\Sigma} \tag{V .11}$$

The inversion of the above relation leads to the following macroscopic stress-train relation:

$$\boldsymbol{\Sigma} = \mathbb{C}^m : (\boldsymbol{E} - \boldsymbol{E}^c) \tag{V .12}$$

The macroscopic strain contribution due to the rth family of open cracks is given by:

$$\boldsymbol{E}^{c,r} = d^r \mathbb{S}^{n,r} : \boldsymbol{\Sigma} \tag{V .13}$$

2.3 Free enthalpy with damage-friction

In the case of open cracks, the crack-induced strain $\boldsymbol{E}^{c,r}$ is fully determined by the effective elastic properties of cracked medium. However, for closed frictional cracks, the crack-induced strain is inelastic and should be determined after defining a suitable local frictional law. Coupled with the crack propagation, the frictional sliding is another energy dissipation mechanisms. The free enthalpy should be extended to include both dissipation mechanisms. According to the classical derivative relation $\boldsymbol{E} = \frac{\partial W^*}{\partial \boldsymbol{\Sigma}}$ and by integration of (V .11), the free enthalpy W^* of the cracked system can be written as:

© 2016 Tous droits réservés.

doc.univ-lille1.fr

Thèse de Mei Qi, Lille 1, 2016

$$W^* = \frac{1}{2}\boldsymbol{\Sigma} : \mathbb{S}^m : \boldsymbol{\Sigma} + \sum_{r=1}^{N} \boldsymbol{\Sigma} : \boldsymbol{E}^{c,r} - W^b \tag{V .14}$$

The term W^b represents the stored energy related to inelastic hardening during frictional sliding along micro-cracks.

On the other hand, the free enthalpy W^* can also be expressed in terms of the effective elastic compliance tensor such that $W^* = \frac{1}{2}\boldsymbol{\Sigma} : \mathbb{S}^{hom} : \boldsymbol{\Sigma}$, which must be equivalent to the quantity in (V .14). Using the expression of $\mathbb{S}^{hom}$ in (V .10) together with (V .13), the free enthalpy of cracked system takes the following general form:

$$W^* = \frac{1}{2}\boldsymbol{\Sigma} : \mathbb{S}^m : \boldsymbol{\Sigma} + \boldsymbol{\Sigma} : \sum_{r=1}^{N} \boldsymbol{E}^{c,r} - \frac{1}{2}\sum_{r=1}^{N} \frac{1}{d_r} \boldsymbol{E}^{c,r} : \mathbb{C}^{n,r} : \boldsymbol{E}^{c,r} \tag{V .15}$$

As mentioned in [Zhu and Shao, 2015], the above general expression of free enthalpy is valid for any open and closed micro-cracks. When the cracks in the rth family are open, the strain $\boldsymbol{E}^{c,r}$ in (V .15) is explicitly given by (V .13). However, when the cracks are closed, $\boldsymbol{E}^{c,r}$ cannot be no more explicitly determined from the elastic properties of cracked medium and its evolution should be determined by making use of some criterion. In the latter case, $\boldsymbol{E}^{c,r}$ becomes an internal variable of inelastic frictional sliding process.

3 Hill tensor for arbitrarily oriented spheroidal cracks in a transversely isotropic material

In order to consider the initially transversely isotropic material, another key point is to determine the fourth order Hill's tensor which is applying in the strain concentration tensor. In this section, we will briefly recall that the numerical method to calculate the Hill polarization tensor of an arbitrarily oriented spheroidal inclusion embedded in a transversely isotropic matrix, for more detail see: Chapter II .

Consider a spheroidal inclusion that verifies the following characteristic equation for its geometry:

$$\frac{(e_1^\alpha)^2 + (e_2^\alpha)^2}{a^2} + \frac{(e_3^\alpha)^2}{a^2\epsilon^2} = 1 \tag{V .16}$$

Here, α refers to all quantities related to the inclusion phase α. $\underline{e}_i^\alpha$ defines the local coordinates frame associated to this inclusion and $\underline{e}_3^\alpha$ its symmetry axis. In this chapter, we mainly deal with oblate spheroidal inclusions as penny shaped cracks, whose half-lengths

© 2016 Tous droits réservés.

doc.univ-lille1.fr

Thèse de Mei Qi, Lille 1, 2016

(centred at the origin $\mathcal{O}$) are denoted respectively by a in the plane $e_1^\alpha - e_2^\alpha$ and by $c = a\epsilon$ along the symmetry axis, ϵ being the aspect ratio of the spheroidal.

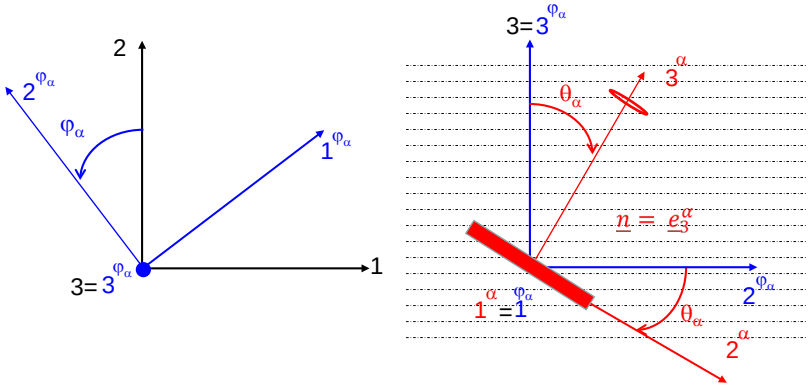

Figure V .2: Rotation between local and global system coordinates

Now let $\underline{e}_i$ be the global coordinates frame associated to the transversely isotropic solid matrix with $\underline{e}_3$ as the symmetry axis. The second-order rotation operator $\boldsymbol{Q}^\alpha$ helps to transfer the components of the global system (e_1, e_2, e_3) to the local one $\underline{e}_i^\alpha$. According to [Giraud et al., 2007], the rotation matrix can be defined as the product of the two rotation matrices $\boldsymbol{Q}^\alpha = \boldsymbol{Q}^{\theta_\alpha} \cdot \boldsymbol{Q}^{\varphi_\alpha}$, which are expressed as:

$$\boldsymbol{Q}^{\theta_\alpha} = \begin{pmatrix} 1 & 0 & 0 \\ 0 & cos(\theta_\alpha) & -sin(\theta_\alpha) \\ 0 & sin(\theta_\alpha) & cos(\theta_\alpha) \end{pmatrix} \quad \boldsymbol{Q}^{\varphi_\alpha} = \begin{pmatrix} cos(\varphi_\alpha) & sin(\varphi_\alpha) & 0 \\ -sin(\varphi_\alpha) & cos(\varphi_\alpha) & 0 \\ 0 & 0 & 1 \end{pmatrix} \tag{V .17}$$

In these relations, two rotation angles are introduced with the help of an intermediate system of coordinates noted by $\underline{e}_i^{\varphi_\alpha}$. The angle between the $\underline{e}_1$ and the $\underline{e}_1^{\varphi_\alpha}$ axis is φ_α ($0 \leqslant \varphi_\alpha \leqslant 2\pi$) and the angle between the $\underline{e}_3$ and the $\underline{e}_3^{\theta_\alpha}$ is θ_α $(0 \leqslant \theta_\alpha \leqslant \pi)$. The Green's function solution of Pan and Chou [Pan and Chou, 1976] for the transversely isotropic material, developed for the coordinate system of a material with the symmetry axis $\underline{e}_3$, is adapted for the calculation in a coordinate system with one axis aligned to the axis of symmetry of matrix, that is: $\underline{e}_i^{\varphi_\alpha} = \underline{\underline{Q}}_{i,j}^{\varphi_\alpha} \underline{e}_j$. Also, it is convenient to express the local coordinate system $\underline{e}_i^\alpha$ in terms of the intermediate one, $\underline{e}_i^{\varphi_\alpha}$, as it is attached to the

© 2016 Tous droits réservés.

doc.univ-lille1.fr

Thèse de Mei Qi, Lille 1, 2016

spheroidal orientation, that is: $\underline{e}_i^{\alpha} = \underline{\underline{Q}}_{i,j}^{\theta_\alpha} \underline{e}_j^{\varphi_\alpha}$. In this way, the $\underline{e}_3^{\varphi_\alpha}$ axis coincides with the symmetry axis $\underline{e}_3$ of the transversely isotropic matrix. Consider the intermediate system φ_α as a global system for the calculation of Hill's tensor. Only one angle θ_α between the symmetry axis of the solid matrix and the symmetry axis of the spheroidal inclusion needs to be taken into account for an arbitrarily oriented spheroidal inclusion in a transversely isotropic matrix. Finally, the fourth-order Hill's tensor can be expressed in terms of the second-order derivatives of Green's function, such as [Giraud et al., 2007]:

$$P_{ijkl}^{\varphi_\alpha}(\underline{e}^{\varphi_\alpha}) = \frac{1}{4}\Big(M_{kijl}^{\varphi_\alpha}(\underline{e}^{\varphi_\alpha}) + M_{kjil}^{\varphi_\alpha}(\underline{e}^{\varphi_\alpha}) + M_{lijk}^{\varphi_\alpha}(\underline{e}^{\varphi_\alpha}) + M_{ljik}^{\varphi_\alpha}(\underline{e}^{\varphi_\alpha}) \Big) \tag{V .18}$$

$$M_{ijkl}^{\varphi_\alpha}(\underline{e}^{\varphi_\alpha}) = \int_\Omega G_{ij,kl}^{\varphi_\alpha}(\underline{e}^{\varphi_\alpha} - \underline{e}'^{\varphi_\alpha}) d\Omega_{e'} = -\frac{\partial}{\partial e_l^{\varphi_\alpha}} \int_\Omega \frac{\partial G_{ij}^{\varphi_\alpha}(\underline{e}^{\varphi_\alpha} - \underline{e}'^{\varphi_\alpha})}{\partial e_k^{\varphi_\alpha}} d\Omega_{e'}, \quad \underline{e}^{\varphi_\alpha} \in \Omega \tag{V .19}$$

Physically, the second-order Green function $G_{ij,kl}^{\varphi_\alpha}(\underline{e}^{\varphi_\alpha} - \underline{e}'^{\varphi_\alpha})$ represents the displacement at a point $\underline{e}^{\varphi_\alpha}$ in a linear elastic solid of stiffness $\mathbb{C}_m$, resulting from a unit force applied at a point $\underline{e}'^{\varphi_\alpha}$ in the solid.

After mathematical manipulations, we can obtain the general forms of the components of the Hill's tensor in the intermediate system and in terms of the arguments θ_α and $\underline{l}_i^{\varphi_\alpha}$.

$$P_{ijkl}^{\varphi_\alpha} = \int_\Sigma (\underline{p}_l^{\varphi_\alpha} g_{kij}^{\varphi_\alpha} + \underline{p}_l^{\varphi_\alpha} g_{kji}^{\varphi_\alpha} + \underline{p}_k^{\varphi_\alpha} g_{lij}^{\varphi_\alpha} + \underline{p}_k^{\varphi_\alpha} g_{lji}^{\varphi_\alpha}) d\omega \tag{V .20}$$

The detailed expressions of $\underline{p}_i^{\varphi_\alpha} = \underline{p}_i^{\varphi_\alpha}(\theta_\alpha, \underline{l}^{\varphi_\alpha}, \epsilon)$ and $g_{ijk}^{\varphi_\alpha} = g_{ijk}^{\varphi_\alpha}(\underline{l}^{\varphi_\alpha}, \mathbb{C}_m)$, are given in Appendix B. The unit vector $\underline{l}_i^{\varphi_\alpha}$ can be expressed in terms of two angles characterizing the spherical coordinates frame:

$$\begin{cases} l_1^{\varphi_\alpha} = cos(\zeta) sin(\psi) \\ l_2^{\varphi_\alpha} = sin(\zeta) sin(\psi) \\ l_3^{\varphi_\alpha} = cos(\psi) \end{cases} \tag{V .21}$$

The integral on the surface of an unit sphere $\mathcal{S}$ can be expressed as:

$$\int_{\mathcal{S}} F(\theta_\alpha, \underline{l}^{\varphi_\alpha}) dw = \int_{\psi=0}^{2\pi} \int_{\zeta=0}^{\pi} F(\theta_\alpha, \psi, \zeta) sin(\psi) d\psi d\zeta \tag{V .22}$$

© 2016 Tous droits réservés.

doc.univ-lille1.fr

Thèse de Mei Qi, Lille 1, 2016

Accordingly, the Hill's tensor can be evaluated numerically using Gauss-Legendre quadrature in terms of the integration angles ζ and ψ. The components of the Hill's tensor in the intermediate coordinate system depend on the aspect ratio of the inclusion ϵ, the angle θ^α of the inclusion, and the elastic properties of the solid matrix:

$$P_{ijkl}^{\varphi_\alpha} = P_{ijkl}^{\varphi_\alpha}(\epsilon, \theta^\alpha, \mathbb{C}_m) \tag{V .23}$$

In order to using Gauss-Legendre quadrature method who is an approximation of the definite integral of a function to evaluate the Hill tensor in the intermediate system, the formulation (V .22) who is the double integral on the surface of an unit sphere S can be stated as a weighted sum of function values at specified points within the domain of integration. On using the spheroidal coordinates, we obtain:

$$\mathbb{P}_{ijkl}^{\varphi_\alpha}(\theta_\alpha) \approx \sum_{k=1}^{N_\zeta^G} \sum_{l=1}^{N_\psi^G} w_k^\zeta w_l^\psi \mathbb{G}_{ijkl}^{\varphi_\alpha}(\theta_\alpha, \zeta_l^G, \psi_k^G) sin(\psi_k^G) \tag{V .24}$$

where w_k^ζ, w_l^ψ, ζ_l^G, ψ_k^G denote respectively the Gauss-Legendre weights and coordinates corresponding to the N_ζ^G and N_ψ^G integrating points which are comprised in the intervals $[0, 2\pi]$ (ζ angle) and $[0, \pi]$ (ψ angle) as previously mentioned. The $\mathbb{G}_{ijkl}^{\varphi_\alpha}$ coefficients can be given by the relation (V .20). The unit vector components $\underline{l}^{\varphi_\alpha}$ in the $\mathbb{G}_{ijkl}^{\varphi_\alpha}$ coefficients defined by relations (V .21) as the functions of angles ψ and ζ, are introduced in the relations presented in Appendix B which are necessary to compute $\mathbb{G}_{ijkl}^{\varphi_\alpha}$ coefficients in the relation (V .20).

Finally, the numerical values of $\mathbb{P}_{ijkl}^{\varphi_\alpha}$ components are computed by using the Gaussian quadrature method (see: (V .24)). The numerical calculations have been achieved by using Fortran software. 5 integrations points of Gaussian quadrature in each subinterval were adopted, and we take the relation $N_\zeta^G = 2N_\psi^G$ in all cases in a division of intervals $[0, 2\pi]$ and $[0, \pi]$ respectively.

Finally, the components of Hill's tensor in the global coordinate system $\mathbb{P}_{ijkl}$ can be determined with the help of the transformation rules between $\underline{e}_i$ and $\underline{e}_i^{\varphi_\alpha}$ coordinates, that is:

$$\mathbb{P} = P_{pqrs}\underline{e}_p \otimes \underline{e}_q \otimes \underline{e}_r \otimes \underline{e}_s = P_{ijkl}^{\varphi_\alpha}\underline{e}_i^{\varphi_\alpha} \otimes \underline{e}_j^{\varphi_\alpha} \otimes \underline{e}_k^{\varphi_\alpha} \otimes \underline{e}_l^{\varphi_\alpha} \tag{V .25}$$

$$P_{ijkl}(\theta_\alpha, \varphi_\alpha) = Q_{p,i}^{\varphi_\alpha}(\varphi_\alpha) Q_{q,j}^{\varphi_\alpha}(\varphi_\alpha) Q_{r,k}^{\varphi_\alpha}(\varphi_\alpha) Q_{s,l}^{\varphi_\alpha}(\varphi_\alpha) P_{pqrs}^{\theta_\alpha} \tag{V .26}$$

© 2016 Tous droits réservés.

doc.univ-lille1.fr

Thèse de Mei Qi, Lille 1, 2016

4 Description of friction-damage evolutions

As mentioned above, for closed frictional micro-cracks, additional constitutive laws should be proposed to describe evolutions of damage and inelastic frictional sliding. To this end, it is convenient to take the inelastic strain $\boldsymbol{E}^{c,r}$ and the crack density parameter d^r as the local internal variables of the two dissipation mechanisms for each family of micro-cracks. The free energy function is then a function of these two international variables as given in (V .15). Note that when multiple families of micro-cracks are considered, a series of discrete local internal variables are defined in the present model. However, the friction and damage evolution law to be developed later are formally common to all families of micro-cracks. For the sake of simplicity, in the following sections, unless specifically mentioned, the superscript r denoting the sequence number of cracks families will be omitted.

The thermodynamic force associated with the inelastic strain $\boldsymbol{E}^{c,r}$, denoted by $\boldsymbol{\sigma}^{c,r}$, is obtained by standard derivative of $W^*(\boldsymbol{E}^{c,r}, d^r)$:

$$\boldsymbol{\sigma}^c = \frac{\partial W^*}{\partial \boldsymbol{E}^c} = \boldsymbol{\Sigma} - \frac{1}{d}\mathbb{C}^n : \boldsymbol{E}^{c,r} \tag{V .27}$$

The thermodynamic force $\boldsymbol{\sigma}^c$ physically defines the local stress applied onto micro-cracks and is the deriving force for the evolution of inelastic strain $\boldsymbol{E}^{c,r}$. It is worth noticing that this thermodynamic force contains a back-stress term, $\frac{1}{d}\mathbb{C}^n : \boldsymbol{E}^{c,r}$. The presence of this term will allow the description of material hardening/softening behaviours. Indeed, the material hardening corresponds to increase of crack shear strength to frictional sliding while the strain softening is induced by crack propagation.

The local stress $\boldsymbol{\sigma}^c$ and be classically decomposed into a normal component σ_n^c and a tangential component $\underline{\tau}^c$, which are obtained by projecting the stress vector $\boldsymbol{\sigma}^c \cdot \underline{n}$ onto the normal direction and cracks plane, as shown in Figure V .3:

$$\sigma_n^c = \underline{n} \cdot \boldsymbol{\sigma}^c \cdot \underline{n}, \quad \underline{\tau}^c = \boldsymbol{\sigma}^c \cdot \underline{n} \cdot (\boldsymbol{\delta} - \underline{n} \otimes \underline{n}) \tag{V .28}$$

On the other hand, the thermodynamic force conjugated with the damage variable d, denoted as F_d, can be also derived from the free enthalpy (V .15):

$$F_d = \frac{\partial W^*}{\partial d} = \frac{1}{2d^2}\boldsymbol{E}^{c,r} : \mathbb{C}^n : \boldsymbol{E}^{c,r} \tag{V .29}$$

© 2016 Tous droits réservés.

doc.univ-lille1.fr

Thèse de Mei Qi, Lille 1, 2016

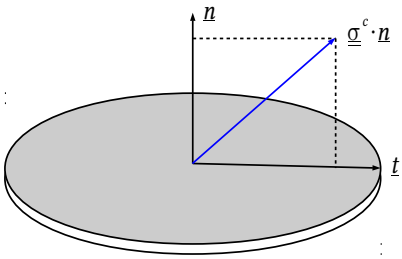

Figure V .3: Decomposition of the local stress vector $\boldsymbol{\sigma}^f \cdot \underline{n}$ onto the normal direction and the crack plane.

4.1 Friction criterion

The frictional sliding is driven by the local shear stress and influenced by the normal stress. In the present study, a linear Coulomb type criterion is applied at the local scale to describe the frictional sliding of micro-cracks. That is:

$$f(\boldsymbol{\sigma}^c) = \|\underline{\tau}^c\| + \eta\sigma_n^c \leqslant 0 \tag{V .30}$$

The parameter η denotes the local friction coefficient on crack surfaces, which can be related to macroscopic shear strength of material as discussed in [Zhu and Shao, 2015]. The presence of the friction term also allows description of confining pressure effects on macroscopic behaviours.

In order to facilitate the formulation of frictional flow rule and numerical implementation, [Zhu and Shao, 2015] proposed the following normal and tangential operators, which are fourth order tensors and both functions of the unit normal vector $\underline{n}$:

$$\mathbb{N} = \underline{n} \otimes \underline{n} \otimes \underline{n} \otimes \underline{n} \tag{V .31}$$

$$\mathbb{T} = (\underline{n} \otimes \underline{n})\overline{\otimes}(\boldsymbol{\delta} - \underline{n} \otimes \underline{n}) + (\boldsymbol{\delta} - \underline{n} \otimes \underline{n})\overline{\otimes}(\underline{n} \otimes \underline{n}) \tag{V .32}$$

with the following properties:

$$\mathbb{N} : \mathbb{N} = \mathbb{N}, \quad \mathbb{T} : \mathbb{T} = \mathbb{T}, \quad \mathbb{N} : \mathbb{T} = \mathbb{T} : \mathbb{N} = \mathbb{O} \tag{V .33}$$

By using these operators, the local normal and tangential stresses can be rewritten as:

$$\|\underline{\tau}^c\| = (\frac{1}{2}\boldsymbol{\sigma}^c : \mathbb{T} : \boldsymbol{\sigma}^c)^{\frac{1}{2}}, \quad \sigma_n^c = -(\boldsymbol{\sigma}^c : \mathbb{N} : \boldsymbol{\sigma}^c)^{\frac{1}{2}} \tag{V .34}$$

© 2016 Tous droits réservés.

doc.univ-lille1.fr

Thèse de Mei Qi, Lille 1, 2016

An associate flow rule is here employed to describe the evolution of inelastic strain. The yield function (V .30) also serves as the potential function. The evolution rate of the inelastic strain $\boldsymbol{E}^{c,r}$ is thus given by the normality rule:

$$\dot{\boldsymbol{E}}^{c,r} = \lambda^s \frac{\partial f(\boldsymbol{\sigma}^c)}{\partial \boldsymbol{\sigma}^c} = \lambda^s \left(\frac{\mathbb{T}}{2\|\underline{\tau}^c\|} + \eta \frac{\mathbb{N}}{\sigma_n^c}\right) : \boldsymbol{\sigma}^c \tag{V .35}$$

The positive multiplier λ^s can be determined by the consistency condition ($g = 0, \dot{g} = 0$), as described later. According to (V .35), the inelastic flow direction can be defined by a second order tensor:

$$\boldsymbol{D}^n = \left(\frac{\mathbb{T}}{2\|\underline{\tau}^c\|} + \eta \frac{\mathbb{N}}{\sigma_n^c}\right) : \boldsymbol{\sigma}^c \tag{V .36}$$

Thus, the evolution of the inelastic strain takes the following form:

$$\dot{\boldsymbol{E}}^{c,r} = \lambda^s \boldsymbol{D}^n \tag{V .37}$$

The Coulomb-type friction criterion can also be reformulated as:

$$f(\boldsymbol{\sigma}^c) = \boldsymbol{\sigma}^c : \boldsymbol{D}^n \leqslant 0 \tag{V .38}$$

4.2 Damage criterion

In the framework of irreversible thermodynamics, the damage criterion is expressed in terms of the thermodynamic forces associated with the damage variables d. Based on the previous works by [Zhu and Shao, 2015], the general expression of damage criterion is adopted:

$$g(F_d, d) = F_d - \mathcal{R}(d) \leqslant 0 \tag{V .39}$$

The conjugate damage force F_d is given in (V .29). The function $\mathcal{R}(d)$ represents the current material toughness to further damage evolution by cracks growth. Following [Zhu and Shao, 2015], the following function is proposed:

$$\mathcal{R}(d) = r_c \frac{2\kappa}{1 + \kappa^2} \tag{V .40}$$

with $\kappa = d/d_c$. The parameter d_c is a critical value of the damage variable and $r_c = \mathcal{R}(d_c)$ being the corresponding value of material toughness. Note that the function $\mathcal{R}(d)$ is increasing when $d \leqslant d_c$ for describing strain hardening process while decreasing when $d \geqslant d_c$ for capturing material softening. The failure of the material takes place when the damage variable d reaches its critical value d_c.

When the damage criterion is reached, the evolution rate of damage variable d can be calculated by using the following normality rule:

$$\dot{d} = \lambda^d \frac{\partial g(F_d, d)}{\partial F_d} = \lambda^d \tag{V .41}$$

© 2016 Tous droits réservés.
doc.univ-lille1.fr

Thèse de Mei Qi, Lille 1, 2016

where λ^d is the damage multiplier which can be determined by the consistency conditions $g(F_d, d) = 0$ and $\dot{g}(F_d, d) = 0$.

4.3 Damage-friction coupling

In general loading conditions, the damage growth and inelastic strain evolution are inherently coupled. In view of numerical implementation of the micro-mechanical model in a computer code and also capturing the post-peak behaviour of materials, it is convenient to carry out the numerical implement with prescribed strain conditions. In the present work, only time-independent behaviours are considered. The rate form of constitutive relations can be equivalently replaced by an incremental form. Consider an incremental variation of macroscopic strain $\Delta \boldsymbol{E}$ applied to the REV. For the ith family of micro-cracks, when the friction criterion is continuously satisfied, the consistency condition ($f^i = 0, \dot{f}^i = 0$) is written as:

$$\Delta f^i = \sum_{j=1}^{N} \frac{\partial f^i}{\partial \boldsymbol{E}^{c,j}} : \Delta \boldsymbol{E}^{c,j} + \frac{\partial f^i}{\partial d^i} \Delta d^i + \frac{\partial f^i}{\partial \boldsymbol{E}} : \Delta \boldsymbol{E} = 0 \tag{V .42}$$

or in an equivalent way

$$\Delta f^i = (\sum_{j=1}^{N} \frac{\partial \boldsymbol{\sigma}^{c,i}}{\partial \boldsymbol{E}^{c,j}} : \Delta \boldsymbol{E}^{c,j} + \frac{\partial \boldsymbol{\sigma}^{c,i}}{\partial d^i} \Delta d^i + \frac{\partial \boldsymbol{\sigma}^{c,i}}{\partial \boldsymbol{E}} : \Delta \boldsymbol{E}) : \boldsymbol{D}^{n,i} = 0 \tag{V .43}$$

Recall that $\Delta \boldsymbol{E}^{c,j} = \lambda_j^s \boldsymbol{D}^{n,j}$ and that the damage increment Δd^i can be expressed in terms of $\Delta \boldsymbol{E}^{c,i}$ by developing the damage consistency condition, that is:

$$\Delta g^i = \frac{\partial g^i}{\partial \boldsymbol{E}^{c,i}} : \Delta \boldsymbol{E}^{c,i} + \frac{\partial g^i}{\partial d^i} \Delta d^i = 0 \tag{V .44}$$

The damage multiplier is obtained:

$$\lambda^d = -\lambda^s \frac{\partial g^i}{\partial \boldsymbol{E}^{c,i}} : \boldsymbol{D}^{n,i} / \frac{\partial g^i}{\partial d^i} \tag{V .45}$$

Finally, the following linear equations are obtained with unknowns $\lambda_j^s, j = 1, ..., N$:

$$X_{ij} \lambda_j^s = Y_i \tag{V .46}$$

with the coefficient X_{ij}:

$$X_{ij} = \boldsymbol{D}^{n,i} : \mathbb{C}^m : \boldsymbol{D}^{n,j} + \frac{1}{d^i} \boldsymbol{I}_{ij} \boldsymbol{D}^{n,i} : \mathbb{C}^{n,i} : \boldsymbol{D}^{n,i} + \frac{1}{(d^i)^4} \boldsymbol{I}_{ij} (\boldsymbol{D}^{n,i} : \mathbb{C}^{n,i} : \boldsymbol{E}^{c,i})^2 / \frac{\partial g^i}{\partial d^i} \tag{V .47}$$

© 2016 Tous droits réservés.

doc.univ-lille1.fr

Thèse de Mei Qi, Lille 1, 2016

and the value of Y_i

$$Y_i = \boldsymbol{D}^{n,i} : \mathbb{C}^m : \Delta\boldsymbol{E} \tag{V .48}$$

In equation (V .47), $\boldsymbol{I}_{ij}$ is the components of a square matrix of dimension $N \times N$. More precisely, $\boldsymbol{I}_{ij} = 1$ when $i = j$, and $\boldsymbol{I}_{ij} = 0$ when $i \neq j$. In the particular case where all cracks are closed and the respective local damage criterion is reached, we will have N linear equations of the same type, which forms a system of N linear equations with N unknowns. Accordingly, the coefficient row X_{ij} in (V .47) is naturally extended to be the matrix of coefficients $[\boldsymbol{X}]$. It is worth noting that this matrix is symmetric and positively define. In this way, the column of unknowns $\{\lambda^s\}$ is given by:

$$\{\lambda^s\} = \boldsymbol{X}^{-1}\{\boldsymbol{D}^n : \mathbb{C}^s\} : \mathrm{d}\boldsymbol{E} \tag{V .49}$$

The incremental form of the macroscopic stress-strain relations (V .12) reads:

$$\Delta\boldsymbol{\Sigma} = \mathbb{C}^m : \Delta\boldsymbol{E} - \sum_{r=1}^{N} \mathbb{C}^m : \Delta\boldsymbol{E}^{c,r} = \mathbb{C}^m : \Delta\boldsymbol{E} - \{\mathbb{C}^m : \boldsymbol{D}^n\}^T\{\lambda^s\} \tag{V .50}$$

Insertion of equation (V .49) into equation (V .50) gives $\Delta\boldsymbol{\Sigma} = \mathbb{C}^{tan} : \Delta\boldsymbol{E}$ with the tangential stiffness tensor:

$$\mathbb{C}^{tan} = \mathbb{C}^m - \{\mathbb{C}^m : \boldsymbol{D}^n\}^T[\boldsymbol{X}]^{-1}\{\boldsymbol{D}^n : \mathbb{C}^m\} \tag{V .51}$$

4.4 Numerical implementation

Due to the nonlinear behaviours related to the inelastic deformation and damage evolution, the loading path is divided into a limited number of steps. At the loading step $j+1$, a new macroscopic strain increment $\Delta\boldsymbol{E}_{j+1}$ is applied. Note that at the end of the previous loading step, the internal variables ($d_{r,j}$, $\boldsymbol{E}^c_j$) as well as the macroscopic stress $\boldsymbol{\Sigma}_j$ and strain $\boldsymbol{E}_j$ are all known. The problem to be solved here is to find the corresponding macroscopic stress increment $\Delta\boldsymbol{\Sigma}_{j+1}$ by using the micro-mechanical model. The numerical algorithm used here is based on the classical operator-splitting method, mainly composed of the elastic predictor and plastic/damage corrector. Further, in the present study, the aspect ratio of micro-cracks is taken as constant. Therefore, for each family of micro-cracks, the fourth order operator $\mathbb{C}^n$ is numerically calculated according to V .9 once for all loading steps. However, in future works, it will be possible to consider variation of crack aspect ratio by updating the Eshelby tensor and operator $\mathbb{C}^n$ for each loading step. The flowchart of the numerical algorithm can be summarized as follows:

a) Elastic prediction:

© 2016 Tous droits réservés.

doc.univ-lille1.fr

Thèse de Mei Qi, Lille 1, 2016

For each rth family of micro-cracks, the two internal variables remain unchanged such that:

$$\begin{cases} d_{r,(j+1)} = d_{r,j} \\ \boldsymbol{E}^{c,r}_{j+1} = \boldsymbol{E}^{c,r}_{j} \end{cases} \tag{V .52}$$

Update the macroscopic strain $\Delta \boldsymbol{E}_{j+1}$ at the step $j+1$ as:

$$\boldsymbol{E}_{j+1} = \boldsymbol{E}_j + \Delta \boldsymbol{E}_{j+1} \tag{V .53}$$

The elastic prediction of the macroscopic stress is calculated by:

$$\boldsymbol{\Sigma}_{j+1} = \mathbb{C}^m : (\boldsymbol{E}_{j+1} - \sum_{r=1}^{N} \boldsymbol{E}^{c,r}_{j+1}) \tag{V .54}$$

b) Friction-damage correction:

(1) Check the friction criterion $f(\boldsymbol{\sigma}^c) \leqslant 0$ for each family of micro-cracks.

(2) Determine the friction multipliers according to (V .49) and calculate the inelastic strain for each family of micro-cracks by using the flow rule:

$$\boldsymbol{E}^c_{j+1} = \boldsymbol{E}^c_j + \lambda^s \boldsymbol{D}^n \tag{V .55}$$

(3) Check the damage criterion for each family of micro-cracks according to (V .39), calculate the damage multiplier using the equation (V .45), and then update the damage variable:

$$d_{r,j+1} = d_{r,j} + \lambda^d \tag{V .56}$$

(4) Update the macroscopic stress according to the stress-strain relation:

$$\boldsymbol{\Sigma}_{j+1} = \mathbb{C}^m : (\boldsymbol{E}_{j+1} - \sum_{r=1}^{N} \boldsymbol{E}^{c,r}_{j+1}) \tag{V .57}$$

If the convergence tolerance in stress $\frac{\|\boldsymbol{\Sigma}_{j+1} - \boldsymbol{\Sigma}_j\|}{\|\boldsymbol{\Sigma}_j\|} \leqslant 10^{-3}$ is not satisfied, carry out the inner iteration.

5 Numerical assessment and experimental verification

In this section, a series of numerical simulations are presented to show the predictive capability of the micro-mechanical model. Experimental verification against laboratory tests is also performed. For this purpose, the proposed model is applied to describe mechanical

© 2016 Tous droits réservés.

doc.univ-lille1.fr

Thèse de Mei Qi, Lille 1, 2016

behaviours of a typical anisotropic clayey rock, Tournemire shale. This rock has been extensively investigated in different contexts such geological disposal of radioactive waste and shale gas production. The Tournemire shale is considered as a typical transversely isotropic material containing a family of parallel bedding planes. A number of laboratory studies have been performed on this material and shown that its mechanical behaviours, in particular elastic properties and mechanical strength, strongly depend on loading orientation. Experimental results obtained from triaxial compression tests by [NianDou et al., 1997] will be used here. For convenience, a structural frame coordinates system is defined. Denote $\underline{e}_3$ the unit vector of the symmetric axis which is perpendicular to bedding planes as shown in V .4. The orientation of each ellipsoidal crack is then defined by two angles, the angle with the symmetric axis θ_α and the angle in the isotropic plane φ_α.

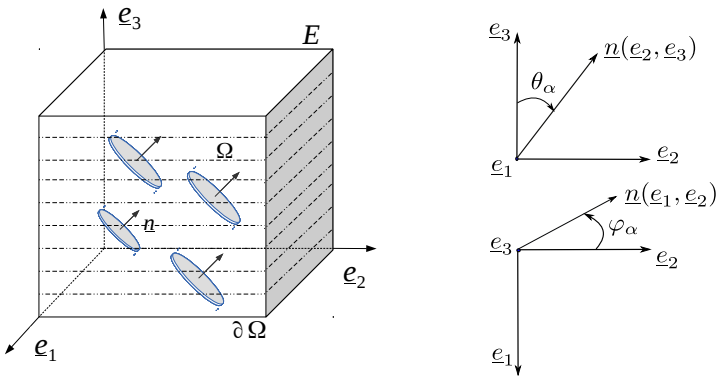

Figure V .4: Definition of structural frame system and crack orientation

5.1 Parameters identification

Compared with most macroscopic models, the proposed micro-mechanical model contains a very small number of parameters and each of them is physically defined. For instance, a part five elastic parameters for transversely isotropic materials, only four parameters are needed for the description of evolutions of induced damage and friction-related inelastic strain.

The elastic properties of a transversely isotropic material at intact state are defined by five initial elastic parameters. With the frame system defined in V .4 and based on the experimental data from [NianDou et al., 1997], the representative values of elastic parameters for the Tournemire shale are given in Table (V .1). It is worth noticing that for most rock materials, the elastic properties may depend on confining pressure due to

© 2016 Tous droits réservés.

doc.univ-lille1.fr

Thèse de Mei Qi, Lille 1, 2016

closure of initial cracks or bedding planes [NianDou et al., 1997, Chen et al., 2012a]). Such a feature is not investigated in the present work because the emphasis is put on the modelling of induced damage and frictional sliding in initially anisotropic materials.

Table V .1: Initially values of elastic parameter of Tournemire shale

E_3 (MPa)	E_1 (MPa)	ν_{12}	ν_{31}	G_{31} (MPa)
3800	10,000	0.202	0.164	2000

As mentioned in the formulation of the micro-mechanical model, the macroscopic strength of materials is controlled by micro-crack density evolution. For instance, in a triaxial compression test, the peak stress is obtained when the local crack toughness reaches its maximal value r_c. Further, the friction coefficient η describes the influence of local normal stress on the inelastic frictional sliding along cracks surface. At the macroscopic scale, this is interpreted by the fact that the macroscopic failure stress varies with confining pressure. Therefore, these two failure parameters are identified from experimental values of peak stress obtained from triaxial compression tests with different confining pressures. Further, the critical value of crack density parameter d_c determines macroscopic strain at the failure state and post-peak responses. Therefore it is fit from stress-strain curves obtained in triaxial compression tests. Finally, it is needed to define an initial value of crack density parameter reflecting a distribution of initial micro-cracks. In the absence of micro-structural analysis, it is usually to take a small value for this parameter. The typical values of four parameters for modelling induced damage and friction are presented in Table V .2.

Table V .2: Parameter values for model

Parameters	η	r_c	d_c	d_0
Values	0.405	0.086	1	0.1

© 2016 Tous droits réservés.

doc.univ-lille1.fr

Thèse de Mei Qi, Lille 1, 2016

5.2 Simulation of triaxial compression test

Mechanical responses of the shale in triaxial compression tests with different confining pressures are first studied. For the sake of simplicity, only one family of micro-cracks is considered in the present study and the case of multiple crack families will be investigated in future works. Two different loading orientations are investigated respectively perpendicular and parallel to bedding planes.

5.2.1 Compression along the axis $\underline{e}_3$

In this case, the loading path is composed of two stages. In the first stage, a hydrostatic stress ($\Sigma_{11} = \Sigma_{22} = \Sigma_{33} = p_c$)is applied to confine the sample. During the second stage, a compressive strain $E_{33} < 0$ is prescribed along the axis $\underline{e}_3$ by maintaining the confining pressure at a constant value to generate a deviatoric stress state in the sample. As the induced damage occurs only during the deviatoric stage, only mechanical responses during the second stage of loading are presented here. Under such a triaxial compression loading condition, three principal stress are all compressive and it is assumed that all induced micro-cracks are closed. Therefore, the frictional sliding and the crack propagation are coupled. In the present work, as mentioned above, only one family of micro-cracks is considered and the most critical one is chosen as the potential failure plane. For initially anisotropic materials, the orientation of the failure plane is influenced by the anisotropy degree of materials and cannot be determined analytically. Thus, a preliminary assessment is performed under uniaxial compression condition by comparing the mechanical strength obtained with different orientations of crack family. In Figure V .5, the numerical results of axial stress-strain curves are presented for different values of the angle θ_α. One can see that the smallest peak stress is obtained when the crack angle is between $\theta_\alpha = 55°$ and $\theta_\alpha = 60°$. Thus, the crack angle $\theta_\alpha = 55°$ is chosen as the failure plane orientation for the transversely isotropic material studied here under compression along the axis $\underline{e}_3$. It is worth noticing that the orientation of failure plane in rock-like materials may vary with confining pressure [Chen et al., 2012a], but this feature is not discussed in the present work.

In Figure V .9, curves are shown comparisons between numerical results and experimental data for triaxial compression tests under different confining pressures. There is a good concordance between the numerical results and the experimental data for inelastic responses and failure stress. Some scatters are observed for the post-peak behaviour of the material. The experimental data show a sharp decrease of the axial stress after the peaks stress while a progressive decrease is obtained in the numerical results. It is useful to point

© 2016 Tous droits réservés.
doc.univ-lille1.fr

Thèse de Mei Qi, Lille 1, 2016

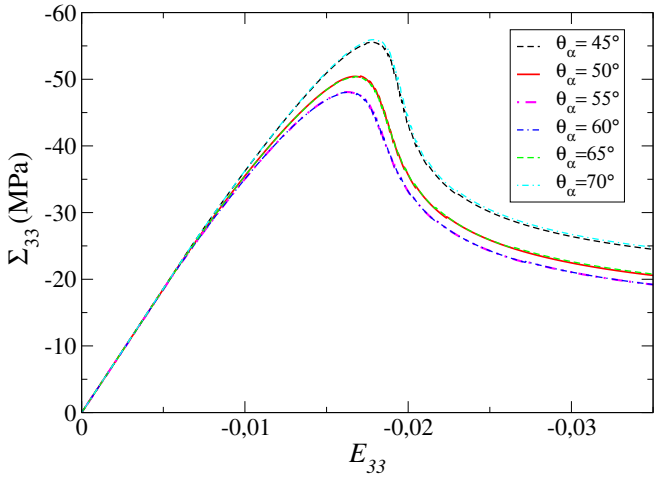

Figure V .5: Stress-strain curves in uniaxial compression test with different crack orientations

out that the post-peak behaviour is inherently related to the onset of strain localization bands and the coalescence of micro-cracks leading to the formation of macroscopic cracks. The overall response of the sample is strongly affected by the deformation of localized bands and cracks. This feature is behind the topic of this work and will be developed in a future investigation.

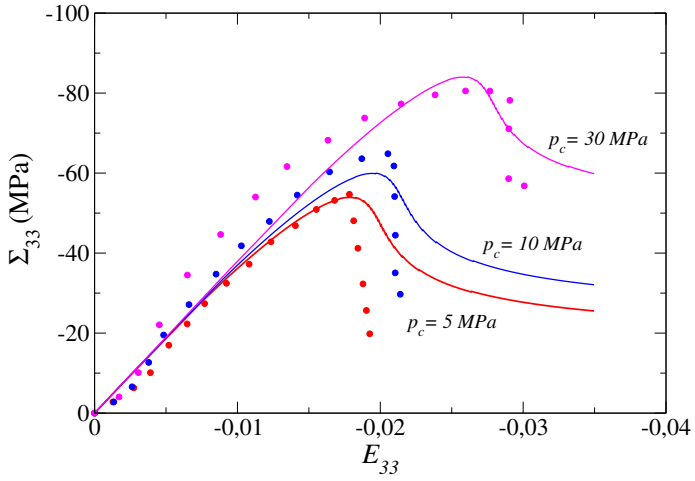

Figure V .6: Stress-strain curves in triaxial compression tests on Tournemire shale with three different confining pressures $(5MPa, 10MPa, 30MPa)$: Comparisons between numerical results (continuous lines) and experimental data

© 2016 Tous droits réservés.

doc.univ-lille1.fr

Thèse de Mei Qi, Lille 1, 2016

5.2.2 Unloading-reloading cycles along the axis e_3

In the proposed micro-mechanical model, the inelastic strain is directly related to the frictional sliding along micro-crack surfaces and coupled with the crack propagation. In order to show effects of the local friction on micro-crack surfaces, stress-strain behaviours during unloading-reloading cycles are studied. Consider now another loading path in the triaxial compression test: cyclic loading path along the axis e_3. To this end, after the stage of confining pressure, some cycles of the axial compressive strain $E_{33} < 0$ is prescribed along the axis $\underline{e}_3$. In Figure V .7, stress-strain curves obtained in such a loading path are presented for three cycles and a $5MPa$ confining pressure. It is found that due to the friction effect, the material exhibits a hysteretic loop during a unloading-reloading cycle. Micro-cracks are locked by the friction during unloading until the friction criterion is reached in an opposite sense. The width of hysteretic loop increases with the accumulated density of micro-cracks, which enhances the inelastic sliding along crack surfaces. Further, the stress-strain curves are compared with those obtained in a monotonic loading path. It is seen that the mechanical strength of material is lower in the cyclic loading than that in the monotonic one. This mechanical strength degradation is due to the accumulation of damage during unloading-reloading cycles.

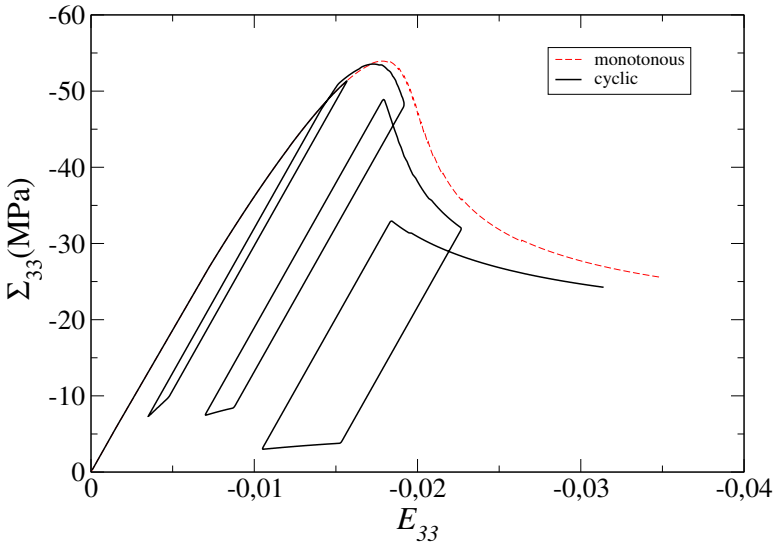

Figure V .7: Stress-strain curves in a triaxial compression test with unloading-reloading cycles under a $5MPa$ confining pressure and comparison with stress-strain envelope obtained in monotonic loading

© 2016 Tous droits réservés.

doc.univ-lille1.fr

Thèse de Mei Qi, Lille 1, 2016

5.2.3 Compression along the axis $\underline{e}_2$

In order to study effects of loading orientation on macroscopic behaviours of transversely isotropic materials, uniaxial and triaxial compression in the direction parallel to bedding planes is now considered. After the application of hydrostatic confining pressure, a compression strain $E_{22} < 0$ is prescribed along the axis $\underline{e}_2$. As for the previous case, preliminary calculations are first performed to choose the orientation of the critical crack orientation considered as that of failure plane. The obtained numerical results under uniaxial compression for four different values of the angle θ_α are presented in Figure V .8. It is seen that the smallest peak stress is obtained for $\theta_\alpha = 43°$. Thus, this angle is chosen as the orientation of failure plane under compression along the axis $\underline{e}_2$.

Comparisons between numerical results and experimental data are given in Figure V .9 for two values of confining pressure. Again, the general trends of mechanical responses of the shale are correctly reproduced by the proposed model. The description of post-peak behaviours should be improved by considering strain localization and crack coalescence.

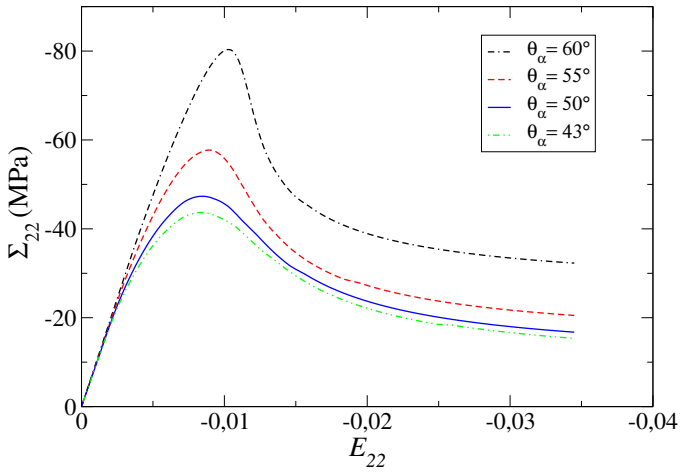

Figure V .8: Stress-strain curves under uniaxial compression for different crack orientations

In Figure V .10, are shown the comparisons of stress-strain curves, obtained in a triaxial compression test under a $5MPa$ confining pressure, respectively in the orientation perpendicular (red color) and parallel (blue color) to bedding planes. One can see that the mechanical response is clearly different between the two loading orientations due to the structural anisotropy of material. The deformation is larger in the perpendicular direction than in the parallel one due to the compressibility of bedding planes. The peak stress is also slightly higher in the perpendicular direction. The results show that the proposed

© 2016 Tous droits réservés.

doc.univ-lille1.fr

Thèse de Mei Qi, Lille 1, 2016

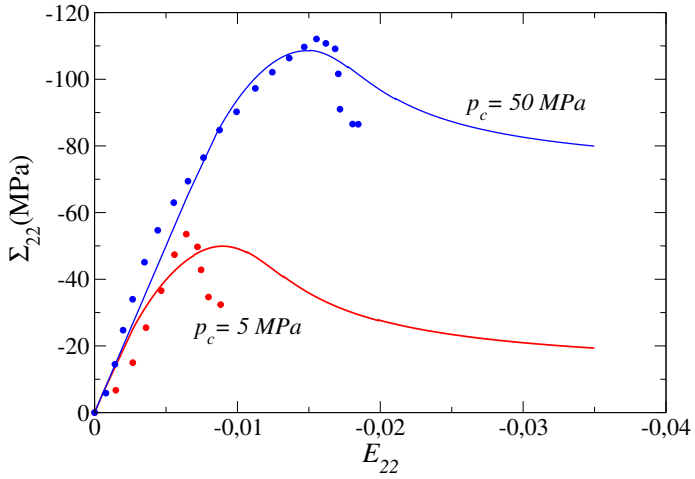

Figure V .9: Stress-strain curves under triaxial compression with two confining pressures $(5MPa, 50MPa)$: Comparisons between numerical results (continuous lines) and experimental data

model is able to describe inelastic deformation and induced damage in initially anisotropic rock-like materials.

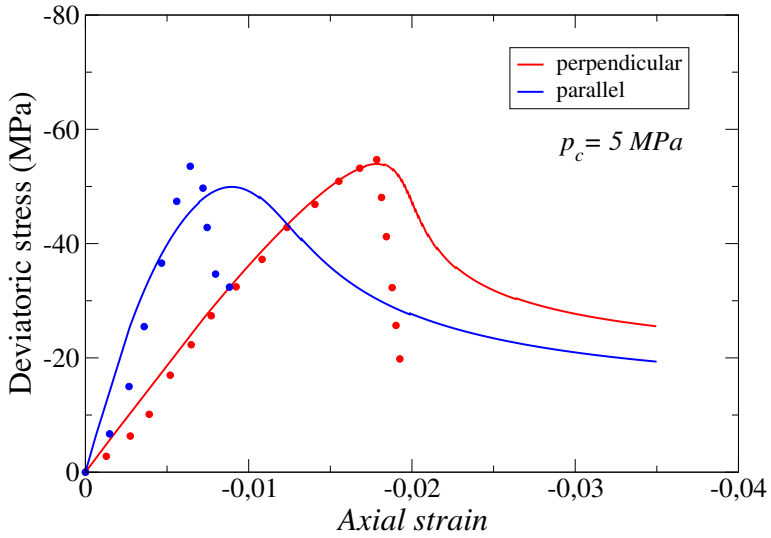

Figure V .10: Stress-strain curves in a triaxial compression test with a $5MPa$ confining pressure: comparison between two loading orientations

© 2016 Tous droits réservés.

doc.univ-lille1.fr

Thèse de Mei Qi, Lille 1, 2016

5.3 Direct shear tests

In order to assess the efficiency of the micro-mechanical model in reproducing mechanical responses of anisotropic materials in different loading conditions, direct shear tests are now considered. The transversely isotropic material contains one family of induced micro-cracks with the crack angles $\theta_\alpha = 55°$, $\varphi_\alpha = 0°$. The emphasis is still put on the description of inelastic friction and damage in closed micro-cracks. For this purpose, the studied unit-cell is under a confining pressure of $5MPa$ to maintain all micro-cracks in the closed state. The values of the initial elastic parameters and of those for the friction and damage are also taken from Tables V .1 and V .2. It is worthy to mention that three are two independent shear moduli in a transversely isotropic material, the transverse shear modulus G_{12} and the longitudinal shear modulus G_{31}=G_{23}. The transverse shear modulus can be calculated from the Young's modulus and Poisson's ratio in the transverse plane by $G_{12} = \frac{E_1}{2(1+\nu_{12})}$ and one obtains $G_{12} \approx 4160MPa$.

In order to investigate effects of the initial material anisotropy on mechanical responses under direct shear, two different shear paths are considered, respectively in the planes $\underline{e}_1\underline{e}_2$ and $\underline{e}_3\underline{e}_1$. For each path, a shear strain, say E_{12} and E_{31}, is prescribed. Further, both monotonic and cyclic paths are considered. In Figures V .11 and V .12, are shown the stress-strain curves obtained for two direct shear paths. It is found that the mechanical responses are clearly dependent on the shear loading path and then affected by the initial material anisotropy. Beside the difference of shear modulus in the elastic stage, the evolutions of inelastic deformation and damage as well as the failure stress are also significantly different between the two paths. For instance, the failure stress is higher for the shear path E_{31} than for the path E_{12}. On these figures, one can also see the comparisons of mechanical responses between the monotonic and cyclic paths. As for compression loading, hysteretic loops due to friction locking of micro-cracks are well described by the micro-mechanical model. The mechanical strength is slightly lower in cyclic paths than that in monotonic ones due to the accumulation of induced damage in unloading-reloading cycles.

6 Conclusion

A micro-mechanics based approach is developed for the description of induced damage and frictional sliding in initially anisotropic quasi-brittle materials. An efficient numerical method is first proposed for the estimation of Hill's tensor for spheroidal micro-cracks in a transversely isotropic solid matrix. Based on this estimation, a three-dimensional micro-mechanical model is formulated for closed frictional micro-cracks by combining a

© 2016 Tous droits réservés.

doc.univ-lille1.fr

Thèse de Mei Qi, Lille 1, 2016

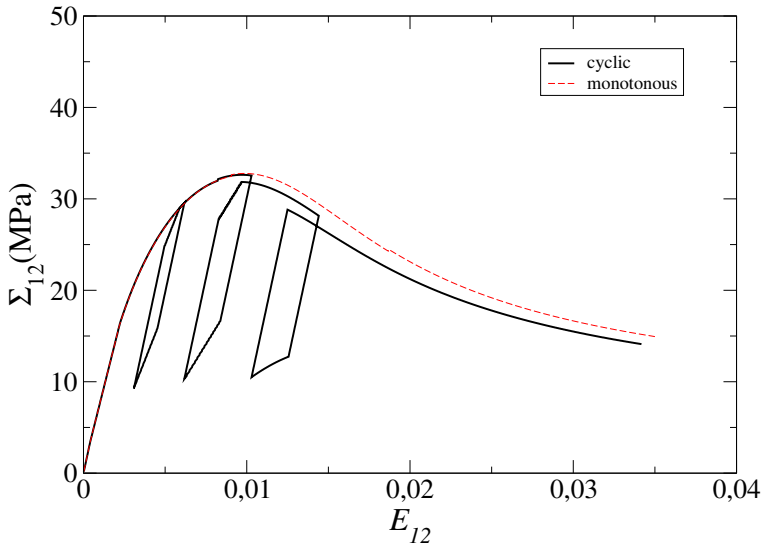

Figure V .11: Stress-strain curves in monotonic and cyclic direct shear tests in the plane $\underline{e}_1\underline{e}_2$

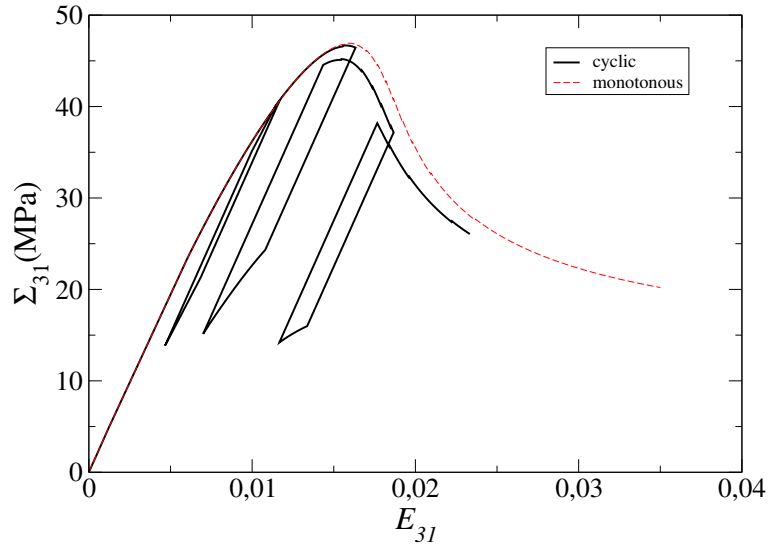

Figure V .12: Stress-strain curves in monotonic and cyclic direct shear tests in the plane $\underline{e}_3\underline{e}_1$

rigorous homogenization procedure and the irreversible thermodynamics framework. The effective elastic properties of cracked materials are estimated using a Mori-Tanaka scheme. The evolutions of inelastic strains due to frictional sliding and induced damage by the propagation of micro-cracks are coupled and described by specific local friction and damage

© 2016 Tous droits réservés.
doc.univ-lille1.fr

Thèse de Mei Qi, Lille 1, 2016

criteria as functions of conjugate thermodynamic forces. The frictional sliding is the driven force of damage growth in closed cracks while the damage enhances the inelastic sliding. With an associated flow rule, the proposed micro-mechanical model contains a smaller number of parameters than most macroscopic models. The efficiency of the model is assessed through a series of numerical examples and comparisons with experimental data for a typical shale. It is found that the micro-mechanical model is able to account for main features of mechanical behaviours of initially anisotropic quasi-brittle materials such as induced growth of micro-cracks, irreversible deformation and hysteretic loops due to friction effects of crack surfaces, coupling between inherent anisotropy and induced anisotropy, effects of confining pressure and volumetric dilatancy. A number of extensions can be considered in future works, for instance, damage and frictional sliding in a general anisotropic solid matrix, study of strain localization and crack coalescence, investigation of limit case for plane cracks with zero aspect ratio.

© 2016 Tous droits réservés.

doc.univ-lille1.fr

Thèse de Mei Qi, Lille 1, 2016

© 2016 Tous droits réservés.

doc.univ-lille1.fr

Thèse de Mei Qi, Lille 1, 2016

Chapter VI

Conclusions and perspectives

This thesis aims to propose a micro-mechanical approach for modelling induced damage and friction sliding for a class of initially anisotropic quasi-brittle materials. To this end, two three-dimensional micro-mechanical damage models have been developed respectively for open and closed micro-cracks. The key step of these two models is an efficient numerical method which is needed for the estimation of Hill's tensor for three dimensional spheroidal micro-cracks in a transversely isotropic solid matrix. The proposed micro-mechanical models are able to account for main features of mechanical behaviour of a large class of quasi-brittle materials such as degradation of elastic properties, induced anisotropy, inelastic frictional sliding, unilateral effects, interaction between inherent anisotropy and induced anisotropy, coupling between crack-growth and frictional sliding.

The micro-mechanical model for open cracks is able to account for interactions between initial material anisotropy and induced growth of cracks. The effective elastic properties of cracked materials have been studied using different homogenization schemes and for different orientations of induced cracks. It was found that the effective elastic properties are strongly affected by the homogenization scheme, and physically affected by the crack interaction and spatial distribution effects. There is also a clear interaction between the initial material anisotropy and induced cracks. Further, based on the irreversible thermodynamics framework, a specific damage evolution criterion has been proposed to describe the progressive growth of induced cracks. The proposed numerical damage model was implemented in a computer code and applied to study mechanical behaviours of cracked materials under different loading paths. Uniaxial tension and compression as well as simple shear tests have been considered. For all cases, the macroscopic stress-strain relations and damage evolutions have been investigated. It was found that the overall mechanical

© 2016 Tous droits réservés.

doc.univ-lille1.fr

Thèse de Mei Qi, Lille 1, 2016

behaviour of cracked material was significantly dependent on the homogenization scheme. With the *Dilute* scheme without considering crack interactions, a too fast damage evolution kinetics was obtained and leading a too sharp material softening after the peak strength. In the case of MT scheme which consider the crack interaction in a simplified way, one generally obtained a too ductile behaviour with a small decrease of stress in the post-peak regime. The PCW scheme, considering both the crack interaction and spatial distribution effects, provided the most typical results compared with a number of experimental evidences observed in a class of brittle materials such as rocks and concrete. The macroscopic behaviour was also affected by the orientation of induced cracks and their interactions with the initial materials anisotropy.

The micro-mechanical model for frictional closed cracks is developed for the description of induced damage and frictional sliding in initially anisotropic quasi-brittle materials. The effective elastic properties of cracked materials are estimated using a Mori-Tanaka scheme. The evolutions of inelastic strains due to frictional sliding and induced damage by the propagation of micro-cracks are coupled and described by specific local friction and damage criteria as functions of conjugate thermodynamic forces. The frictional sliding is the driven force of damage growth in closed cracks while the damage enhances the inelastic sliding. With an associated flow rule, the proposed micro-mechanical model contains a smaller number of parameters than most macroscopic models. The efficiency of the model is assessed through a series of numerical examples and comparisons with experimental data for a typical shale. It is found that the micro-mechanical model is able to account for main features of mechanical behaviours of initially anisotropic quasi-brittle materials such as induced growth of micro-cracks, irreversible deformation and hysteretic loops due to friction effects of crack surfaces, coupling between inherent anisotropy and induced anisotropy, effects of confining pressure and volumetric dilatancy.

The efficiency of proposed models should still be verified by further experimental data and also by their application to different engineering applications. Many extensions can be considered in future works, for instance, damage and frictional sliding in a general anisotropic solid matrix, investigation of limit case for plane cracks with very small aspect ratio, hydro-mechanical coupling considering effects of interstitial pressure, study of strain localization and crack coalescence.

© 2016 Tous droits réservés.

doc.univ-lille1.fr

Appendix A

Walpole decomposition of elasticity tensor for transversely isotropic materials

In the case of an arbitrary transversely isotropic material, the elasticity tensor $\mathbb{C}$ can be expressed with Walpole decomposition, in terms of the six tensors [Castañeda, 2002] :

$$\mathbb{C} = l_1\,\mathbb{E}_1 + l_2\,\mathbb{E}_2 + l_3\,\mathbb{E}_3 + l_4\,\mathbb{E}_4 + l_5\,\mathbb{E}_5 + l_6\,\mathbb{E}_6 \tag{A.1}$$

The matrix expressions of these six tensors $\mathbb{E}_i$ with Voigt notations and axis $\underline{n}_3 = \underline{e}_3$ can be written as following:

$$\mathbb{E}_1 = \frac{1}{2}\begin{bmatrix} 1 & 1 & 0 & 0 & 0 & 0 \\ 1 & 1 & 0 & 0 & 0 & 0 \\ 0 & 0 & 0 & 0 & 0 & 0 \\ 0 & 0 & 0 & 0 & 0 & 0 \\ 0 & 0 & 0 & 0 & 0 & 0 \\ 0 & 0 & 0 & 0 & 0 & 0 \end{bmatrix} \quad ; \qquad \mathbb{E}_2 = \begin{bmatrix} 0 & 0 & 0 & 0 & 0 & 0 \\ 0 & 0 & 0 & 0 & 0 & 0 \\ 0 & 0 & 1 & 0 & 0 & 0 \\ 0 & 0 & 0 & 0 & 0 & 0 \\ 0 & 0 & 0 & 0 & 0 & 0 \\ 0 & 0 & 0 & 0 & 0 & 0 \end{bmatrix}$$

© 2016 Tous droits réservés.

doc.univ-lille1.fr

Thèse de Mei Qi, Lille 1, 2016

$$\mathbb{E}_3 = \frac{1}{2}\begin{bmatrix} 1 & -1 & 0 & 0 & 0 & 0 \\ -1 & 1 & 0 & 0 & 0 & 0 \\ 0 & 0 & 0 & 0 & 0 & 0 \\ 0 & 0 & 0 & 0 & 0 & 0 \\ 0 & 0 & 0 & 0 & 0 & 0 \\ 0 & 0 & 0 & 0 & 0 & 1 \end{bmatrix} ; \; \mathbb{E}_4 = \frac{1}{2}\begin{bmatrix} 0 & 0 & 0 & 0 & 0 & 0 \\ 0 & 0 & 0 & 0 & 0 & 0 \\ 0 & 0 & 0 & 0 & 0 & 0 \\ 0 & 0 & 0 & 1 & 0 & 0 \\ 0 & 0 & 0 & 0 & 1 & 0 \\ 0 & 0 & 0 & 0 & 0 & 0 \end{bmatrix} \tag{A.2}$$

$$\mathbb{E}_5 = \begin{bmatrix} 0 & 0 & 0 & 0 & 0 & 0 \\ 0 & 0 & 0 & 0 & 0 & 0 \\ 1 & 1 & 0 & 0 & 0 & 0 \\ 0 & 0 & 0 & 0 & 0 & 0 \\ 0 & 0 & 0 & 0 & 0 & 0 \\ 0 & 0 & 0 & 0 & 0 & 0 \end{bmatrix} ; \qquad \mathbb{E}_6 = \begin{bmatrix} 0 & 0 & 1 & 0 & 0 & 0 \\ 0 & 0 & 1 & 0 & 0 & 0 \\ 0 & 0 & 0 & 0 & 0 & 0 \\ 0 & 0 & 0 & 0 & 0 & 0 \\ 0 & 0 & 0 & 0 & 0 & 0 \\ 0 & 0 & 0 & 0 & 0 & 0 \end{bmatrix}$$

© 2016 Tous droits réservés.

doc.univ-lille1.fr

Appendix B

Derivative of Green's function for transversely isotropic materials

The calculations of Hill's tensor in this appendix are given in the intermediate φ_α coordinates $\underline{e}_i^{\varphi_\alpha}$. The Hill's tensor in the global coordinate system $\mathbb{P}_{ijkl}$ can be determined with the help of the transformation rules between $\underline{e}_i$ and $\underline{e}_i^{\varphi_\alpha}$ coordinates.

It is necessary to note that the relation $C_{13}^* - C_{13} - 2C_{44} \neq 0$ is considered here for the case of transversely isotropic materials ([Pan and Chou, 1976]).

$$\mathbb{P}_{ijkl}^{\varphi_\alpha} = \int_\Sigma (\underline{p}_l^{\varphi_\alpha} g_{kij}^{\varphi_\alpha} + \underline{p}_l^{\varphi_\alpha} g_{kji}^{\varphi_\alpha} + \underline{p}_k^{\varphi_\alpha} g_{lij}^{\varphi_\alpha} + \underline{p}_k^{\varphi_\alpha} g_{lji}^{\varphi_\alpha}) d\omega \tag{B.1}$$

with

$$p_1^{\varphi_\alpha} = \frac{\alpha^2 l_1^{\varphi_\alpha}}{\alpha^2 (l_1^{\varphi_\alpha})^2 + (l_3^{\varphi_\alpha} cos(\theta_\alpha) + l_2^{\varphi_\alpha} sin(\theta_\alpha))^2 + \alpha^2 (l_2^{\varphi_\alpha} cos(\theta_\alpha) - l_3^{\varphi_\alpha} sin(\theta_\alpha))^2} \tag{B.2}$$

$$p_2^{\varphi_\alpha} = \frac{(l_3^{\varphi_\alpha} cos(\theta_\alpha) + l_2^{\varphi_\alpha} sin(\theta_\alpha)) * sin(\theta_\alpha) + \alpha^2 (l_2^{\varphi_\alpha} cos(\theta_\alpha) - l_3^{\varphi_\alpha} sin(\theta_\alpha)) * cos(\theta_\alpha)}{\alpha^2 (l_1^{\varphi_\alpha})^2 + (l_3^{\varphi_\alpha} cos(\theta_\alpha) + l_2^{\varphi_\alpha} sin(\theta_\alpha))^2 + \alpha^2 (l_2^{\varphi_\alpha} cos(\theta_\alpha) - l_3^{\varphi_\alpha} sin(\theta_\alpha))^2} \tag{B.3}$$

$$p_3^{\varphi_\alpha} = \frac{(l_3^{\varphi_\alpha} cos(\theta_\alpha) + l_2^{\varphi_\alpha} sin(\theta_\alpha)) * cos(\theta_\alpha) - \alpha^2 (l_2^{\varphi_\alpha} cos(\theta_\alpha) - l_3^{\varphi_\alpha} sin(\theta_\alpha)) * sin(\theta_\alpha)}{\alpha^2 (l_1^{\varphi_\alpha})^2 + (l_3^{\varphi_\alpha} cos(\theta_\alpha) + l_2^{\varphi_\alpha} sin(\theta_\alpha))^2 + \alpha^2 (l_2^{\varphi_\alpha} cos(\theta_\alpha) - l_3^{\varphi_\alpha} sin(\theta_\alpha))^2} \tag{B.4}$$

© 2016 Tous droits réservés.

doc.univ-lille1.fr

$$
\begin{aligned}
g_{111}^{\varphi_\alpha} &= -\nu_1 A\prime_1 l_1^{\varphi_\alpha}[-8\tfrac{(l_2^{\varphi_\alpha})^2\nu_1^2(l_3^{\varphi_\alpha})^2}{(\rho^{\varphi_\alpha})^2}+\tfrac{(l_1^{\varphi_\alpha})^2\nu_1^2(l_3^{\varphi_\alpha})^2}{(R_1^{\varphi_\alpha})^2}-3(l_2^{\varphi_\alpha})^2+2\nu_1^2(l_3^{\varphi_\alpha})^2](\rho^{\varphi_\alpha})^{-4}(R_1^{\varphi_\alpha})^{-1}\\
&\quad -\nu_2 A\prime_2 l_1^{\varphi_\alpha}[-8\tfrac{(l_2^{\varphi_\alpha})^2\nu_2^2(l_3^{\varphi_\alpha})^2}{(\rho^{\varphi_\alpha})^2}+\tfrac{(l_1^{\varphi_\alpha})^2\nu_2^2(l_3^{\varphi_\alpha})^2}{(R_2^{\varphi_\alpha})^2}-3(l_2^{\varphi_\alpha})^2+2\nu_2^2(l_3^{\varphi_\alpha})^2](\rho^{\varphi_\alpha})^{-4}(R_2^{\varphi_\alpha})^{-1}\\
&\quad -Dl_1^{\varphi_\alpha}[8\tfrac{(l_3^{\varphi_\alpha})^2\nu_2^2(l_3^{\varphi_\alpha})^2}{(\rho^{\varphi_\alpha})^2}+\tfrac{(l_2^{\varphi_\alpha})^2\nu_3^2(l_3^{\varphi_\alpha})^2}{(R_3^{\varphi_\alpha})^2}-(l_1^{\varphi_\alpha})^2+2(l_2^{\varphi_\alpha})^2-2\nu_3^2(l_3^{\varphi_\alpha})^2](\rho^{\varphi_\alpha})^{-4}(R_3^{\varphi_\alpha})^{-1}
\end{aligned}
\tag{B.5}
$$

$$
\begin{aligned}
g_{112}^{\varphi_\alpha} &= -\nu_1 A\prime_1 l_2^{\varphi_\alpha}[8\tfrac{(l_1^{\varphi_\alpha})^2\nu_1^2(l_3^{\varphi_\alpha})^2}{(\rho^{\varphi_\alpha})^2}+\tfrac{(l_1^{\varphi_\alpha})^2\nu_1^2(l_3^{\varphi_\alpha})^2}{(R_1^{\varphi_\alpha})^2}+2(l_2^{\varphi_\alpha})^2-(l_2^{\varphi_\alpha})^2-2\nu_1^2(l_3^{\varphi_\alpha})^2](\rho^{\varphi_\alpha})^{-4}(R_1^{\varphi_\alpha})^{-1}\\
&\quad -\nu_2 A\prime_2 l_2^{\varphi_\alpha}[8\tfrac{(l_1^{\varphi_\alpha})^2\nu_2^2(l_3^{\varphi_\alpha})^2}{(\rho^{\varphi_\alpha})^2}+\tfrac{(l_1^{\varphi_\alpha})^2\nu_2^2(l_3^{\varphi_\alpha})^2}{(R_2^{\varphi_\alpha})^2}+2(l_1^{\varphi_\alpha})^2-(l_2^{\varphi_\alpha})^2-2\nu_2^2(l_3^{\varphi_\alpha})^2](\rho^{\varphi_\alpha})^{-4}(R_2^{\varphi_\alpha})^{-1}\\
&\quad -Dl_2^{\varphi_\alpha}[-8\tfrac{(l_1^{\varphi_\alpha})^2\nu_3^2(l_3^{\varphi_\alpha})^2}{(\rho^{\varphi_\alpha})^2}+\tfrac{(l_2^{\varphi_\alpha})^2\nu_3^2(l_3^{\varphi_\alpha})^2}{(R_3^{\varphi_\alpha})^2}-3(l_1^{\varphi_\alpha})^2+2\nu_3^2(l_3^{\varphi_\alpha})^2](\rho^{\varphi_\alpha})^{-4}(R_3^{\varphi_\alpha})^{-1}
\end{aligned}
\tag{B.6}
$$

$$
\begin{aligned}
g_{113}^{\varphi_\alpha} &= 2\nu_1^3 A\prime_1 l_3^{\varphi_\alpha}[2(l_1^{\varphi_\alpha})^2-(l_2^{\varphi_\alpha})^2-\tfrac{\nu_1^2(l_1^{\varphi_\alpha})^2(l_3^{\varphi_\alpha})^2}{(R_1^{\varphi_\alpha})^2}](\rho^{\varphi_\alpha})^{-4}(R_1^{\varphi_\alpha})^{-1}\\
&\quad +2\nu_2^3 A\prime_2 l_3^{\varphi_\alpha}[2(l_1^{\varphi_\alpha})^2-(l_2^{\varphi_\alpha})^2-\tfrac{\nu_2^2(l_1^{\varphi_\alpha})^2(l_3^{\varphi_\alpha})^2}{(R_2^{\varphi_\alpha})^2}](\rho^{\varphi_\alpha})^{-4}(R_2^{\varphi_\alpha})^{-1}\\
&\quad -D\nu_3^2 l_3^{\varphi_\alpha}[(l_1^{\varphi_\alpha})^2-2(l_2^{\varphi_\alpha})^2+\tfrac{\nu_3^2(l_2^{\varphi_\alpha})^2(l_3^{\varphi_\alpha})^2}{(R_3^{\varphi_\alpha})^2}](\rho^{\varphi_\alpha})^{-4}(R_3^{\varphi_\alpha})^{-1}
\end{aligned}
\tag{B.7}
$$

$$
\begin{aligned}
g_{121}^{\varphi_\alpha} &= -\nu_1 A\prime_1 l_2^{\varphi_\alpha}[8\tfrac{(l_1^{\varphi_\alpha})^2\nu_1^2(l_3^{\varphi_\alpha})^2}{(\rho^{\varphi_\alpha})^2}+\tfrac{(l_1^{\varphi_\alpha})^2\nu_1^2(l_3^{\varphi_\alpha})^2}{(R_1^{\varphi_\alpha})^2}+2(l_2^{\varphi_\alpha})^2-(l_2^{\varphi_\alpha})^2-2\nu_1^2(l_3^{\varphi_\alpha})^2](\rho^{\varphi_\alpha})^{-4}(R_1^{\varphi_\alpha})^{-1}\\
&\quad -\nu_2 A\prime_2 l_2^{\varphi_\alpha}[8\tfrac{(l_1^{\varphi_\alpha})^2\nu_2^2(l_3^{\varphi_\alpha})^2}{(\rho^{\varphi_\alpha})^2}+\tfrac{(l_1^{\varphi_\alpha})^2\nu_2^2(l_3^{\varphi_\alpha})^2}{(R_2^{\varphi_\alpha})^2}+2(l_1^{\varphi_\alpha})^2-(l_2^{\varphi_\alpha})^2-2\nu_2^2(l_3^{\varphi_\alpha})^2](\rho^{\varphi_\alpha})^{-4}(R_2^{\varphi_\alpha})^{-1}\\
&\quad -Dl_2^{\varphi_\alpha}[8\tfrac{(l_1^{\varphi_\alpha})^2\nu_3^2(l_3^{\varphi_\alpha})^2}{(\rho^{\varphi_\alpha})^2}+\tfrac{(l_1^{\varphi_\alpha})^2\nu_3^2(l_3^{\varphi_\alpha})^2}{(R_3^{\varphi_\alpha})^2}+2(l_1^{\varphi_\alpha})^2-(l_2^{\varphi_\alpha})^2-2\nu_3^2(l_3^{\varphi_\alpha})^2](\rho^{\varphi_\alpha})^{-4}(R_3^{\varphi_\alpha})^{-1}
\end{aligned}
\tag{B.8}
$$

$$
\begin{aligned}
g_{123}^{\varphi_\alpha} &= 2\tfrac{\nu_1^3 A\prime_1 l_1^{\varphi_\alpha} l_2^{\varphi_\alpha} l_3^{\varphi_\alpha}(3(\rho^{\varphi_\alpha})^2+2\nu_1^2(l_3^{\varphi_\alpha})^2)}{(\rho^{\varphi_\alpha})^4(R_1^{\varphi_\alpha})^3}+2\tfrac{\nu_2^3 A\prime_2 l_1^{\varphi_\alpha} l_2^{\varphi_\alpha} l_3^{\varphi_\alpha}(3(\rho^{\varphi_\alpha})^2+2\nu_2^2(l_3^{\varphi_\alpha})^2)}{(\rho^{\varphi_\alpha})^4(R_2^{\varphi_\alpha})^3}\\
&\quad -\tfrac{D\nu_3^2 l_1^{\varphi_\alpha} l_2^{\varphi_\alpha} l_3^{\varphi_\alpha}(3(\rho^{\varphi_\alpha})^2+2\nu_3^2(l_3^{\varphi_\alpha})^2)}{(\rho^{\varphi_\alpha})^4(R_3^{\varphi_\alpha})^3}
\end{aligned}
\tag{B.9}
$$

$$
\begin{aligned}
g_{131}^{\varphi_\alpha} &= \nu_1^2 A_1 l_3^{\varphi_\alpha}(1-2\tfrac{(l_1^{\varphi_\alpha})^2}{\rho^{\varphi_\alpha}}-\tfrac{(l_1^{\varphi_\alpha})^2}{(R_1^{\varphi_\alpha})^2})(\rho^{\varphi_\alpha})^{-2}(R_1^{\varphi_\alpha})^{-1}\\
&\quad +\nu_2^2 A_2 l_3^{\varphi_\alpha}(1-2\tfrac{(l_1^{\varphi_\alpha})^2}{\rho^{\varphi_\alpha}}-\tfrac{(l_1^{\varphi_\alpha})^2}{R_2^2})(\rho^{\varphi_\alpha})^{-2}(R_2^{\varphi_\alpha})^{-1}
\end{aligned}
\tag{B.10}
$$

© 2016 Tous droits réservés.

doc.univ-lille1.fr

$$\begin{aligned} g_{312}^{\varphi_\alpha} &= 2k_1\nu_1^3 A\prime_1 l_1^{\varphi_\alpha} l_2^{\varphi_\alpha} l_3^{\varphi_\alpha} (2(\rho^{\varphi_\alpha})^{-2} + (R_1^{\varphi_\alpha})^{-2})(\rho^{\varphi_\alpha})^{-2}(R_1^{\varphi_\alpha})^{-1} \\ &+2k_2\nu_2^3 A\prime_2 l_1^{\varphi_\alpha} l_2^{\varphi_\alpha} l_3^{\varphi_\alpha} (2(\rho^{\varphi_\alpha})^{-2} + (R_2^{\varphi_\alpha})^{-2})(\rho^{\varphi_\alpha})^{-2}(R_2^{\varphi_\alpha})^{-1} \end{aligned} \tag{B.11}$$

$$g_{313}^{\varphi_\alpha} = -2\frac{k_1\nu_1^3 A\prime_1 l_1^{\varphi_\alpha}}{(R_1^{\varphi_\alpha})^3} - 2\frac{k_2\nu_2^3 A\prime_2 l_1^{\varphi_\alpha}}{(R_2^{\varphi_\alpha})^3} \tag{B.12}$$

$$g_{331}^{\varphi_\alpha} = \frac{k_1\nu_1^2 A_1 l_1^{\varphi_\alpha}}{(R_1^{\varphi_\alpha})^3} + \frac{k_2\nu_2^2 A_2 l_1^{\varphi_\alpha}}{(R_2^{\varphi_\alpha})^3} \tag{B.13}$$

$$g_{333}^{\varphi_\alpha} = \frac{k_1\nu_1^4 A_1 l_1^{\varphi_\alpha}}{(R_1^{\varphi_\alpha})^3} + \frac{k_2\nu_2^4 A_2 l_3^{\varphi_\alpha}}{(R_2^{\varphi_\alpha})^3} \tag{B.14}$$

where:

$$\rho^{\varphi_\alpha} = \sqrt{(l_1^{\varphi_\alpha})^2 + (l_2^{\varphi_\alpha})^2};\quad R_i^{\varphi_\alpha} = (\rho^{\varphi_\alpha})^2 + \nu_i^2 (l_3^{\varphi_\alpha})^2;\quad k_i = \frac{\frac{C_{11}}{\nu_i^2} - C_{44}}{C_{13}+C_{44}}$$

$$A_1 = \tfrac{1}{4}\frac{C_{13}+C_{44}}{\nu_1\pi(\nu_2^2-\nu_1^2)C_{33}C_{44}};\quad A_2 = -\frac{\nu_1 A_1}{\nu_2}$$

$$A_1' = \tfrac{1}{8}\frac{C_{44}-\nu_1^2 C_{33}}{\pi(\nu_2^2-\nu_1^2)\nu_1^2 C_{33}C_{44}};\quad A_2' = \tfrac{1}{8}\frac{C_{44}-\nu_2^2 C_{33}}{\pi(\nu_2^2-\nu_1^2)\nu_2^2 C_{33}C_{44}}$$

$$D = \tfrac{1}{4}\frac{1}{\pi C_{44}\nu_3};\quad C_{13}^* = \sqrt{C_{11}C_{33}};\quad C_{66} = \tfrac{1}{2}(C_{11}-C_{12})$$

$$\nu_1 = \sqrt{\frac{(C_{13}^*-C_{13})(C_{13}^*+C_{13}+2C_{44})}{4C_{33}C_{44}}} + \sqrt{\frac{(C_{13}^*+C_{13})(C_{13}^*-C_{13}-2C_{44})}{4C_{33}C_{44}}}$$

$$\nu_2 = \sqrt{\frac{(C_{13}^*-C_{13})(C_{13}^*+C_{13}+2C_{44})}{4C_{33}C_{44}}} - \sqrt{\frac{(C_{13}^*+C_{13})(C_{13}^*-C_{13}-2C_{44})}{4C_{33}C_{44}}}$$

$$\nu_3 = \sqrt{\frac{C_{44}}{C_{66}}}$$

$$\overline{\rho}^{\varphi_\alpha} = \sqrt{(e_1^{\varphi_\alpha})^2 + (e_2^{\varphi_\alpha})^2};\quad \overline{R}_i^{\varphi_\alpha} = (\rho^{\varphi_\alpha})^2 + \nu_i^2 (e_3^{\varphi_\alpha})^2$$

© 2016 Tous droits réservés.

doc.univ-lille1.fr

© 2016 Tous droits réservés.

doc.univ-lille1.fr

Appendix C

Chapter 3 supplements

1 Some illustrations of effect of the microcracks on the macrocopic property for initially isotropic matrix

It is proposed to illustration and compare here the predictions of the various homogenisation schemes of effect of the microcracks on the macrocopic property for initially isotropic matrix. First of all, we consider the case of anisotropic distribution of cracks in the initially isotropic matrix. For complete the result, we extend to examine the influence of the microcracks system in any one direction defined by a unit vector $\underline{m}$, considering the Young's modulus $E^{hom}(\underline{m})$ as mentioned in the Chapter II . Then the simple case of the isotropic distribution of cracks are proposed. As indicated in Chapter II , we will consider a spherical distribution of the PCW scheme.

1.1 Anisotropic distribution of microcracks

To present an anisotropic distribution of microcracks in an initially isotopic matrix, we consider here the same parallel cracks system, normal $\underline{e}_3$ as previously mentioned for the case of initially transversely isotropic matrix, which induces an isotropic transverse of the matrix. The results are shown in a modification of the longitudinal Young modulus and the shear modulus in the cracks plan. We can deduce the analytical formulation because of the property of the initially isotropic matrix. Due to the transverse isotropy, we using a standard notation (Walpole notation) to simplify the calculation of fourth-order transversely isotropic tensor ([Walpole, 1981]). It construct from the tensor $\mathbb{E}^i, i = 1, ..., 6$, (see Chapter II). We rappel the analytical results of the different estimation schemes for this system:

© 2016 Tous droits réservés.

doc.univ-lille1.fr

Thèse de Mei Qi, Lille 1, 2016

- Dilute scheme:

Case of open cracks

$$\frac{E_3^{dil}}{E^s} = \frac{1 - r(1-\nu^s)d}{1 - 2r(\nu^s)^2 d} \quad ; \quad \frac{\mu_{31}^{dil}}{\mu^s} = \frac{\mu_{23}^{dil}}{\mu^s} = 1 - \frac{1-2\nu^s}{2-\nu^s} rd \tag{C.1}$$

with $r = \frac{16(1-\mu^s)}{3(1-2\mu^s)}$,

Case of frictionless close cracks

$$\frac{E_3^{dil}}{E^s} = 1 \quad ; \quad \frac{\mu_{31}^{dil}}{\mu^s} = \frac{\mu_{23}^{dil}}{\mu^s} = 1 - \frac{1-2\nu^s}{2-\nu^s} rd \tag{C.2}$$

- Mori Tanaka scheme:

Case of open cracks

$$\frac{E_3^{MT}}{E^s} = \frac{1}{1 + \frac{16}{3}[1-(\nu^s)^2]d} \quad ; \quad \frac{\mu_{31}^{MT}}{\mu^s} = \frac{\mu_{23}^{MT}}{\mu^s} = \frac{1}{1 + \frac{16(1-\nu^s)}{3(2-\nu^s)} d} \tag{C.3}$$

Case of frictionless close cracks

$$\frac{E_3^{MT}}{E^s} = 1 \quad ; \quad \frac{\mu_{31}^{MT}}{\mu^s} = \frac{\mu_{23}^{MT}}{\mu^s} = \frac{1}{1 + \frac{16(1-\nu^s)}{3(2-\nu^s)} d} \tag{C.4}$$

- Ponte-Castaneda and Willis scheme estimations:

Case of open cracks

$$\frac{E_3^{PCW}}{E^s} = 1 - \frac{240[1-(\nu)^2]d}{45+16[7-15(\nu)^2]d}$$

$$\frac{\mu_{31}^{PCW}}{\mu^s} = \frac{\mu_{23}^{PCW}}{\mu^s} = 1 - \frac{240(1-\nu^s)d}{45(2-\nu^s)+32(4-5\nu^s)d} \tag{C.5}$$

Case of frictionless close cracks

$$\frac{E_3^{PCW}}{E^s} = 1 \quad ; \quad \frac{\mu_{31}^{PCW}}{\mu^s} = \frac{\mu_{23}^{PCW}}{\mu^s} = 1 - \frac{240(1-\nu^s)d}{45(2-\nu^s)+32(4-5\nu^s)d} \tag{C.6}$$

With regard to the effect of the close cracks, the analytical results show that a complete restitution of modulus of the elasticity in the normal direction at the crack, and as for the

© 2016 Tous droits réservés. doc.univ-lille1.fr

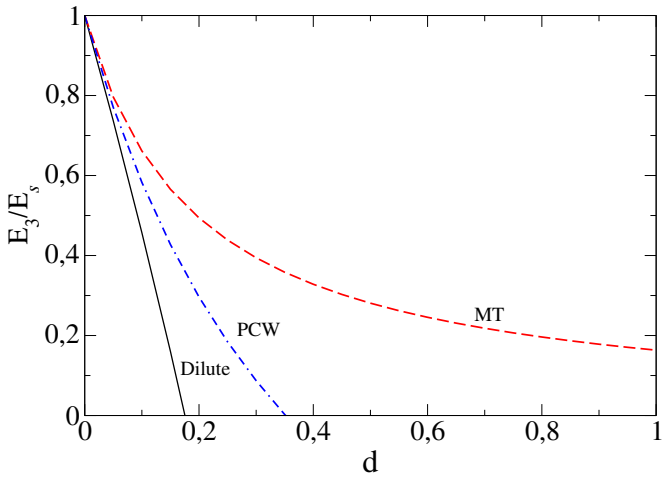

Figure C.1: Parallel cracks: Comparison of the predictions of the different schemes for the longitudinal Young modulus with initially isotropic matrix

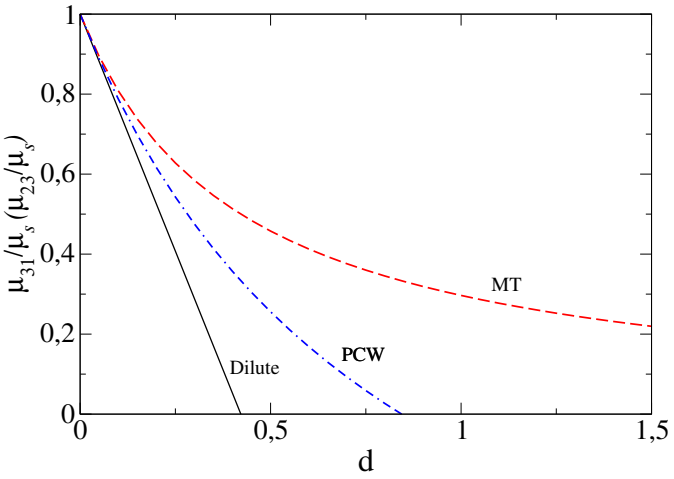

Figure C.2: Parallel cracks: Comparison of the predictions of the different schemes for the shear modulus with initially isotropic matrix

shear modulus in the cracks plane, the value is the same as the open cracks. We adopt the numerical value of the Poisson ratio $\nu^s = 0.2$.

A comparison of these predictions of the difference estimation schemes is provided in the figure (C.1) for the longitudinal Young modulus and in the figure (C.2) for the shear modulus in the plan of the cracks who are the only affected elastic characteristics by the crack. The general variation of the anisotropic distribution of cracks of initially isotropic matrix are quite similar with the initially transversely isotropic matrix. Here, the results

© 2016 Tous droits réservés.

doc.univ-lille1.fr

Thèse de Mei Qi, Lille 1, 2016

are shown in the case of open cracks.

1.2 Effects of the microcracks on the elastic modulus in arbitrary direction: comparison with the initially transversely isotropic matrix

We recall the same system in the subsection (3.2) which a set of parallel microcracks, its unit normal $\underline{n}(\underline{e}_2, \underline{e}_3)$ associated to the angle θ_α is coincident with the normal $\underline{e}_3$ of the isotropic matrix (see Fig. III .1).

We take into account also the Young's modulus $E^{hom}(\underline{m})$ in the normal direction $\underline{e}_3$ to compare the influence of the Young's moduli between isotropic matrix and transversely isotropic matrix produced by a parallel open and close cracks with 3 different estimation schemes.

The results are normalized with the initial values of the Young moduli, which are represented by the unit circle. The figure (C.3) and (C.4) presented perspectively the variation of transverse and longitudinal Young moduli in any one direction for $\theta_\alpha = 0°$. We can see that there are sensibly different between the isotropic matrix and transversely isotropic matrix in these two case. For the case of initially isotropic matrix, it can obtain the same curve in the (Fig: C.4), when we take a simple rotation of the previous one $\theta_\alpha = 0°$. But for the case of transversely isotropic matrix, we can not obtain the same curve with a rotation $\pi/2$ because of the effect anisotropy of the materials.

© 2016 Tous droits réservés.

doc.univ-lille1.fr

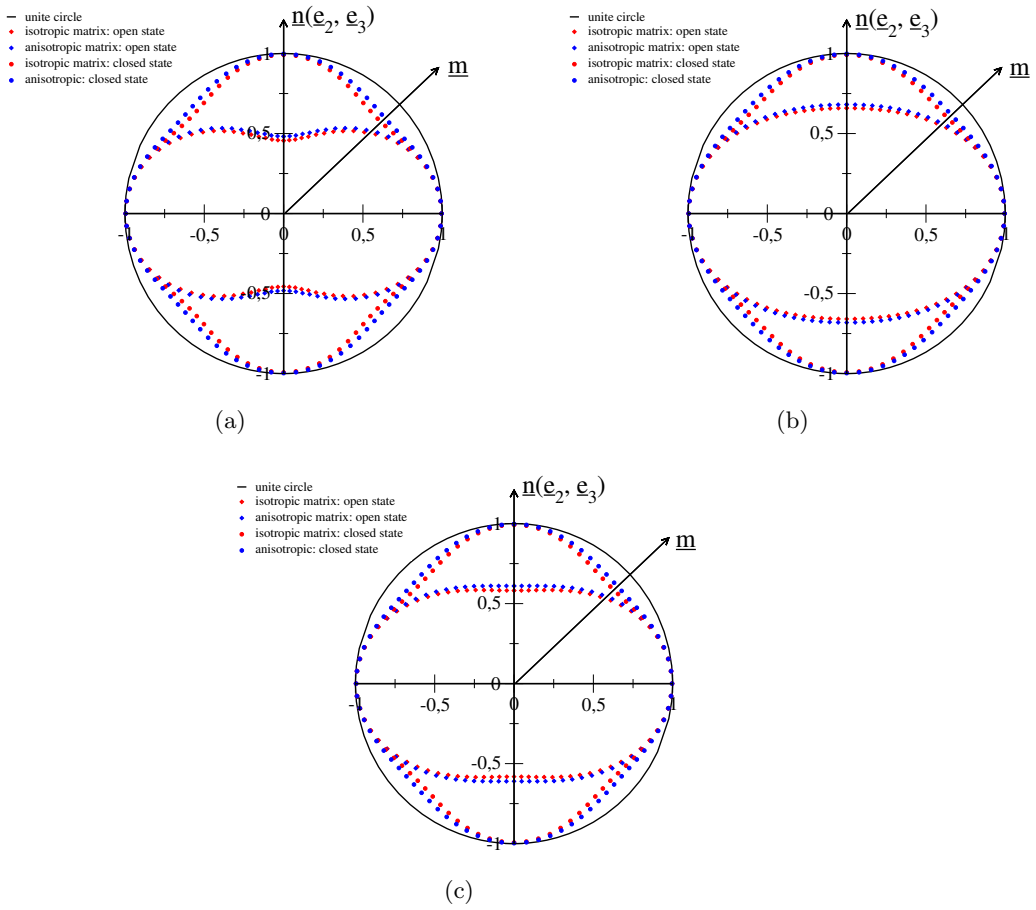

Figure C.3: Comparison the variation of the Young's moduli between isotropic and transversely isotropic matrix produced by parallel open/close cracks media for $\theta_\alpha = 0°$: (a) Dilute scheme, (b) Mori-Tanaka scheme, (c) Ponte-Castaneda et Willis scheme.

© 2016 Tous droits réservés.

doc.univ-lille1.fr

Thèse de Mei Qi, Lille 1, 2016

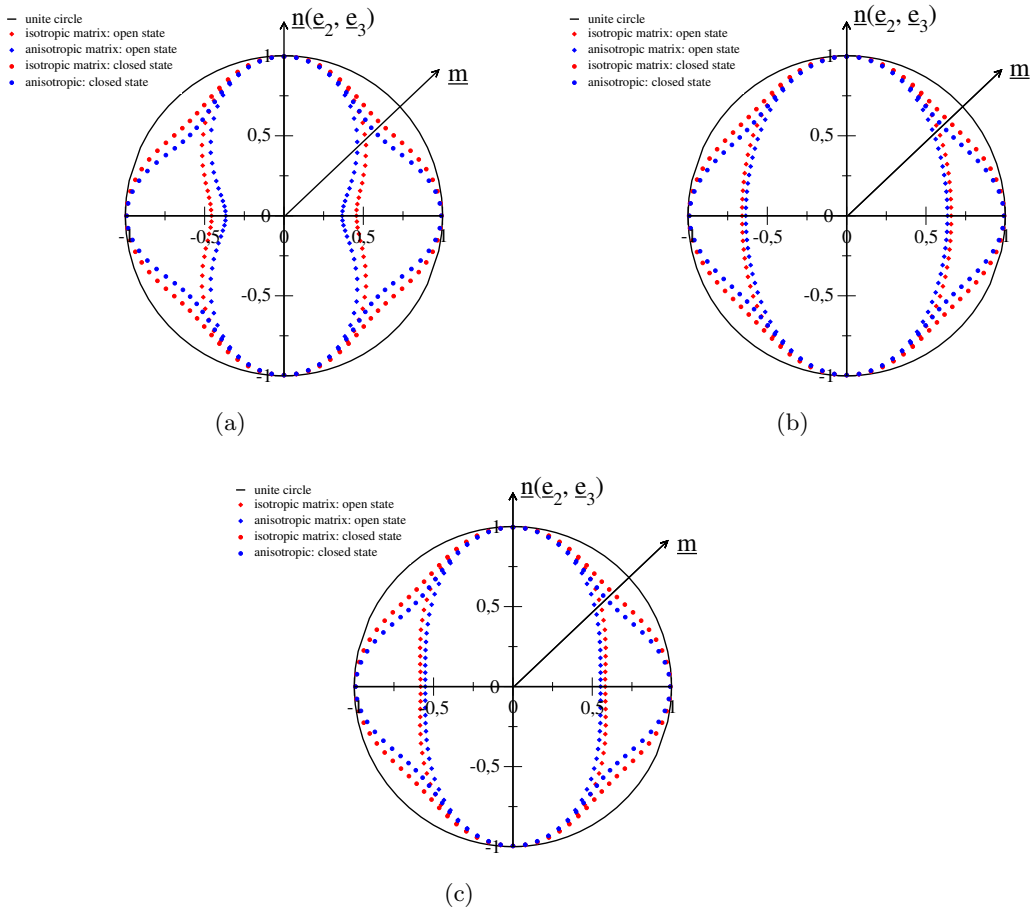

Figure C.4: Comparison the variation of the Young's moduli between isotropic and transversely isotropic matrix produced by parallel open/close cracks media for $\theta_\alpha = 90°$: (a) Dilute scheme, (b) Mori-Tanaka scheme, (c) Ponte-Castaneda et Willis scheme.

© 2016 Tous droits réservés.

doc.univ-lille1.fr

Thèse de Mei Qi, Lille 1, 2016

1.3 Isotropic distribution of microcracks

The crack system here implies the macroscopic elastic isotropy of the cracked media. The effect of the microcracks results in a modification of the shear modulus and bulk modulus. For all application of the end of the chapter, we utilise the numerical value of $\nu = 0.2$. Here, we set $\vartheta = \frac{5-\nu^s}{3}$.

- Dilute scheme:

Case of open cracks

$$\frac{k^{dil}}{k^s} = 1 - \frac{16(1-(\nu^s)^2)}{9(1-2\nu^s)}d \quad ; \quad \frac{\mu^{dil}}{\mu^s} = 1 - \frac{32(1-\nu^s)\vartheta}{15(2-\nu^s)}d \tag{C.7}$$

Case of frictionless close cracks

$$\frac{k^{dil}}{k^s} = 1 \quad ; \quad \frac{\mu^{dil}}{\mu^s} = 1 - \frac{32(1-\nu^s)}{15(2-\nu^s)}d \tag{C.8}$$

- Mori Tanaka scheme:

Case of open cracks

$$\frac{k^{MT}}{k^s} = \frac{1}{1+\frac{16(1-(\nu^s)^2)}{9(1-2\nu^s)}d} \quad ; \quad \frac{\mu^{MT}}{\mu^s} = \frac{1}{1+\frac{32(1-\nu^s)\vartheta}{15(2-\nu^s)}d} \tag{C.9}$$

Case of frictionless close cracks

$$\frac{k^{MT}}{k^s} = 1 \quad ; \quad \frac{\mu^{MT}}{\mu^s} = \frac{1}{1+\frac{32(1-\nu^s)\vartheta}{15(2-\nu^s)}d} \tag{C.10}$$

- Ponte-Castaneda and Willis scheme estimations:

Case of open cracks

$$\frac{k^{PCW}}{k^s} = 1 - \frac{16(1-(\nu^s)^2)d}{9(1-2\nu^s)+\frac{16d}{3}(1+\nu^s)^2}$$

$$\frac{\mu^{PCW}}{\mu^s} = 1 - \frac{480(1-\nu^s)d}{255(2-\nu^s)+64(4-5\nu^s)d} \tag{C.11}$$

© 2016 Tous droits réservés.

doc.univ-lille1.fr

Thèse de Mei Qi, Lille 1, 2016

Case of frictionless close cracks

$$\frac{k^{PCW}}{k^s} = 1 \quad ; \quad \frac{\mu^{PCW}}{\mu^s} = 1 - \frac{480(1-\nu^s)d}{255(2-\nu^s) + 64(4-5\nu^s)d} \tag{C.12}$$

The comparison of the predictions of the different homogenisation schemes for isotropic distribution of cracks are present in the figure (C.5 and C.6). The general variation of the isotropic distribution of cracks are quite similar with the two case that we presented in the subsection (**??**) and (1.1).

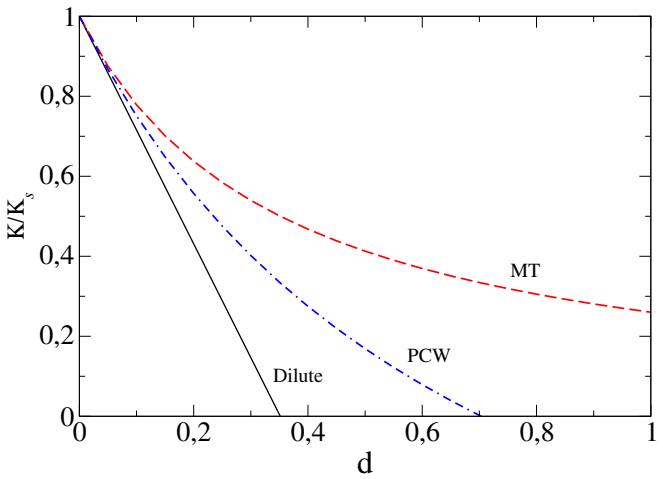

Figure C.5: Isotropic distribution of cracks: Comparison of the predictions of the different schemes for the Young modulus with initially isotropic matrix

© 2016 Tous droits réservés.

doc.univ-lille1.fr

Thèse de Mei Qi, Lille 1, 2016

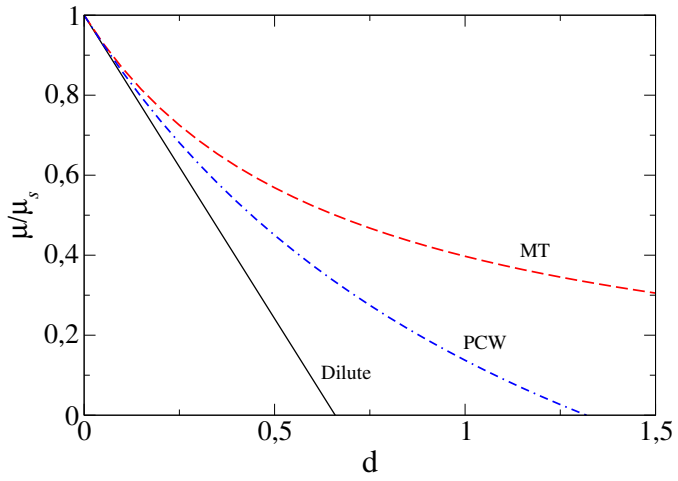

Figure C.6: Isotropic distribution of cracks: Comparison of the predictions of the different schemes for the shear modulus with initially isotropic matrix

© 2016 Tous droits réservés.

doc.univ-lille1.fr

Thèse de Mei Qi, Lille 1, 2016

© 2016 Tous droits réservés.

doc.univ-lille1.fr

Bibliography

[Akai and Arioka, 1970] Akai, K.and Yamamoto, K. and Arioka, M. (1970). Experimental research on the structural anisotropy of crystalline schists. *Proc 2nd, Int, progress international Soc Rock Mechanics Belgrade*, 2:181–186.

[ALLIROTE and BOEHLER, 1970] ALLIROTE, D. and BOEHLER, J. (1970). Evaluation of mechanical properties of a stratified rock under confining pressure. *Proceedings of the Fourth Congress on. I.S.R.M.*, 1:15–22.

[Amadei et al., 1987] Amadei, B., Sa Vage, W. Z., and SWOLFS, H. S. (1987). Gravitational stresses in anisotropie rock masses. *Int. J. Rock Mech. Min. Sei and Geomech.*, 24:5–14.

[Andrieux et al., 1986] Andrieux, S., Bamberger, Y., and Marigo, J. (1986). Un modèle de matériau microfissuré pour les roches et les bétons. *Journal de mécanique théorique et appliquée*, 5(3):471–513.

[Attewell, 1974] Attewell, P. B.and Sandford, M. R. (1974). Intrinsic shear strength of a brittle anisotropie rock- 1. experimental and mechanical interpretation. *Int. J. Rock Mech. Min. Sei and Geomech. Abstr.*, 11:423–430.

[Barthelemy et al., 2003] Barthelemy, J., Dormieux, L., and Kondo, D. (2003). Détermination du comportement macroscopique d'un milieu à fissures frottantes. *C.R. Mecanique*, 331:7–84.

[Barthélémy, 2009] Barthélémy, J.-F. (2009). Compliance and hill polarization tensor of a crack in an anisotropic matrix. *International Journal of Solids and Structures*, 46(22–23):4064 – 4072.

[Benveniste, 1986] Benveniste, Y. (1986). On the mori-tanaka method in cracked bodies. *Mech.Res. Commun.*, 13(4):193–210.

[Bieniawski, 1967] Bieniawski, Z. (1967). Mechnism of brittle fracture of rock. part i: Thoery of the fracture process, part ii expermental study. *Int.J. Rock Mech. Min. Sci.*, 4:395–430.

[Boehler and Sawczuk, 1977] Boehler, J. and Sawczuk, A. (1977). On yielding of oriented solids. *Acta Mechanica*, page 185–206.

© 2016 Tous droits réservés.

doc.univ-lille1.fr

Thèse de Mei Qi, Lille 1, 2016

[Boehler and Sawczuk, 1980] Boehler, J. and Sawczuk, A. (1980). The failure of transversely isotropic rocks in triaxial compression. *Int. J. Rock Mech. Min. Sci*, 17(6):325–332.

[Boehler and Sawczuk, 1986] Boehler, J. and Sawczuk, A. (1986). An extended cam-clay model for soft anisotropic rocks. *Computer and Geotechnics*, 2:69–88.

[Bornert et al., 2001] Bornert, M., Bretheau, T., and Gilormini, P. (2001). *Homogénéisation en mécanique des matériaux 1. Matériaux aléatoires élastiques et milieux périodiques*. Hermes Sciences Europe Ltd.

[Brace and Bombolakis, 1963] Brace, W. and Bombolakis, E. (1963). A note on brittle crack growth in compression. *Journal of Geophysical Research—Solid Earth*, 68(12):3709–3713.

[Castañeda, 2002] Castañeda, P. P. (2002). *Heterogeneous materials. Lecture Notes*. Department of Mechanics, Ecole Polytechnique.

[Chen et al., 2012a] Chen, L., Shao, J., Zhu, Q., and Duveau, G. (2012a). Induced anisotropic damage and plasticity in initially anisotropic sedimentary rocks. *International Journal of Rock Mechanics and Mining Sciences*, 51:13–23.

[Chen et al., 2012b] Chen, Y., Hu, S., Wei, K., Zhou, C., and L, J. (2012b). Experimental characterization and micromechanical modeling of damage-induced permeability variation in beishan granite. *International Journal of Rock Mechanics and Mining Sciences*, 71:64–76.

[Chen et al., 2014] Chen, Y., Li, D., Jiang, Q., and Zhou, C. (2014). Micromechanical analysis of anisotropic damage and its in uence on effective thermal conductivity in brittle rocks. *International Journal of Rock Mechanics and Mining Sciences*, 50:102–116.

[Chenevert and Gatlin, 1965] Chenevert, M. and Gatlin, C. (1965). Mechanical anisotropies of laminated sedimentary rocks. *Soc. Petrol. Eng. J.*, 5:67–77.

[Dafalias, 1979] Dafalias, Y. (1979). Anisotropic hardening of initially orthotropic materials. *ZAMM*, 59:437–446.

[Dafalias, 1982] Dafalias, Y. (1982). Anisotropic critical state clay plasticity model. *In Constitutive Laws for Engineering Materials. Theory and Applications. Elsevier Science Publishing co, Inc.*

© 2016 Tous droits réservés. doc.univ-lille1.fr

Thèse de Mei Qi, Lille 1, 2016

[Deude et al., 2002] Deude, V., Dormieux, L., Kondo, D., and Pensee, V. (2002). Conewise linear elastic materials. *C.R. Mécanique*, 330:587–592.

[Donath, 1964] Donath, F. (1964). Strength variation and deformational behavior in anisotropic rock. *State of stress in the earth's crust: New York*, page 281–297.

[Dormieux and Kondo, 2005] Dormieux, L. and Kondo, D. (2005). Diffusive transport in disordered media. application to the determination of the tortuosity and the permeability of cracked materials. *Applied Micromechanics of Porous Media, L. Dormieux and F-J.Ulm (Eds.), CISM Courses and lectures 480*, pages 83–106.

[Dormieux et al., 2006] Dormieux, L., Kondo, D., and Ulm, F.-J. (2006). *Microporomechanics*. WILEY.

[Eshelby, 1961] Eshelby, J. (1961). Elastic inclusions and inhomogeneities. *In: Sneddon, I.N., Hill, R.(Eds), Progress in solid Mechanics 2.*, 241:89–140.

[Eshelby, 1957] Eshelby, J. D. (1957). The determination of the elastic field of an ellipsoidal inclusion, and related problems. *Proceedings of the Royal Society of London*, 241(1226):376–396.

[Gambarotta and Lagomarsino, 1993] Gambarotta, L. and Lagomarsino, S. (1993). A microcrak damage model for brittle materials. *Int. J. Solids Structures*, 30(2):177–198.

[Gavazzi and Lagoudas, 1990] Gavazzi, A. C. and Lagoudas, D. C. (1990). On the numerical evaluation of eshelby's tensor and its application to elastoplastic fibrous composites. *Comp. Mech.*, 7:13–19.

[Ghahremani, 1977] Ghahremani, F. (1977). Numerical evaluation of the stresses and strains in ellipsoidal inclusions in an anisotropic elastic material. *Mech. Res. Commun.*, 4(2):88–91.

[Giraud et al., 2007] Giraud, A., Huynh, Q., Hoxha, D., and Kondo, D. (2007). Effective poroelastic properties of transversely isotropic rock like composites with arbitrarily oriented ellipsoidal inclusions. *Mechanics of materials*, 39:1006–1024.

[Hayes, 1972] Hayes, M. (1972). Connexions between the moduli for anisotropic elastic materials. *J.Elast*, 2 (1-2):99–110.

[He and Curnier, 1995] He, Q.-C. and Curnier, A. (1995). A more fundamental appraoch to damaged elastic stress-strain relations. *International Journal of Solids and Structures*, 32 (10):1433–1457.

© 2016 Tous droits réservés. doc.univ-lille1.fr

Thèse de Mei Qi, Lille 1, 2016

[Hobbs, 1964] Hobbs, D. W. (1964). The strength and the stress-strain characteristics of coal in triaxial compression. *J. Geol.*, 72:214–231.

[Hoek, 1964] Hoek, E. (1964). Fracture of anisotropie rock. *J. S. Afr. Inst. Min. Metall.*, 64(10):501–518.

[Hoek and Brown, 1980] Hoek, E. and Brown, E. (1980). Underground excavations in rock. *Institution of Mining and Metallurgy, London.*

[Homand et al., 2000] Homand, F., Hoxha, D., Belem, T. andPons, M.-N., and Hoyeit, N. (2000). Geometric analysis of damaged microcracking in granites. *Mech. Mater.*, 32:361–376.

[Homand et al., 1993] Homand, F., Morel, E., Henry, J., Cuxac, P., and Hammade, E. (1993). Characterization of the moduli of elasticity of an anisotropic rock using dynamic and static methods. *Int. J. Rock Mech. Min. Sci.*, 30(5):527–535.

[Hori and Nemat-Nasser, 1983] Hori, M. and Nemat-Nasser, S. (1983). Overall moduli of solids with microcracks: load-induced anisotropy. *J. Mech. Phys. Solids*, 31(2):155–171.

[Hori and Nemat-Nasser, 1985] Hori, M. and Nemat-Nasser, S. (1985). Compression-induced microcrack growth in brittle solids: axial splitting and shear failure. *Journal of Geophysical Research—Solid Earth*, 90(B4):3105–3125.

[Horino and Ellickson, 1970] Horino and Ellickson (1970). A method of estimating strength of rock containing planes of weakness. *Report of Investigation 7449.*

[Huang and Liu, 1998] Huang, J. H. and Liu, H.-K. (1998). On a flat ellipsoidal inclusion or crack in three dimensional anisotropic media. *International Journal of Engineering Science*, 36(2):143 – 155.

[Jaeger, 1960] Jaeger, J. (1960). Shear failure of transversely isotropic rock. *Geology Magazine*, 97:65–72.

[JALBOUT, 2005] JALBOUT, A. (2005). *Etude expérimentale de l'influence de l'endommagement induit sur le comportement mécanique d'une roche fragile.* PhD thesis, Université des sciences et technologies de Lille.

[Jefferson and Bennett, 2007] Jefferson, A. and Bennett, T. (2007). Micro-mechanical damage and rough crack closure in cementitious composite materials. *International Journal for Numerical and Analytical Methods in Geomechanics*, 31:133–146.

© 2016 Tous droits réservés.

doc.univ-lille1.fr

Thèse de Mei Qi, Lille 1, 2016

[Jiang et al., 2010] Jiang, T., Shao, J., Xu, W., and CB, Z. (2010). Experimental investigation and micromechanical analysis of damage and permeability variation in brittle rocks. *International Journal of Rock Mechanics and Mining Sciences*, 47:703–713.

[Kachanov, 1982] Kachanov, M. (1982). A microcrack model of rock inelasticity - part i: frictional sliding on microcracks; part ii : propagation of microcraks. mechanics of materials. *Mechanics of Materials*, 1:19–41.

[Khazraei, 1995] Khazraei (1995). *Etude expéimental et modélisation de l'endommagement anisotrope des roches fragiles.* PhD thesis, University lille 1.

[Kunin, 1983] Kunin, I. A. (1983). *Elastic Media with Microstructure.* Springer, Berlin.

[KWASNIEWSKI, 1993] KWASNIEWSKI, M. (1993). Mechanical behaviour of anisotropic rocks. *Mechanical behaviour of anisotropic rocks.*, 1:313–329.

[Lawn and Marshall, 1998] Lawn, B. and Marshall, D. (1998). Nonlinear stress-strain curves for soilds containing closed cracks with friction. *Journal of the Mechanics and Physics of Solids*, 46:85–113.

[Levassseur et al., 2015] Levassseur, S., Welemane, H., and Kondo, D. (2015). A microcracks-induced damage model for initially anisotropic rocks accounting for microcracks closure. *Int. J. Rock Mech. Min. Sci*, 77:122–132.

[Levin and Alvarez-Tostado, 2006] Levin, V. M. and Alvarez-Tostado, J. M. (2006). Explicit effective constants for an inhomogeneous porothermoelastic medium. *Arch. Appl. Mech.*, 76:199–214.

[Markenscoff and Dascalu, 2012] Markenscoff, X. and Dascalu, C. (2012). Asymptotic homogenization analysis for damage amplification due to singular interaction of microcracks. *Journal of the Mechanics and Physics of Solids*, 60:1478–1485.

[Masson, 2008] Masson, R. (2008). New explicit expression of the hill polarization tensor for general anisotropic elastic solids. *International Journal of solids and structures*, 45:757–769.

[McClintock and Walsh, 1962] McClintock, F. and Walsh, J. (1962). Friction on griffith cracks in rocks under pressure. *Proc. 4th U.S Nat. Congress of Applied Mechanics*, II:1015–1021.

© 2016 Tous droits réservés.

doc.univ-lille1.fr

Thèse de Mei Qi, Lille 1, 2016

[McLAMORE and GRAY, 1967] McLAMORE, R. and GRAY, K. (1967). The mechanical behavior of anisotropie sedimentory rocks. *Journal of Engineering for Industry*, 89:62–73.

[Monchiet and Bonnet, 2012] Monchiet, V. and Bonnet, G. (2012). A polarization-based fft iterative scheme for computing the effective properties of elastic composites with arbitrary contrast. *International Journal for Numerical Methods in Engineering*, 89:1419–1436.

[Mori and Tanaka, 1973a] Mori, T. and Tanaka, K. (1973a). Average stress in a matrix and average elastic energy of materials with misfitting inclusions. *Acta Metall. Mater.*, 42(7):597–629.

[Mori and Tanaka, 1973b] Mori, T. and Tanaka, K. (1973b). Average stress in matrix and average elastic energy of materials with misfitting inclusions. *Acta Metallurgica*, 21:571–574.

[Mori and Tanaka, 1973c] Mori, T. and Tanaka, K. (1973c). Averages stress in matrix and average elastic energy of materials with misfitting inclusions. *acta metall.*, 21:571–574.

[Muller, 1930] Muller, H. (1930). Types of visible variations induced by x-rays in drosophila. *J. Genet.*, 22(3):299–334.

[Mura, 1987] Mura, T. (1987). *Micromechanics of defects in solids, 2nd edition.* Martinus Nijhoff Publ., The Hague, Boston.

[Nasseri et al., 2003] Nasseri, M., Rao, K., and Ramamurthy, T. (2003). Anisotropic strength and deformational behaviour of himalayan schist. *International Journal of Rock Mechanics and Mining Sciences*, 40:3–23.

[Nemat-Nasser and Hori, 1993] Nemat-Nasser, S. and Hori, M. (1993). *Micromechanics : overall properties of heterogeneous materials.* North-Holland, Amsterdam, The Netherlands.

[NIANDOU, 1994] NIANDOU, H. (1994). *Etude du comportement rhéologique et modélisation de l'argilite de Tournemire. Application à la stabilité d'ouvrages souterrains.* PhD thesis, Université des sciences et technologies de Lille.

[NianDou et al., 1997] NianDou, H., Shao, J., Henry, J., and Fourmaintraux, D. (1997). Laboratory investigation of the mechanical behaviour of tournemire shale. *Int. J. Rock. Mech. Min. Sci.*, 34:3–16.

© 2016 Tous droits réservés. doc.univ-lille1.fr

Thèse de Mei Qi, Lille 1, 2016

[Ouyang et al., 1997] Ouyang, C., Barzin, M., and Surendra, P. (1997). An r-cruve approach for fracture of quasi brittle materials. *Engineering Fracture Mechanics*, 37:901–913.

[Paliwal and Ramesh, 2008] Paliwal, B. and Ramesh, K. (2008). An interacting micro-crack damage model for failure of brittle materials under compression. *Journal of the Mechanics and Physics of Solids*, 56:896–923.

[Pan and Chou, 1976] Pan, Y. and Chou, T. (1976). Point force solution for an infinite transversely isotropic solid. *Journal of Applied Mechanics*, 43:608–612.

[Pariseau, 1972] Pariseau, W. (1972). Plasticity theory for anisotropic rocks and soils. *Proc. 10th Symposium on Rock Mechanics*, page 267–295.

[Paterson, 1978] Paterson, M. (1978). Experimantal rock deformation: The brittle field. *Springer-Verlag, Berlin.*

[paterson, 1982] paterson, M. (1982). Micromechanics of faulting in westerly granite. *Int. J. Rock Mech. Min. Sci.*, 19:49–62.

[Peng and Johnson, 1972] Peng, S. and Johnson, A. (1972). Crack growth and faulting in cylindrical specimens of chemsford granite. *Int. J. Rock Mech. Min. Sci.*, 9:37–86.

[Pensee et al., 2002a] Pensee, V., Kondo, D., and Dormieux, L. (2002a). Micromechanical analysis of anisotropic damage in brittle materials. *J. Engng. Mech., ASCE*, 128(8):889–897.

[Pensee et al., 2002b] Pensee, V., Kondo, D., and Dormieux, L. (2002b). Micromechanical analysis of anisotropic damage in brittle materials. *Journ. of engineering mechanics*, 128(8):889–897.

[POMEROY et al., 1971] POMEROY, C., HOBBS, D., and MAHMOUD, A. (1971). The effect of weakness plane orientation on the fracture of barnsley hard coal by triaxial compression. *Int. J. Rock Mech. Min. Sci.*, pages 227–238.

[Ponte-Castañeda and Willis, 1995] Ponte-Castañeda, P. and Willis, P. (1995). The effect of spatial distribution on the behaviour of composite materials and cracked media. *J. Mech. Phys. Solids*, 43:1919–1951.

[Ponte Castañeda and Suquet, 1997] Ponte Castañeda, P. and Suquet, P. (1997). Nonlinear composites. *Advances in Applied Mechanics*, 34:171–302.

© 2016 Tous droits réservés.

doc.univ-lille1.fr

Thèse de Mei Qi, Lille 1, 2016

[Ponte-Castaneda and Willis, 1995] Ponte-Castaneda, P. and Willis, J.-R. (1995). The effect of spatial distribution of effective behavior of composite materials and cracked media. *Journ. Mech. Phys. Solids*, 43:1919–1951.

[Prat and Bazant, 1997] Prat, P. and Bazant, Z. (1997). Tangential stiffness of elastic materials with systems of growing or closing cracks. *Journal of the Mechanics and Physics of Solids*, 45:611–636.

[RAO et al., 1984] RAO, K., RAO, G., and RAMAMURTHY, T. (1984). A strength criterion for anisotropic rocks. *Ind. Geotech. J.*, pages 317–333.

[Reuss, 1910] Reuss, A. (1910). Berechnung der fließgrenze von mischkristallen auf grund der plastizitätsbedingung für einkristalle. *Journal of Applied Mathematics and Mechanics Zeitschrift für Angewandte Mathematik und Mechanik*, 9:49–58.

[Santarelli, 1987] Santarelli, F. (1987). Theorical and experimental investigation of the stability of the axisymmetric wellbore. *Ph.D. Thesis, University of London.*

[Sevostianov and Kachanov, 2007] Sevostianov, I. and Kachanov, M. (2007). Explicit elasticity-conductivity connections for composites with anisotropic inhomogeneities. *Journal of the Mechanics and Physics of Solids*, 55(10):2181 – 2205.

[Sevostianov et al., 2005] Sevostianov, I., Yilmaz, N., Kushch, V., and Levin, V. (2005). Effective elastic properties of matrix composites with tranversely-isotropic phases. *International Journal of Solids and Structures*, 42(3):455–476.

[Singh, 1973] Singh, B. (1973). Continuum characterization ofjointed rock mass. *lnt. J. Rock Mech. Min. Sei and Geomech. Abstr.*, 10:319–349.

[Singh et al., 1973] Singh, J., RAMAMURTHY, T., and RAO, G. (1973). Strengh anisotropies in rocks. *Indian geotech*, 19:147–166.

[Steif, 1984] Steif, P. (1984). Crack extension under compressive loading. *Engineering Fracture Mechanics*, 20(3):463–473.

[Suvorov and Dvorak, 2002] Suvorov, A. P. and Dvorak, G. J. (2002). Rate form of the Eshelby and Hill tensors. *International Journal of Solids and Structures*, 39:5659–5678.

[Tapponier and Brace, 1976] Tapponier, P. and Brace, W. (1976). Developpement of stress induced microcracks in westerly granite. *Int. J. Rock Min. Sci. Geomech*, 13:103–112.

© 2016 Tous droits réservés.

doc.univ-lille1.fr

Thèse de Mei Qi, Lille 1, 2016

[Voigt, 1889] Voigt, W. (1889). Über die beziehung zwischen den beiden elasticität constanten isotroper körper. *Ann. Phys.(Leipzig)*, 38:573–587.

[Walpole, 1981] Walpole, L. (1981). Elastic behavior of composite materials: theoretical foundations. *Advances in Applied Mechanics, ed. C. S. Yih,Vol.*, 21:169–242.

[Walpole, 1984] Walpole, L. (1984). Fourth-rank tensors in the thirty-two crystal cliasses: multiplication tables. *Proceedings Royal Society London A*, 391:149–179.

[Welemane and Cormery, 2002] Welemane, H. and Cormery, F. (2002). Some remarks on the damage unilateral effect modelling for microcracked materials. *International Journal of Damage Mechanics*, 11:65–86.

[Welemane and Cormery, 2003] Welemane, H. and Cormery, F. (2003). An alternative 3d model for damage induced anisotropy and unilateral effect in microcracked materials. *Journ. Phys*, 105:329–336.

[Welsh and Brace, 1964] Welsh, J. and Brace, W. (1964). A fracture criterion for bittle anisotropic rock. *Journal of Geophysical Research*, 69(16):3449–3456.

[Withers, 1989] Withers, P, J. (1989). The determination of the elastic field of an ellipsoidal inclusion in a transversely isotropic medium, and its relevance to composite materials. *Philosophical Magazine A*, 59(4):759–781.

[Xie et al., 2012] Xie, N., Zhu, Q., Shao, J., and Xu, L. (2012). Micromechanical analysis of damage in saturated quasi brittle materials. *International Journal of Solids and Structures*, 49:918–928.

[Xie et al., 2011] Xie, N., Zhu, Q., Xu, L., and Shao, J. (2011). A micromechanics-based elastoplastic damage model for quasi-brittle rocks. *Computers and Geotechnics*, 38:970–977.

[Zaoui, 2002] Zaoui, A. (2002). Structural morphology and constitutive behavior of microheterogeneous materials. *Dans : Continuum micromechanics, Ed. P. Suquet, Springer, New-York*, pages 291–347.

[Zhao, 1998] Zhao, Y. (1998). Crack pattern evolution and a fractal damage constitutive model for rock. *Int.J. Rock Mech. Min. Sci.*, 35(3):349–366.

[Zhu, 2006] Zhu, Q. (2006). Applications des approches d'homogénéisation à la modélisation tridimensionnel de l'endommagement des matériaux quasi fragile: For-

© 2016 Tous droits réservés. doc.univ-lille1.fr

Thèse de Mei Qi, Lille 1, 2016

mulations, validations et implémentations numérique. *Ph.D Thesis University of Lille 1 (In French)*.

[Zhu et al., 2011] Zhu, Q., Shao, J., and Kondo, D. (2011). A micromechanics-based thermodynamic formulation of isotropic damage with unilateral and friction effects. *European Journal of Mechanics-A/Solids*, 30:316–325.

[Zhu et al., 2008a] Zhu, Q.-Z., Kondo, D., and Shao, J.-F. (2008a). Micromechanical analysis of coupling between anisotropic damage and friction in quasi brittle materials: role of the homogenization scheme. *International Journal of Solids and Structures*, 45(5):1385–1405.

[Zhu et al., 2008b] Zhu, Q.-Z., Kondo, D., Shao, J.-F., and Pensee, V. (2008b). Micromechanical modelling of anisotropic damage in brittle rocks and application. *International Journal of Rock Mechanics and Mining Sciences*, 45:467–477.

[Zhu and Shao, 2015] Zhu, Q.-Z. and Shao, J.-F. (2015). A refined micromechanical damage–friction model with strength prediction for rock-like materials under compression. *International Journal of Solids and Structures*, 60-61:75–83.

© 2016 Tous droits réservés.

doc.univ-lille1.fr